

THIS IS AN ORIGINAL MANUSCRIPT
IT MAY NOT BE COPIED WITHOUT
THE AUTHOR'S PERMISSION

EVOLUTION OF GALAXIES AND ITS SIGNIFICANCE FOR COSMOLOGY

ACKNOWLEDGMENTS

I wish to thank my Supervising Professor, Dr. Rainer K. Sachs, whose advice, stimulating questions, and encouragement have enabled me to undertake and continue this research. It is also a pleasure to thank Dr. Harlan J. Smith, Dr. Neville J. Woolf, and Dr. Gerard [REDACTED] interest and suggestions.

APPROVED BY SUPERVISORY COMMITTEE:

To my husband, Brian A [REDACTED] my deepest gratitude for the most support, and cooperation he has [REDACTED] iation with The University of Te [REDACTED]

This research has been [REDACTED] Aerospace Research, United States [REDACTED] out during the tenure of a Unive [REDACTED]

December, 1966.

THE LIBRARY
THE UNIVERSITY
OF TEXAS

THIS IS AN ORIGINAL MANUSCRIPT
IT MAY NOT BE COPIED WITHOUT
THE AUTHOR'S PERMISSION

EVOLUTION OF GALAXIES AND ITS SIGNIFICANCE FOR COSMOLOGY
EVOLUTION OF GALAXIES AND ITS SIGNIFICANCE FOR COSMOLOGY

by

BEATRICE MURIEL HILL TINSLEY, B.Sc., M.Sc.

APPROVED BY SUPERVISORY COMMITTEE:

Primer K. Lach
DISSERTATION

Presented to the Faculty of the Graduate School of
The University of Texas in Partial Fulfillment
of the Requirements

W. J. Woolf
For the Degree of

E. L. Shuck
G. L. Van der Kruit
DOCTOR OF PHILOSOPHY

THE UNIVERSITY OF TEXAS

Austin, Texas

January, 1967

ABSTRACT

ACKNOWLEDGMENTS

I wish to thank my Supervising Professor, Dr. Rainer K. Sachs, whose advice, stimulating questions, and encouragement have enabled me to undertake and continue this research. It is also a pleasure to thank Dr. Harlan J. Smith, Dr. Neville J. Woolf, and Dr. Gerard de Vaucouleurs for their interest and suggestions.

To my husband, Brian A. Tinsley, I wish to express my deepest gratitude for the most essential encouragement, support, and cooperation he has given me throughout my association with The University of Texas.

This research has been sponsored by the Office of Aerospace Research, United States Air Force, and was carried out during the tenure of a University of Texas Fellowship.

December, 1966.

Theoretical magnitude-redshift relations ($m-z$) are constructed, for a variety of cosmological models, using the computed past history of giant elliptical systems. Three

ABSTRACT

values of Hubble's constant are considered, since effects of evolution are greater if this is small. The color-redshift relation is also discussed, but effects of evolution are small.

Evolution of the content and light of galaxies are studied to determine their significance for cosmology.

A numerical computation of evolution starts from gas with Population I composition; then stars are formed at all times, at rates which are functions of stellar mass and mass of gas in the galaxy. Discrete time steps of 10^9 years are used, and 13 stellar masses. The stars are placed on the H-R diagram according to their masses and ages; each star finally becomes a white dwarf, while its excess mass enriches the interstellar gas. Different evolutionary sequences are constructed by adjusting four parameters of a stellar birth-rate function. Then 'galaxies' resulting from each sequence of $10-12 \times 10^9$ years are compared with observed local galaxies, with respect to colors in Johnson's 8-color (UBVRIJKL) system, mass/light ratio, relative mass of gas, and types of stars contributing to the light.

'Galaxies' closely resembling all normal types, Im to E, can be formed with a stellar birthrate proportional to the inverse square of stellar mass, and to the mass of gas in the galaxy; the types differ in initial rate of gas consumption and in the birthrate of very low mass stars. These types can all have the same age, and do not form an evolutionary sequence.

Theoretical magnitude-redshift relations ($m-z$) are constructed, for a variety of cosmological models, using the computed past history of giant elliptical systems. Three values of Hubble's constant are considered, since effects of evolution are greater if this is small. The color-redshift relation is also discussed, but effects of evolution are small in the range observed. Inclusion of galactic evolution greatly reduces the differences in $m-z$ relations between models. This is because those models with the greatest luminosity distance at a given redshift also have the greatest light travel-time, so the galaxies would be seen earlier when they were brighter.

Many cosmological models are found to be consistent with the observed m_V-z relation, including models also consistent with empirical limits on the mean density of matter, with the minimum age of the universe inferred from evolution of star clusters, and with a steep number-flux density relation for radio sources.

Bibliography.

TABLE OF CONTENTS

List of Tables.	vii
List of Figures.	viii
Chapter I. Introduction.	17
Chapter II. Construction of Galactic Evolution Sequences.	30
Chapter III. Results and Comparison with Observed Galaxies.	40
Chapter IV. Magnitude-Redshift Relations.	38
Chapter V. Other Observational Cosmology.	55
Figures 1 - 12.	62
Appendix I. Stellar Evolution Tracks.	84
Appendix II. Formulae for Cosmological Calculations.	92
Appendix III. Magnitude-Redshift Relations.	98
Appendix IV. Revised Colors of Elliptical Galaxies.	104
Bibliography.	108

LIST OF TABLES

1.	Parameters of the Stellar Birthrate Function.	10
2.	Times for Stellar Evolution.	12
3.	Observed Properties of Galaxies.	27
4.	Properties of Computed Galaxies.	30
5.	Comparison with Wood's Photometry.	33
6.	Redshifts.	40
7.	Cosmological Models.	43
8.	Magnitude-Redshift Relation in the B Band.	47
9.	Change in Color B-V at Redshift 0.22.	56
10.	Coefficients in Linear Color-Redshift Relations.	59
5.	Colors of Observed E and SO Galaxies, and Computed Galaxies at 12×10^9 Years.	66
6.	Changes in Time of Computed Galaxy Properties:	
	(a) B-V,	67
	(b) Bolometric Luminosity,	67
	(c) Fraction of Mass as Hydrogen Gas,	68
	(d) Proportion by Weight of Heavy Elements in the Gas.	68
7.	Absolute Spectral Energy Distribution in Sequence E2 at Different Times, Compared with Observed E Galaxies.	69

8.	Ages and Densities of Cosmological Models.	70
9.	Past Behaviour of <u>LIST OF FIGURES</u> Models.	71
10.	Magnitude-Redshift Relations for V Magnitudes.	72
1.	Hertzsprung-Russell Diagram showing Stellar	76
12.	Evolution Tracks Used.	62
2.	Hertzsprung-Russell Diagram showing Old Galactic Clusters and Stellar Evolution Tracks.	63
3.	Color-Color Relation for Mean Observed Galaxies and Computed Galaxies at 12×10^9 Years.	64
4.	Relations between Color and	
	(a) Mass/Light Ratio in B Light, and	65
	(b) Fraction of Total Mass in Hydrogen Gas, for Observed Galaxies and Computed Galaxies at 12×10^9 Years.	65
5.	Colors of Observed E and SO Galaxies, and Computed Galaxies at 12×10^9 Years.	66
6.	Changes in Time of Computed Galaxy Properties:	
	(a) B-V,	67
	(b) Bolometric Luminosity,	67
	(c) Fraction of Mass as Hydrogen Gas,	68
	(d) Proportion by Weight of Heavy Elements in the Gas.	68
7.	Absolute Spectral Energy Distribution in Sequence E2 at Different Times, Compared with Observed E Galaxies.	69

8.	Ages and Densities of Cosmological Models.	70
9.	Past Behaviour of Cosmological Models.	71
10.	Magnitude-Redshift Relations for V Magnitudes.	72
11.	Magnitude-Redshift Relations for R Magnitudes.	76
12.	Magnitude-Redshift Relations for I Magnitudes.	80

The aim of the investigation described here has been to provide estimates of the effect of galactic evolution on the cosmological interpretation of the observed relation between redshifts and apparent magnitudes of galaxies.

The observations used in attempts to choose between theoretical world models extend now to such great distances that light travel-times of several billion years are involved, so that neglecting changes in the luminosity and colors of galaxies over such times is clearly not justified.

Extensive calculations of relations between observable properties of galaxies, for General Relativistic and Steady State world models, have been published by several authors, notably Sandage (1961a) and Clanfield (1966), but these were based on the assumption that evolution of galaxies is negligible. Some estimates of the effects of evolution have been made, e.g. by Crampin and Hoyle (1961), Sandage (1961b), Gratton (1964), and Eastmond (1965), but the arguments used were rather simplified and qualitative. The estimates published to date have not been definite enough to show more than the necessity for considering evolution when trying to choose between world models.

One of the incentives to determine the effects of

CHAPTER I

INTRODUCTION

The aim of the investigation described here has been to provide estimates of the effect of galactic evolution on the cosmological interpretation of the observed relation between redshifts and apparent magnitudes of galaxies.

The observations used in attempts to choose between theoretical world models extend now to such great distances that light travel-times of several billion years are involved, so that neglecting changes in the luminosity and colors of galaxies over such times is clearly not justified.

Extensive calculations of relations between observable properties of galaxies, for General Relativistic and Steady State world models, have been published by several authors, notably Sandage (1961a) and Glanfield (1966), but these were based on the assumption that evolution of galaxies is negligible. Some estimates of the effects of evolution have been made, e.g. by Crampin and Hoyle (1961), Sandage (1961b), Gratton (1964), and Eastmond (1965), but the arguments used were rather simplified and qualitative. The estimates published to date have not been definite enough to show more than the necessity for considering evolution when trying to choose between world models.

One of the incentives to determine the effects of

galactic evolution has been that the General Relativistic model which best fits the magnitude-redshift relation, if interpreted without evolution, appears to be too young and too dense to agree with other evidence. The best model is that with $\Lambda = 0$, $q_0 = +1$, according to Sandage (1965). This has an age measured from the initial singularity given by $t_0 = 7.42 \times 10^9 (75/H_0)$ years, where H_0 is Hubble's constant in $\text{km sec}^{-1} \text{Mpc}^{-1}$, and a mean local density of matter given by $\rho_0 = 2 \times 10^{-29} (H_0/75)^2 \text{ gm cm}^{-3}$. However, estimates of the ages of star clusters (e.g. by Demarque and Larson, 1964, and Woolf, 1962) indicate a minimum age for this Galaxy of 10 or 20×10^9 years, while Abell (1965) concludes that the mean density of matter is probably about $10^{-30} (H_0/75)^2 \text{ gm cm}^{-3}$, and is probably not more than ten times that value. The age problem is not likely to be solved by a reduction in H_0 since most current estimates (Sandage, 1962c; Sérsic, 1962) are greater than $100 \text{ km sec}^{-1} \text{Mpc}^{-1}$. None of the recent attempts to find intergalactic matter at densities near the required value has been successful (Field, Solomon, and Wampler, 1966; Gunn and Peterson, 1965; Kinman, 1966; Koehler, 1965).

The present investigation has shown that when evolution of galaxies is considered, there is a wide range of cosmological models consistent with the observed magnitude-redshift relation, and consistent with reasonable limits on the age and density of the universe.

The galaxies observed at great distances are giant galactic evolution are discussed in Chapter V.

E and SO systems, but in order to develop a theory of evolution of these types it was necessary also to study irregulars and spirals. The evolutionary histories of galaxies constructed here show that it is possible that systems with characteristics of irregular, normal spiral, and E-SO galaxies all have arisen in the same length of time (about 12×10^9 years) since the start of formation of stars with Population I composition. The different types are not found to form an evolutionary sequence in the sense that irregulars evolve through spirals into ellipticals, or vice versa. The type of galaxy eventually formed depends on the fractional rate at which gas is used to form stars, and on the number of stars born less massive than 0.1 solar units. The same power law for rate of star formation, inverse square, is found to be the most successful in giving rise to all the types of galaxies.

The method used to construct evolutionary histories of galaxies is described in Chapter II. In Chapter III, the results of the theory are given, and the close agreement between observed galactic properties and the computed properties of final galaxies of all types is described. Applications to cosmology are given in Chapters IV and V. Chapter IV presents the magnitude-redshift relations for representative cosmological models, incorporating the evolution of giant elliptical (gE) galaxies, and these are compared with the available observational data. Some other observable relations relevant to cosmology and affected by these calculations of galactic evolution are discussed in Chapter V.

Appendix I gives details of the stellar evolution tracks used in constructing galaxies; Appendix II summarizes the formulae needed for calculations with cosmological models, in forms found convenient for numerical computation; Appendix III gives tables of the magnitude-redshift relations discussed in Chapter IV. A revision of the observed colors of gE galaxies, made by de Vaucouleurs (private communication) after the calculations reported here were completed, is discussed in Appendix IV.

The evolution of a galaxy should, ideally, be followed following its history either backwards in time from the present population of stars and gas, or forwards from the beginning. The former method is not feasible because the integrated features do not give enough details. The latter is also subject to great uncertainties, especially as to whether the primeval gas contained helium (Peebles, 1966), and as to the nature of first generation stars. However, evidence that the gas in our Galaxy was rapidly enriched with heavy elements at an early stage is provided by the apparently normal composition of very old galactic clusters (Johnson and Sandage, 1955; Sandage, 1962a). The composition of most galaxies also appears to be similar to that of local Population I stars (Roberts, 1963), and metal-poor stars (Population II) are not important contributors to the light.

Therefore, the starting point chosen here was gas with a Population I composition. The fractions by weight of hydrogen, helium, and heavier elements were taken as $X = .708$, $Y = .272$, $Z = .020$, as deduced by Sears (1964) for the initial composition of the sun. The mass of gas used was 5×10^{11}

CHAPTER II

CONSTRUCTION OF GALACTIC EVOLUTION SEQUENCES

STARTING POINT

The evolution of a galaxy should, ideally, be deduced by following its history either backwards in time from a known population of stars and gas, or forwards from primeval gas. The former method is not feasible because observable integrated features do not give enough details. The latter is also subject to great uncertainties, especially as to whether the primeval gas contained helium (Peebles, 1966), and as to the nature of first generation stars. However, evidence that the gas in our Galaxy was rapidly enriched with heavy elements at an early stage is provided by the apparently normal composition of very old galactic clusters (Johnson and Sandage, 1955; Sandage, 1962a). The composition of most galaxies also appears to be similar to that of local Population I stars (Roberts, 1963), and metal-poor stars (Population II) are not important contributors to the light.

Therefore, the starting point chosen here was gas with a Population I composition. The fractions by weight of hydrogen, helium, and heavier elements were taken as $X = .708$, $Y = .272$, $Z = .020$, as deduced by Sears (1964) for the initial composition of the sun. The mass of gas used was 5×10^{11}

solar masses (M_{\odot}), which is about the mass of a large elliptical galaxy, but all observable integrated properties are independent of this scale factor. A rough estimate was made of the time required for stars of mass about $30M_{\odot}$ to increase the value of Y+Z of the gas from zero to .292, the result being about 10^8 years and involving 10^{10} stars. To allow for these, 10^{10} white dwarfs were added to the gas at the starting point. These stars were found to be of no consequence in the subsequent history, so the uncertainty in their number and formation time is not important.

the HR diagram, with known bolometric corrections (BC) and colors for these positions, luminosity of the galaxy at

NATURE OF A COMPUTED SEQUENCE

A computed time sequence representing the evolutionary history of a galaxy from the above starting point to 12×10^9 years later will be referred to as a 'sequence'. Many different sequences were computed, using the same program after several trials had enabled a suitable one to be developed, but changing four parameters of the stellar birthrate function.

Calculations were made in 12 discrete time steps of 10^9 years. At each time t_j , $j \times 10^9$ years from the start, the numbers of stars, n_{ij} , of mass m_i born in the preceding time interval were calculated, 13 masses m_i being chosen to represent the whole range. These and the already existing stars were placed at appropriate positions in the Hertzsprung-Russell diagram, with the number at each point proportional to the time spent there, corresponding to a uniform stellar

birthrate during each interval of 10^9 years. All stars at the end of their evolutionary tracks were assumed to become white dwarfs of mass $0.5 M_{\odot}$, returning the remainder of their mass to the interstellar medium. The mass of gas, $m_{g,j}$, remaining at t_j was also found, considering the gas consumed in star formation and the gas returned by dying stars.

The change in total fraction by mass of elements heavier than hydrogen (Y+Z) was also found for the gas at each time, considering the mass of such elements returned by dying stars.

The star numbers and positions on the H-R diagram, with known bolometric corrections (BC) and colors for these positions, gave the integrated colors and luminosity of the galaxy at each time.

Details of the stellar birthrate, stars chosen and their evolutionary tracks, and compilation of BC and colors, will now be given.

STELLAR BIRTHRATE

The stellar birthrate is obviously the most important function determining the history of a galaxy. Discussions for the solar neighborhood, in terms of an 'initial luminosity function', have been published by Salpeter (1955, 1959), and in more detail by Schmidt (1959, 1962, 1963). It is unlikely that the solar neighborhood initial luminosity function is widely applicable: Limber (1960) and Salpeter (1965) note that it does not seem compatible with the observed color and

mass/light ratio of most galaxies; also, the present solar neighborhood is not typical of any whole galaxy because of the large numbers of A-F stars which evidently are not important in the integrated light of galaxies (de Vaucouleurs and de Vaucouleurs, 1958, 1959; de Vaucouleurs, 1961; Roberts, 1963).

The stellar birthrate could depend on the local density, temperature, turbulence, angular momentum, and magnetic field of the interstellar gas, but no definitive theory is available to give the birthrate in terms of these or other quantities (e.g. Burbidge, E.M., 1962; Burbidge, G.R., 1962; Spitzer, 1965). Therefore, a function was adopted here with four parameters, apparently providing sufficient generality since, as will be shown, it can give rise to the main present galactic types.

The birthrate function adopted gives n_{ij} , the number of stars of mass m_i formed in the time interval 10^9 years before t_j :

$$n_{ij} = C \xi_i (m_{g,j-1}/m_{g,0})^{1+q_1} \cdot m_{g,0} \quad (1)$$

$m_{g,j-1}$ is the mass of gas in the galaxy at the start of the interval (t_{j-1}), and $m_{g,0}$ is the initial mass of gas ($5 \times 10^{11} M_{\odot}$). C is a constant chosen so that

$$m_{g,1} = \beta m_{g,0} \quad (2)$$

ξ_i depends on the star mass, and is calculated according to a power law integrated between limits that are the geometric means (arithmetic means of log mass) of m_i and the masses

immediately above and below it:

$$\xi_1 = \frac{1}{x} \int_{\sqrt{m_1 m_{i-1}}}^{\sqrt{m_1 m_{i+1}}} m^{-(x+1)} dm = (m_1 m_{i-1})^{-x/2} - (m_1 m_{i+1})^{-x/2} \quad (3)$$

For ξ_1 of maximum i , the value of m_{i+1} is unimportant but was taken to be $100 M_{\odot}$. The value of ξ_1 was taken as

$$\xi_1 = D \xi_2 \quad (4)$$

In equation (1), q_1 was either taken to be zero for all masses, or to be given by:

$$q_1 = \begin{cases} 0 & \text{if } m \leq M_{\odot} \\ 2 \log \bar{m}_1 & \text{if } m > M_{\odot} \end{cases} \quad (5)$$

where \bar{m}_1 is the mass of the star with mean absolute visual magnitude in the range m_{i-1} to m_{i+1} . (5) thus gives a greater proportion of massive stars earlier in the galactic history. The dependence of n_{1j} on gas mass corresponds to the law given by Schmidt (1963), with his parameter $n=1$ and his parameter $\alpha=0$ (if all q_1 in (1) are zero) or $q=2$ (if (5) is used). These two sets of values of q_1 will be referred to by the value of Schmidt's 'q', 0 or 2 respectively.

Power laws similar to equation (3) are discussed by Reddish (1961, 1962a and b, 1965), who finally adopts $x=1.5$.

The four parameters of the birthrate function, and their values used to give different sequences, are listed in Table 1. Many of the possible combinations of parameters

were not tried, because the results from others made it clear that they would lead to totally unrealistic 'galaxies'.

TABLE 1
PARAMETERS OF THE STELLAR BIRTHRATE FUNCTION

Parameter	Significance	Values Tried
β	Initial fractional rate of gas consumption, eq. (2).	.0001, .01, .1, .3, .5, .7, .9, .99
x	Power of stellar mass, eq. (3).	0.5, 1.0, 1.5, 2.0 2.5
D	Birthrate of very low mass stars, eq. (4).	10, 100, 1000, 10000
a	Possibility of more massive stars earlier, eq.(5).	0, 2

CHOICE OF STELLAR MASSES

It was found after several trials that the 13 stellar masses given below were suitable. Solar units will be used for mass throughout.

Mass .05. This star does not reach the main sequence (MS) but evolves into the very faint red dwarf region.

Mass .26. This star reaches the MS in the region of M3 dwarfs, but further evolution is negligible, in 12×10^9 years.

Mass .80. This evolves up, but not away from, the MS, and is

typical of late G to late K dwarfs.

Masses 1.00, 1.03, 1.06, 1.09, 1.18, 1.25. These are all about G dwarfs at the zero-age main sequence (ZAMS), but evolve into red giants in times of 5 to 11×10^9 years. For this reason, many masses were needed to give smooth changes in time of the properties of the galaxy.

Masses 1.5, 2.0, 3.0, 15.0. These all complete their evolution to white dwarfs in 10^7 to 2×10^9 years. They evolve from the upper MS into giants and supergiants.

STELLAR EVOLUTION TRACKS TAKEN FROM THEORETICAL CALCULATIONS

Theoretical calculations of stellar evolution give the bolometric luminosity, L , and effective temperature, T_e , as a function of time, for a star of known mass and initial composition. The tracks on the theoretical H-R diagram used are shown in Figure 1, and the times at various stages of evolution are summarized in Table 2. Details are given in Appendix I.

All stars were given the composition $X=.708$, $Y=.272$, $Z=.020$ at birth, for simplicity in calculation, even though the interstellar medium becomes enriched in heavy elements. The probable effects of changing the initial composition, or allowing for changes in time, will be discussed below.

In this and the next section, sources of the stellar evolution data will be described.

Masses 0.8 to 15.0, pre-MS. These tracks were all taken from Iben (1965a), with graphical interpolation between masses

TABLE 2

TIMES FOR STELLAR EVOLUTION

Mass of star (solar units)	Times (10^9 years) On MS	Birth to white dwarf	Mass of star (solar units)	Times (10^9 years) On MS	Birth to white dwarf
0.05	-	-	1.18	5.50	6.44
0.26	> 12	-	1.25	4.40	4.94
0.8	> 12	-	1.5	1.40	1.83
1.00	10.8	> 12	2.0	0.78	0.98
1.03	9.50	11.04	3.0	0.22	0.33
1.06	8.50	9.84	15.0	0.011	0.012
1.09	7.50	8.74			

Masses .05 and .26. The calculations of Hayashi and Nakano (1963) were used, with an adjustment of $\log T_e$ to allow for the composition differences: in accordance with the authors' estimates of the effects of changing opacity, $\log T_e$ was reduced by .01 at each luminosity. The track for mass .26 was interpolated in their Figure 2, ending at their ZAMS point; above $\log L/L_\odot = .5$, the track was interpolated in Figure 4-4 of Hayashi et al. (1962; hereafter referred to as HHS). The final point for mass .05 was taken just beyond the last point of Hayashi and Nakano, and the possible effects of uncertainty here are discussed below.

Masses 0.8 to 15.0, pre-MS. These tracks were all taken from Iben (1965a), with graphical interpolation between masses

where necessary. The composition used by Iben was that adopted here. Masses 0.8, 1.00, 1.03, MS. The tracks given by Demarque and Larson (1964) for composition $X=.67$, $Z=.03$ (case $1/H=1.6$) were used, but shifted in $\log L$ and $\log T_e$, and correspondingly in time, by the difference between these authors' and Iben's (1965a) ZAMS values; this was consistent with the effects of composition found by these authors: $\log L$ was increased by .011 and $\log T_e$ by .01 at each point, and the time changed by a factor equal to the change in ratio X/L .

Masses 1.06 to 1.5, MS. For mass 1.5, the track of Henyey et al. (1959) was used, but shifted, because of the composition differences, in $\log L$ and $\log T_e$ at all points by the difference between these authors' and Iben's (1965a) ZAMS values. This shift is consistent with that predicted from the calculations of Kelsall (1965) for mass 1.78, when these are used to derive increments in $\log L$ and $\log T_e$ for small changes in X and Z . The times were also changed, by a factor proportional to X/L .

For masses 1.06, 1.09, 1.18, and 1.25, the ZAMS luminosities were calculated from the law $L \propto M^5$ indicated by the results of Demarque and Larson (1964), and then values of $\log T_e$ were interpolated graphically between Iben's (1965a) ZAMS positions. The times spent on the MS were assumed proportional to mass/luminosity at the ZAMS. Subsequent parts of the MS were drawn parallel to that for mass 1.00,

for masses 1.06 and 1.09, but for 1.18 and 1.25 the track was drawn similar to that for 1.5, since these stars all have convective cores. Unfortunately, no more accurate tracks seem to be available in this critical range of mass where the structure of the star changes from having a radiative to a convective core. The uncertainties are probably not important for the integrated light of galaxies, however.

Mass 2.0, MS. The track of Auman (1965) was used, shifted in $\log L$ and $\log T_e$ and changed in time because of the composition differences, by the method described for mass 1.5.

Mass 3.0. The complete track of Iben (1965a and b) was used, from pre-MS through core helium burning.

Mass 15.0. Iben's (1965a and 1966b) track from pre-MS through core helium burning was used, and the carbon burning phase was taken from the calculations of Hayashi and Cameron for mass 15.6 (see HHS), with an adjustment of $\log T_e$ for the mass difference as in HHS (page 150).

White dwarfs. The approximation used was that every star at the end of nuclear burning forms a white dwarf with mass 0.5 and the same composition, which cools as a degenerate body at constant radius. The mass-radius relations of Hamada and Salpeter (1961) show that for pure helium or pure magnesium the cooling line in the H-R diagram is close to:

of one star, the $\log L/L_{\odot} - 4 \log T_e = -18.8$.

The cooling time at any luminosity is proportional to the

composition parameter $\mu_A^{-1} Z^{2/7}$ (μ_A = mean molecular weight

of atomic nuclei), for which the value 1/20 was chosen.

Then the general equations, given by Schwarzschild (1958), show that for this mass and composition the time is given by:

$$t = 3 \times 10^6 (L/L_{\odot})^{-5/7} \text{ years.}$$

The rather arbitrary choice of composition parameters is not important because at no stage does the light of white dwarfs contribute significantly to that of the galaxy. A different choice of mass would affect the quantity and composition of gas returned to the interstellar medium, but for reasonable white dwarf masses the change would be less than the uncertainty of observations of gas in galaxies, so would not affect any conclusions drawn from this study.

1.5 by NGC 7789; and 2.0 by NGC 2158. The calculated MS

STELLAR EVOLUTION TRACKS TAKEN FROM GALACTIC CLUSTERS

sketches. Theoretical calculations of stellar evolution tracks beyond the main sequence are fewer and less reliable than those for stages up to hydrogen burning in the stellar core. Therefore it was decided, following a suggestion by Woolf (1966), to use the red giant branches of old galactic clusters to represent later stages of evolution of stars with masses 1 to 2. The time required for a star to ascend the red giant branch is so short compared to its time on the MS that the cluster red giant branches can be regarded as tracks of one star, the population at any point indicating the relative time spent there.

red giant The four clusters and sources of data used were:

NGC 188 (Sandage, 1962a and b), M 67 (Johnson and Sandage, 1955), NGC 7789 (Burbidge and Sandage, 1958; Arp, 1962), and NGC 2158 (Arp and Cuffey, 1962). H-R diagrams for these clusters were reduced from the observed magnitude and color (V, B-V), first to corrected absolute magnitude and color (M_{V_0} , $(B-V)_0$) using the authors' distance moduli and reddening corrections, and then to $(\log L/L_\odot, \log T_e)$ using the calibration data described below. These were compared with the calculated evolutionary tracks discussed above for the MS of stars of masses 1 to 2, and it was decided to represent the further evolution of masses 1.00 and 1.03 by NGC 188; 1.06, 1.09, and 1.18 by M 67; 1.25 by a track between M 67 and NGC 7789; 1.5 by NGC 7789; and 2.0 by NGC 2158. The calculated MS tracks and the cluster giant branches were joined by freehand sketches. For masses 1.0 to 1.5, the cluster tracks were extended up to the luminosity of the helium flash, $\log L/L_\odot = 3.14$ (HHS, page 110). (NGC 2158 has stars more luminous than this, consistent with theory which indicates that a star of mass 2 would not undergo a helium flash.) Figure 2 shows the reduced cluster H-R diagrams and the stellar evolution tracks adopted.

The numbers of stars in the clusters were too small to give reliable estimates of the relative times at each part of the track, so theoretical estimates were used. For masses 1.00 to 1.25, the luminosity and structure of the core in the red giant stage is almost independent of mass (HHS, page 109),

so for all masses the time depends on the increase in core mass, M_1 , according to:

$$dt = E X_0 dM_1 / L$$

where E is the number of ergs released per gram of hydrogen, and X_0 is the fraction by mass of hydrogen in the envelope (.708). A graph was drawn of M_1 versus L^{-1} , using data from Hoyle and Schwarzschild (1955, Population I star) and from HHS (Table 6-11) at highest L , and the area under this graph was used to determine the time at several points on the giant branch. These times agreed within statistical error (i.e. \sqrt{N}) with the numbers of stars in corresponding areas of the H-R diagram of NGC 188, listed by Johnson and Sandage (1955). No stars are observed in the region corresponding to the top of the adopted track, but the number predicted is 0.6. (No list was published for M 67, and this is not suitable for comparison being a less rich cluster. The luminosity function published by Sandage (1957) does not provide enough information since B-V or $\log T_e$ must also be known.) The time spent by each star at a point between the MS and the cluster giant tracks was adjusted so that at the tip of the track ($\log L/L_\odot = 3.14$) the total fuel burned would give a helium core of mass 0.42, as required for the helium flash (HHS).

For mass 1.5, the relative times at points of the giant track were taken proportional to star counts in corresponding areas of the H-R diagram of NGC 7789, the cluster being rich enough to give significant counts at all points;

the total time was chosen to give a core mass 0.42 at the tip. The resulting times were very close to those given by the graph of M_1 versus L^{-1} mentioned above, which is a satisfactory check on the method.

For mass 2.0, the relative times were taken proportional to star counts in NGC 2158. Because no better method was available, the total time was estimated by extrapolating the ratios of times given by Iben (1965b, 1966a) for masses 3 and 5, in core hydrogen burning, rapid core contraction, and later stages. The resulting time for mass 2 in the giant region led to a total fuel requirement near to the limit available to the star, so may be an overestimate. However, this star is never of importance to the total light of the galaxy, so the uncertainty is not important in the present study.

ALTERNATIVE FINAL STAGES OF STELLAR EVOLUTION

Two sources of uncertainty in the above stellar evolution tracks could have important effects on the integrated light of the galaxy.

In constructing most galactic evolution sequences, it was assumed that when a star reaches the end of its track shown in Figure 1 it loses mass and becomes a white dwarf in negligible time. However, there is evidence (summarized by Deutsch, 1961, and Weymann, 1963) that red giants are losing mass at a rate which could slow down the later stages of evolution considerably. This possibility should be con-

sidered for stars which evolve into the region of the H-R diagram where mass loss is observed. Very red giants, in that region of the H-R diagram, have been observed in some old galactic clusters; Walker and Bidelman (1960) report on stars of types M0III and M1II-III in NGC 7789, and Walker (1958) reports on a variable of type M5II in NGC 6940.

The second source of uncertainty is the small number of stars in the clusters, making it statistically possible that such red giants as these are part of the evolutionary history of stars with masses 1 to 2.

The effect of these uncertainties was tested by computing some sequences with alternative final positions for the stars. These positions had to be chosen rather arbitrarily, but they should provide a reasonable upper limit to the effect on the whole galaxy.

The alternative for stars with masses 1.0 to 1.5 was a position corresponding to a typical long period variable, spectrum M4III and absolute magnitude $M_V = -1.8$ (Allen, 1963), replacing the previous tip of the giant branch. The time spent there was such that the fuel burnt was the same as before. The expected number of such stars in NGC 188 would be about 0.5.

For mass 2.0, the alternative was the star observed by Walker (1958) in NGC 6940 (M5II, $M_V = -2.4$). The time previously at the tip of the giant branch was halved, and the time at the alternative position chosen to give the same

amount of fuel burnt; also this makes the number of stars observed in NGC 2185 (near the previous tip but not at M5II) not too improbable.

For mass 15.0, the time estimated by HHS for stages later than carbon burning (6×10^5 years) was added to the final point of the previous track, at M4Ib.

The effect on the whole galaxies was noticeable only in the far infrared (J, K, and L filter bands), where there are observations only for E and SO galaxies. For these, differences between sequences with alternative star tracks were 0.01 to 0.05 magnitudes in the colors, which is much less than the scatter in observations. Thus the comparison of computed with observed galaxies is not affected by these uncertainties in stellar evolution.

BOLOMETRIC CORRECTIONS AND COLORS OF STARS

The greatest wavelength range for which there are adequate observations of stars and galaxies is given by the UBVRIJKL wide band photometry of Johnson and his collaborators. The effective wavelengths are .36, .44, .55, .70, .90, 1.25, 2.2, and 3.4 microns, respectively. The necessary data, BC and seven colors U-V to V-L, were obtained for all 136 points shown on Figure 1, as follows.

Graphs were drawn of BC and each color versus $\log T_e$, separately for luminosity classes I, III, and V, using data given by Johnson (1964, 1965a and b) and Mendoza and Johnson

(1965), and by Harris (1963) for BC not available in the preceding papers. Then for each point in Figure 1, the BC and colors were read for the appropriate $\log T_e$ and luminosity, interpolating between luminosity classes where necessary. The values adopted are given in Appendix I.

These data, with the bolometric luminosity for each point, enable the integrated bolometric luminosity, magnitudes, and colors of a galaxy to be computed when the number of stars at each point is known. The absolute energy distribution, in $\text{ergs sec}^{-1} \text{micron}^{-1}$ at the effective wavelength of each band, can also be found using the absolute calibration of this photometric system (Johnson, 1965c).

The final point for mass .05 was taken at $\log L/L_{\odot} = -3.75$, $\log T_e = 3.33$, with colors for that T_e (M7III) given by Mendoza and Johnson (1965). The position was somewhat arbitrary as the star continues cooling beyond the last point calculated by Hayashi and Nakano (1963). Since this star dominates the light in the J, K, and L bands, several sequences were computed using alternatively the colors of M9III. Changes in the integrated colors of galaxies were less than 0.01 except in V-J, V-K, and V-L, where they were up to 0.2, but less than the errors and scatter in observation, so this uncertainty is not important.

After the present computations were completed, a revision of the stellar data (Johnson, 1966b) became available. Compared with the $\log T_e$ -BC-color relationships described

above, the new data are different in two ways that would affect the properties of computed galaxies:

(a) There is a change of several hundredths of a magnitude in the BC and colors for given $\log T_e$. Since the values of $\log T_e$ used here were taken from theoretical stellar evolution tracks for all pre-MS and MS stars, and later stages of massive stars, the data for these should be changed accordingly.

(b) There is a similar change in other colors and BC for giant stars with given B-V. Since the red giants used here for stars of masses 1.0 to 2.0 were placed on the H-R diagram according to their observed B-V and M_V , their bolometric luminosities and other colors should be changed.

In order to test the importance of these changes, a galactic evolution sequence was computed with the same stellar birthrate parameters as sequence E2 (see Chapter III and Table 4), but with the four MS stars and three giants that contribute most light in U, B, V recalibrated. The resulting colors of the computed galaxy at 12×10^9 years were reduced from their previous values by .06, .01, .03, .01, .03, .03, .05 in U-V, B-V, V-R, V-I, V-J, V-K, V-L, respectively. The most important change is in U-V, and improves the agreement with observed galaxies. The changes in far infrared colors are not significant since the main stars contributing there were not recalibrated, and since the observed values are from very few galaxies (Johnson, 1966a) and are uncertain by several

tenths of a magnitude.

These changes show the importance of having an accurate knowledge of stellar effective temperatures, BC, and colors. They also show that differences of several hundredths of a magnitude between observed and computed galactic colors must be expected, because of uncertainties in stellar data.

QUANTITIES COMPUTED

The following quantities were printed during computation of sequences, at some or all of the times t_j ; they were chosen to make possible a thorough comparison with observed galaxies at times 10, 11, and 12×10^9 years, and to show essential features of the history:

Mass of gas.

Composition parameter: relative mass of elements heavier than hydrogen, $Y+Z$ of the gas.

Ratio mass of hydrogen/mass of galaxy, m_H/m_{tot} .

Bolometric luminosity, L_{bol} .

Mass/light ratios in V and B bands, in solar units, $f(V)$ and $f(B)$; and mass of hydrogen gas/luminosity in B band, $f_H(B)$.

Absolute spectral energy, in $\text{ergs sec}^{-1} \text{micron}^{-1}$, at effective wavelengths of U, B, V, R, I, J, K, L filter bands.

Integrated colors, U-V, B-V, V-R, V-I, V-J, V-K, V-L.

Stellar birthrates, n_{ij} , for each mass m_i .

Those stars (i.e. positions in the H-R diagram,

Figure 1) contributing more than 10% of the light in any filter band, and their relative contributions, for qualitative estimates of spectral features.

Number of stars at each of the 136 points on the H-R diagram, so that further details of spectra, colors in other photometric systems, etc., could be calculated.

alternatives in star tracks, and then the resulting galaxies were compared with galaxies observed nearby in time and space.

The final age cannot be less than 10×10^9 years after the start of Population I star formation, or no stars have evolved up the NGC 188 track, which would be inconsistent with our own Galaxy; also calculations showed that for ages greater than 12×10^9 years earlier types of galaxies are too red for consistency with their other properties, while ellipticals would have too much contribution to the red light from giant stars. Possible parameter combinations for obtaining good final galaxies at ages 10 to 12×10^9 years ago surprisingly few. As remarked in Chapter II, the alternatives in star tracks did not make significant differences.

DETERMINATION OF GALACTIC TYPE

The parameter μ determines the mass of gas remaining in the galaxy, and this property was shown to be the approximate Hubble type represented by the sequence.

CHAPTER III

RESULTS AND COMPARISON WITH OBSERVED GALAXIES

A large number of sequences were computed, using different combinations of stellar birthrate parameters and alternatives in star tracks, and then the resulting galaxies were compared with galaxies observed nearby in time and space.

The final age cannot be less than 10×10^9 years after the start of Population I star formation, or no stars have evolved up the NGC 188 track, which would be inconsistent with our own Galaxy; also calculations showed that for ages greater than 12×10^9 years earlier types of galaxies are too red for consistency with their other properties, while ellipticals would have too much contribution to the red light from giant stars. Possible parameter combinations for obtaining good final galaxies at ages 10 to 12×10^9 years are surprisingly few. As remarked in Chapter II, the alternatives in star tracks did not make significant differences.

DETERMINATION OF GALACTIC TYPE

The parameter β determines the mass of gas remaining in the galaxy, and this property was chosen to give the approximate Hubble type represented by the sequence. Then

the combinations of other parameters (x, D, q) were found which gave agreement with other properties. The relative masses of gas observed in galaxies of type Im, Sc to Sm, Sa to Sb, and E to S0 were obtained using β values .9, .7, .5, and .3 or .1, respectively.

OBSERVED PROPERTIES OF GALAXIES

Table 3 gives observed properties of the galactic types which the computed final galaxies were required to match.

TABLE 3 OBSERVED PROPERTIES OF GALAXIES

Type (1)	zE and S0 (E)	Sa to Sb	Sc to Sm
m_H/m_{tot}	$\leq .001$.0001 to .01	.01 to .1
$f(B) = m_B/L(B)$ m_{tot}	20 to 200, or greater (2)	10 to 20	5 to 10
$f_B(B) = m_B/L(B)$	$\leq .03$ (only observation! SGC 4472; .007)	.005 to .05	.05 to .1
Range of B-V & corresponding U-V (3)	.75 to .95 .95 to 1.6	.70 to 1.00 .75 to 1.55	.45 to .75 .25 to .85
Colors & spectral energy (4)	5 E galaxies: Mean: Range U-V 1.56:1.64, 1.70 B-V 1.02:1.00, 1.07 V-R 0.92:0.82, 1.00 V-I 1.67:1.50, 1.77 V-J 2.23:1.54, 2.79 V-K 3.04:2.71, 3.16 V-L 3.46:3.04, 3.87		
Contributing types of stars	4 S0s of V contributing light in red dwarf (prob- ably 50%), ad- just of B light in red dwarf.	65-early B stars, not dwarfs, domin- ant in UV (4) S0s dwarfs in (5), red dwarf in B, few A or early F stars. V155-55, 58, 6.	20-4 or early F stars. For (part of 10) (C); spectral type changes to 25 in B

TABLE 3 OBSERVED PROPERTIES OF GALAXIES

Type (1)	gE and SO (E)	Sa to Sb	Sc to Sm	Im	References
m_H/m_{tot}	$\lesssim .001$.0001 to .01	.01 to .1	$\geq .1$	Epstein (1964) Holmberg (1964) Roberts (1963) Robinson & Koehler (1965) de Vaucouleurs (1959, 1966)
$f(B) = m_H/L(B)$ m_{tot}	20 to 200, or greater (2)	10 to 20	5 to 10	1 to 5	
$f_H(B) = m_H/L(B)$	$\lesssim .03$ (only observation: NGC 4472::007)	.005 to .05	.05 to .1	.23 to 2	
Range of B-V & correspond- ing U-V (3)	.75 to .95 .95 to 1.6	.70 to 1.00 .75 to 1.55	.45 to .75 .25 to .85	.2 to .6 -.25 to .4	de Vaucouleurs (1961)
Colors & spectral energy. U-V (4)	5 E galaxies: Mean: Range 1.56:1.44, 1.70 1.02:1.00, 1.07 0.92:0.82, 1.00 1.67:1.50, 1.77 2.23:1.54, 2.79 3.04:2.71, 3.18 3.48:3.04, 3.87				Johnson (1966a) (5) (See App. IV.)
Contributing types of stars	< 50% of V light in red dwarfs (prob- ably 40%). 40- 50% of R light in red dwarfs.	G8-early M giants, not dwarfs, domin- ant in UBV (< 50% dwarfs in V). Red dwarfs in R. Few A or early F stars.	Few A or early F stars. For Sm (part of LM C): spectral type changes B0 to F5 in U to B; order in V: B0-B5, K, M, G.	From NGC 4449: type A-F in B wavelengths.	Code (1959) Morgan (1959a & b) Morgan & Mayall (1957) Roberts (1963) Spinrad (1962) Tull (1966) de Vaucouleurs & de Vaucou- leurs (1958, 1959)

NOTES TO TABLE 3

(1) The approximate galactic type is all that can be indicated. Computed galaxies were not required to have gas and light characteristics corresponding to the mean observed galaxy of any type, but to have consistent relations between these characteristics. (See Figures 3 and 4, discussed below.) Dwarf ellipticals were not considered. gE and SO were grouped together, and will be referred to as 'E' systems hereafter.

(2) Mass/light ratios for E and SO galaxies are usually quoted as less than 100, but mass estimates are so uncertain that ratios of several hundred are consistent with the observations (de Vaucouleurs, 1966).

(3) The colors listed in this line of the table are corrected for Galactic absorption and redshift.

(4) These are Johnson's (1966a) observed colors for 5 E galaxies. His observations on spirals refer to nuclear regions only, so are not relevant here. Revisions to the reduction of these observations are discussed in Appendix IV.

(5) The photometry of Wood (1966) was published after the present calculations were completed, but comparison of the final E galaxies with this is given below.

Figures 3, 4, and 5
of the computer
In Figure 3 all the galaxies
from Holmberg (1964), his
sent between computed and
too large. Figure 5
by Johnson (1966a).
found for the population of
at this age, so the conclusions
each. For the computer
were those of the
used were those of the

TABLE 4
PROPERTIES OF COMPUTED GALAXIES

Seq.	Type	β	x	D	q	Final age	$\frac{m_H}{m_{tot}}$	B-V	U-V	f(B)	$f_H(B)$	Y+Z
(1)	(2)	(3)	(4)	(5)	(6)	(7)	(8)	(9)	(10)	(11)	(12)	(13)
I1	Im	.9	.5	10	2	10,11, 12	.21	.50	.43	3.1	.65	.48
I2	Im	.9	1.0	10	0	10,11, 12	.19	.44	.23	3.7	.70	.41
Sc1	Sc to Sm	.7	.5	10	2	10,11, 12	.035	.80	1.18	4.8	.17	.56
Sc2	Sc to Sm	.7	1.0	10	0	10,11, 12	.014	.68	.75	5.7	.08	.57
Sc3	Sc to Sm	.7	1.5	10	0	10,11	.013	.82	1.19	14	.18	.38
Sa1	Sa to Sb	.5	.5	10	2	12	.0089	.87	1.38	5.6	.050	.59
Sa2	Sa to Sb	.5	1.0	10	0	12	.0032	.82	1.17	8.0	.026	.53
Sa3	Sa to Sb	.5	.5	100	2	12	.0018	.92	1.52	28	.050	.39
Sa4	Sa to Sb	.5	1.0	100	0	12	.0008	.90	1.45	52	.042	.38
E1	E	.3	.5	1000	0,2	12	1.0×10^{-4}	.92	1.60	262	.026	.31
E2	E	.3	1.0	1000	0,2	12	4.5×10^{-5}	.88	1.59	516	.023	.30
E3	E	.1	.5	1000	0,2	12	7.4×10^{-5}	.96	1.70	266	.020	.30
E4	E	.1	1.0	1000	0,2	12	3.4×10^{-5}	.93	1.66	520	.018	.30

Figures 3, 4, and 5 show how closely the properties of the computed final galaxies agree with those observed. In Figure 3, all the computed galaxies shown lie well within the observed range of colors (de Vaucouleurs, 1961), except for Sc1 and Sc3 which have rather larger U-V and B-V than observed. The observational data in Figures 4(a) and (b) are from Holmberg (1964), his color index being converted to B-V by the relations given by de Vaucouleurs (1961). The agreement between computed and observed relations is seen to be excellent within the range observed (which does not include the E systems), except that sequences Sa1 and Sc1 seem to have too large B-V. Figure 5 compares the computed colors of E systems with the mean and range for 5 such systems observed by Johnson (1966a).

After the present calculations were completed, narrow band photometry between 3459\AA and 7331\AA , for 22 galaxies and 25 star types, was published by Wood (1966). In order to check on the sequences used in cosmological calculations, integrated colors and line indices on Wood's system were found for the population of sequence E2 at 12×10^9 years; sequence E4, also used in Chapter IV, is very similar to E2 at this age, so the conclusions drawn for E2 will apply to both. For the computed star population, the colors used were those given by Wood for the star type with the same B-V and nearest absolute magnitude, and the absolute magnitudes used were those of the 136 points on the H-R diagram. The

data enable one to calculate 6 integrated color differences and 5 line indices. These are given in Table 5, and compared with the mean values for the 7 E and S0 galaxies observed by Wood. The result shows agreement between observed and computed indices: the mean observed-minus-computed is 0.00 magnitudes, and root-mean-square O-C is 0.04, compared to the root-mean-square probable error of the observations used in the means, 0.06. The population of sequence E4 or E2 at 12×10^9 years is rather different from any synthesized by Wood to match E or S0 galaxies, which is possible because there are 25 star types to match 12 colors, and because some of the stars in the sequences have different absolute magnitudes from Wood's. The main differences are the absence of horizontal branch stars from the computed population, and the presence here of many very red dwarfs, which give a much larger mass/light ratio than Wood could obtain but are too red to contribute appreciably at 7000\AA .

The approximate indications given in Table 3 for relative numbers of giant and dwarf stars contributing in V and R light were rather sensitive criteria for choosing E and Sa to Sb sequences and ages. Further quantitative indications of spectral and luminosity classes of contributing stars, such as measurements of equivalent widths of lines, would clearly be very valuable.

AGE AND STELLAR BIRTHRATE

For sequences with $\rho = 0.9$ or 0.7 the changes in ρ are slow enough that agreement with observed properties is hardly altered from 10 to 100 Myr, except that only good sequences are compared with Wood's photometry.

TABLE 5

COMPARISON WITH WOOD'S PHOTOMETRY

Index	Computed Seq. E2	Wood's mean observed E & SO	O-C
C ₃₅ -C ₅₅	+2.45	+2.45	0.00
C ₄₁ -C ₅₅	+1.16	+1.16	0.00
C ₄₇ -C ₅₅	+0.44	+0.48	+0.04
C ₆₀ -C ₅₅	-0.20	-0.21	-0.01
C ₆₇ -C ₅₅	-0.38	-0.39	-0.01
C ₇₃ -C ₅₅	-0.57	-0.66	-0.09
L ₅₂	+0.10	+0.08	-0.02
L ₅₉	-0.09	-0.05	+0.04
L ₆₆	-0.04	-0.08	-0.04
L ₆₂	+0.05	+0.07	+0.02
L ₇₁	-0.07	0.00	+0.07

AGE AND STELLAR BIRTHRATE

For sequences with $e = .9$ or $.7$ the changes in time are slow enough that agreement with observed properties is hardly altered from 10 to 12×10^9 years, except that Sc3 (the only good sequence with $x=1.5$) is definitely too red after the twelfth time interval. In Sa to Sb and E sequences, the evolution of stars near one solar mass from the MS into the red giant region controls the light of the galaxy in bands U to R, and it is only after 12×10^9 years that there are enough red giants to agree with the observations listed in the last row of Table 3. At this age, the Sa to Sb and E sequences listed in Table 4 have both enough giants contributing in U, B, and V, and enough red dwarfs in R. At greater ages, there would be too many giants contributing in the R band. Thus there are sequences representing all the types considered, at 12×10^9 years after the start of Population I star formation.

None of the sequences studied passes through stages representing other galactic types in all properties. For example, the sequences finally giving E systems pass through B-V values of the other types but have always too large mass/light ratios for these types. While the calculations cannot prove that the sequence irregular-spiral-elliptical is not an evolutionary sequence, they show that all the principal galactic types may have originated at the same time, but with some differences in physical conditions that led to different

stellar birthrates.

The stellar birthrate laws also may be surprisingly uniform. Table 4 shows that it is possible to have all types of galaxies with the same age, x , and q , in two ways: age 12×10^9 years, and either $x=0.5$, $q=2$ or $x=1.0$, $q=0$. The first represents a differential stellar birthrate proportional to $m^{-1.5} dm$ with the value preferred by Schmidt (1963) for q , while the second represents a differential stellar birthrate proportional to $m^{-2} dm$ with a linear dependence on gas mass for all stars. When $q=2$ there are relatively fewer massive stars formed at later times, so consequently less gas, less enrichment with heavy elements, and less blue light. The massive stars are unimportant to E systems, so q makes little difference. It does not seem possible to obtain a good Sc to Sm galaxy with $q=2$: the sequence Sc1 is the worst of any listed in Table 4 for agreement with observed galaxies, having too large B-V and especially U-V to go with its other properties. Thus it seems necessary to reject Schmidt's conclusion, which was derived for the solar neighborhood only, and the most reasonable conclusion is that one should take q to be zero for all galactic types. Therefore, while other laws of star formation are not excluded, all the types of galaxies considered can be formed with a stellar birthrate proportional to the mass of gas present, and to the inverse square of star mass per unit mass. The respects in which the types of galaxies differ are the initial rate of gas consumption to

form stars and the relative number of stars formed less massive than $0.1 M_{\odot}$. The latter determines mainly the mass/light ratio and the far infrared luminosity of the final galaxy; a result equivalent to the large value of D for E systems was found by Page (1964).

TIME CHANGES IN GALAXIES

Some representative features of the history of each galactic type are shown in Figures 6(a) to (d), for the sequences with $x=1.0$, $q=0$. The data for E types are from the final detailed computations (for use in cosmology, Chapter IV), smoothed in time where necessary because the use of discrete star masses instead of a continuum resulted in some irregularities. The data for the other types are from detailed computations at times $10-12 \times 10^9$ years, but partly interpolated at earlier times for which not all the quantities were computed. In Figure 6(b), the luminosities are all for the arbitrarily chosen galactic mass $5 \times 10^{11} M_{\odot}$, but would vary in proportion to mass if this were different.

It can be seen from Figure 6(d) that changes in composition of the interstellar gas should not be neglected for Sc to Sm systems if an accurate account of their history is required. But for the purposes of comparing observed and final computed properties this change is not important, because the stars which contribute most light are formed early. For E systems, whose exact history is of interest

here, it should be safe to neglect the change. The rise and fall of Y+Z for sequence E4 is probably greatly exaggerated, being due to the gap between the lifetimes of stars with masses 1.5 and 1.25 (1.83 and 4.94×10^9 years). For Sa to Sb and Im systems, the change would alter the rate of evolution appreciably, as discussed in another context at the end of Chapter IV; but for the former only the stars formed early are important contributors at the end, and for the latter the evolution of the galaxy is slow enough that such changes would not critically affect the comparison with observed properties.

The absolute spectral energy distributions at different times, for sequence E2, are shown in Figure 7. A shift of the energy maximum towards longer wavelengths occurs, and a rapid early drop in luminosity; these are due mainly to the decreasing number of massive blue stars as the rate of star formation decreases, and to the increasing number of red giants. For comparison with the final computed galaxy, the energy distribution corresponding to Johnson's (1966a) mean colors for E galaxies is shown on an arbitrary scale.

Relations have been calculated and plotted in the form $\log cz$ versus $m_{\lambda} - M_{\lambda}$, where c is the redshift velocity, z is the increase in wavelength between emission and observation, c is the speed of light, m_{λ} is the observed apparent magnitude at effective wavelength λ , and M_{λ} is the absolute magnitude at λ at the present time. The ordinate, $\log cz$, is expressed

CHAPTER IV

MAGNITUDE-REDSHIFT RELATIONS

Magnitude-redshift relations ($m-z$) have been calculated for a variety of cosmological models, incorporating the changes in time found for giant elliptical galaxies. The relations are plotted in Figures 10 to 12 and tabulated in Appendix III.

The calculations have been made for the two sequences E2 and E4, chosen because they have values of parameters x and q which can be used to form irregular and spiral galaxies also. The differences in their histories, illustrated partly in Figure 6, show up in the $m-z$ relations and provide an estimate of the effect on these relations of uncertainties in the history of galaxies.

The present epoch has been taken as 12×10^9 years after the start of the galactic evolution sequences.

METHOD OF CALCULATION

Relations have been calculated and plotted in the form $\log cz$ versus $m_\lambda - M_{0\lambda}$, where z is the redshift (relative increase in wavelength between emission and observation), c is the speed of light, m_λ is the observed apparent magnitude at effective wavelength λ , and $M_{0\lambda}$ is the absolute magnitude at λ at the present time. The ordinate, $\log cz$, is convention-

ally used. The abscissa is independent of the absolute magnitude of the galaxy, and so independent of the mass chosen in the computations, and further differs from the conventional abscissa in not being altered by a 'K correction' to convert broad band magnitudes to a bolometric scale. Comparison with observation is therefore as direct as possible, the only corrections necessary being for Galactic absorption. Inter-galactic absorption is neglected.

The necessary equation has been expressed conveniently by Davidson (1959a). His equation (4.10) is used here, slightly simplified by replacing the observer's sensitivity function by a delta function at the effective wavelength λ :

$$m_{\lambda} - M_{\text{ol}} = 5 \log_{10} D - 5 + 2.5 \log_{10} (1+z) - 2.5 \log_{10} \left[\frac{E(\lambda/(1+z), t_0 - \tau)}{E(\lambda, t_0)} \right] \quad (6)$$

In equation (6), $E(\lambda, t)$ is the absolute monochromatic luminosity, measured in proper units at the source (ergs sec⁻¹ micron⁻¹), at wavelength λ and time t ; t_0 is the present time; τ is the light travel-time, so $t_0 - \tau$ is the time of emission; $\lambda/(1+z)$ is the wavelength at emission, if observed at λ ; and D is the luminosity distance ($=r_1 R_0 (1+z)$ in the notation of Sandage, 1961a). τ and D depend on the redshift, z , on the cosmological model, and on the value of Hubble's constant, H_0 , in such a way that $H_0 \tau$ and $H_0 D$ can be found as functions only of z for any model specified by two parameters besides H_0 . Further details are given in Appendix II. The last term in equation (6) clearly depends on evolution of the galaxy.

Values of $m_{\lambda} - M_{0\lambda}$ have been calculated for the effective wavelengths of the B, V, R, and I bands, at the redshifts which bring each of the shorter wavelengths up to the value observed. These values of redshift and wavelength are given in Table 6. The redshift at which U is shifted to the observed band is the greatest for which the present analysis can give information, and observations of stars and nearby galaxies further into the ultraviolet will be necessary to extend this. It is clear that observations of the $m-z$ relation at B (photographic) wavelength cannot be interpreted in detail beyond $z=0.22$.

TABLE 6
REDSHIFTS

Observed band	λ_{eff} (microns)	Emitted band			
		U	B	V	R
B	0.44	0.22			
V	0.55	0.53	0.25		
R	0.70	0.94	0.59	0.27	
I	0.90	1.50	1.05	0.64	0.29

The final term of equation (6) was evaluated by reading $E(\lambda, t)$ from graphs of E versus t (smoothed in time for reasons discussed in Chapter III), drawn for each sequence at the wavelengths of U to I bands. t_0 was taken to be

12×10^9 years after the start of the sequences, and values of $t_0 - \tau$ were first computed for all the cosmological models and values of z and H_0 considered. The computed sequences give $E(\lambda, t_0 - \tau)$ only for τ no greater than 11×10^9 years. Extrapolated values of $E(\lambda, t)$, marked '??' on the graphs, were used up to 12×10^9 years, but no attempt was made to guess the luminosities at earlier times. Because of the artificial starting point used for the sequences, luminosities for τ greater than 10×10^9 years are probably unreliable, and these are marked '?' on the graphs.

CHOICE OF COSMOLOGICAL MODELS TO STUDY

Several homogeneous, isotropic, pressure-free models of General Relativity have been considered, and the Steady State model for comparison (without, of course, any galactic evolution). The General Relativistic models can be specified by the values of three parameters, as has been shown by many authors, e.g. Robertson (1955). The parameters could be taken as Hubble's constant, H_0 , the age of the universe (time since the scale factor $R(t)$ was zero), t_0 , and the density parameter, σ_0 ($= 4\pi G \rho_0 / 3H_0^2$, where ρ_0 is the local mean density), which is a useful set since certain limits can be placed on all of these by observation.

For consistency in the present discussion, it is necessary that t_0 is greater than 12×10^9 years. A recent review by Abell (1965) gives limits for ρ_0 if H_0 is taken as

75 km sec⁻¹Mpc⁻¹, but all the observations are such that the derived density is proportional to H_0^2 , so the limits are actually on σ_0 , and show that probably $.015 \leq \sigma_0 \leq .5$. Estimates of H_0 vary widely (e.g. Sandage, 1962c), so three values have been considered: 75, 98, and 120 km sec⁻¹Mpc⁻¹.

To find cosmological models consistent with these limits, Figure 8 was constructed, $H_0 t_0$ versus $\log \sigma_0$. This is the most general form of Figure 3 of Robertson (1955), showing the positions of models in terms of the other two parameters when H_0 is specified. The limit $H_0 t_0 \geq .92$ shown corresponds to $t_0 \geq 12 \times 10^9$ years, $H_0 \geq 75$ km sec⁻¹Mpc⁻¹. It will be seen from Figure 8 that the model with $\Lambda=0$, $q_0 = \sigma_0=1.0$, regarded usually as giving best fit to the m-z relations (Sandage, 1961a, 1965), is both too young and too dense for the limits accepted above.

Representative models selected for study are shown on Figure 8, and their properties listed in Table 7. The cosmological constant Λ , the deceleration parameter q_0 , and curvature k are determined for any model with given σ_0 , H_0 , t_0 by well-known formulae given in Appendix II. In practice, except for models with $\Lambda=0$ and some other special cases, q_0 and σ_0 must be specified and $H_0 t_0$ computed by numerical integration. Column (7) of Table 7 gives z_m , the redshift at which the rate of expansion of the model, \dot{R}/R , passes through a minimum. For the Eddington-Lemaitre model, \dot{R}/R tends to zero as z tends to z_m , corresponding to the finite radius

($R_m = R_o / (1+z_m)$) from which the expansion begins at past infinity. Column (8) lists the values of H_o of those used which give the model an age greater than 12×10^9 years.

TABLE 7
COSMOLOGICAL MODELS

Model (1)	σ_o (2)	$H_o t_o$ (3)	$\frac{\Lambda c^2}{H_o^2}$ (4)	q_o (5)	k (6)	z_m (7)	H_o used (km sec ⁻¹ Mpc ⁻¹) (8)
1	.015	.953	0	.015	-1		75
2	.03	.927	0	.03	-1		75
3	.015	.921	-.375	.14	-1		75
4	.015	1.65	2.91	-.955	0	7.61	75, 98, 120
5	.18	.92	1.92	-.46	0	3.35	75
6 Eddington-Lemaitre	.018	∞	$\Lambda_c = 3.53$	-1.17	+1	3.00	75, 98, 120
7 Lemaitre	.05	1.44	3.15	-1.0	+1	1.76	75, 98
8 Lemaitre	.10	1.26	3.30	-1.0	+1	1.22	75, 98
9 Lemaitre	.25	1.35	5.13	-1.46	+1	.90	75, 98
10 Lemaitre	.50	1.63	7.50	-2.0	+1	.71	75, 98, 120

Figure 9 illustrates the past behaviour of the models, with the present epoch shown at $R/R_o = 1$, $\tau = 0$, $z = 0$. This method of plotting $R(t)$ shows clearly the redshifts to which observations must be made to show up differences between models. The models were chosen to give as wide a range of behaviour as possible within the limits on H_o , t_o ,

and σ_0 ; all types of models are illustrated by Bondi (1960). The only possible types here with $\Lambda=0$ are open, monotonic expanding models with $k=-1$; models 1 and 2 are the extreme cases. Model 3 with $\Lambda<0$, $k=-1$ is an oscillating model but its maximum radius is so far in the future that it is scarcely distinguishable from 1 or 2. The Eddington-Lemaitre model, 6, has a finite minimum radius in the past and corresponding maximum redshift, $z_m=3$. Eddington-Lemaitre models with z_m between .7 and 3.3 are allowed by the limits on σ_0 , although the lower values are ruled out if the redshifts of quasi-stellar objects are cosmological. Models 7 to 10 were chosen by testing a grid of models with σ_0 values from .015 to .5 and q_0 values from -3 to +1, to determine which σ_0 , q_0 gave Lemaitre models with $H_0 t_0 \geq .92$, then selecting four with interesting σ_0 or z_m . If z_m is less than the greatest redshift observed, τ may be very large and the effects of evolution of galaxies very important.

EXPLANATION OF FIGURES 10, 11, AND 12

Figures 10, 11, and 12 show the calculated $m-z$ relations, which are also tabulated in Appendix III. The upper portion of some figures is redrawn on a larger scale, to show more details.

1. At small enough redshifts, the effects of galactic evolution are negligible, and for all models equation (6) reduces to:

best straight line is $m_{\lambda} - M_{0\lambda} = 5 \log cz - 5 \log H_0 + 25$,
 if H_0 is in $\text{km sec}^{-1} \text{Mpc}^{-1}$, and c is in km sec^{-1} . This is the
 straight line to which all curves tend asymptotically at small
 z .

2. On all graphs, two cosmological models are shown without galactic evolution, i.e. with τ set to zero in equation (6). The upper curve is for the model $\Lambda=0$, $q_0 = \sigma_0 = 1.0$, which was regarded by Sandage (1961a, 1965) as giving the best fit to the observed relation in the V band. The $m-z$ relation here is not that tabulated by Sandage (1961a), since he included a 'K correction' to give a bolometric scale. The lower curve is for the Steady State model. At other wavelengths than V, the curves for these models provide a framework for comparison purposes on the graph, but neither is regarded as agreeing with observations.

3. In the V band, the clusters observed by Humason et al. (1956; hereafter referred to as HMS) are plotted. Magnitudes are means for the first, third, fifth, and tenth galaxies, with the authors' corrections for latitude but without their 'K correction'. This was included by HMS to bring their magnitudes to a bolometric scale, and was calculated from the energy distribution in local galaxies; subtracting their $K(z, t_0)_V$ from their \bar{V}_c restores the observed magnitude in the V band, corrected for latitude. The HMS clusters were placed on the horizontal scale of Figure 10 by first fitting to all their points, from $\log cz = 3.055$, the

best straight line of slope $\Delta m / \Delta \log cz = 5$ at small z . It is not known whether the galaxies observed by HMS were all ellipticals or SO, which would be necessary for a detailed comparison with the present calculations.

4. The graphs (a), labeled 'No Evolution', were obtained from equation (6) with τ set to zero and H_0 to 75 km sec⁻¹ Mpc⁻¹. In this case, H_0 appears only in the product $H_0 D$ for each model, so 'No Evolution' graphs for other values of H_0 could be obtained by shifting these curves to smaller magnitudes by 0.58 or 1.02 for $H_0 = 98$ or 120 km sec⁻¹ Mpc⁻¹, respectively. Values of $E(\lambda, t_0)$ for 'No Evolution' were taken from sequence E2 at 12×10^9 years, which is very similar to E4 at the same age.

5. Graphs for different models are not drawn separately if they lie too close together; similarly, sequence E4 is not shown separately if it is too close to E2. The limiting separation is about .05 magnitudes at given $\log cz$ in most figures, and about .02 magnitudes in the detailed portions of Figure 10.

6. No graph is drawn for the B band, because data were available only at $z=0.22$. Values of $m_B - M_{OB}$ are given in Table 8.

The effects are greatest if H_0 is smaller. This is because $H_0 z$ is a function of z only, for any value of H_0 . The smallest H_0 one sees furthest back into the past. If H_0 is 120 km sec⁻¹ Mpc⁻¹ evolution has striking effects on

TABLE 8

MAGNITUDE-REDSHIFT RELATION IN THE B BAND*

Model	No Evolution, $H_0=75$		$H_0=75$		$H_0=98$		$H_0=120$	
	Seq.E2	E4	E2	E4	E2	E4	E2	E4
1	41.46	41.52	41.09	41.08				
2	41.38	41.44	41.01	41.00				
3	41.37	41.43	41.01	41.00				
4	41.60	41.66	41.19	41.19	40.70	40.70	40.33	40.33
5	41.48	41.54	41.10	41.09				
6	41.70	41.76	41.28	41.27	40.79	40.78	40.41	40.41
7	41.60	41.66	41.19	41.19	40.71	40.70		
8	41.59	41.65	41.18	41.18	40.70	40.69		
9	41.69	41.75	41.27	41.26	40.78	40.77		
10	41.82	41.88	41.37	41.36	40.89	40.88	40.51	40.55
SS	41.61	41.67						

* Tabulated is $m_B - M_{OB}$ at $z=0.22$.

DISCUSSION OF MAGNITUDE-REDSHIFT RELATIONS

The effects of galactic evolution can be seen by comparing Figures (b), (c), and (d) with (a) for each filter band.

The effects are greatest if H_0 is smallest. This is because H_0 is a function of z only, for any model, so at smallest H_0 one sees furthest back into the past. Even if H_0 is $120 \text{ km sec}^{-1} \text{ Mpc}^{-1}$ evolution has striking effects beyond

about $z=.5$.

The most interesting fact brought to light by Figures 10 to 12 is that evolution of galaxies reduces the differences in $m-z$ relations between most models. This is because the models with fainter magnitudes at given redshift without evolution also have the greater light travel-time at given z , so the galaxies are seen at brighter absolute magnitude. The formulae for light travel-time and luminosity distance at small z , expressed as a power series to terms in z^2 , show this: if models are specified by the parameters H_0 , σ_0 , and q_0 , equations (A18) and (A20) in Appendix II reduce to:

$$H_0 \tau = z \left[1 - \frac{1}{2}(2+q_0)z + \dots \right] \quad (7)$$

$$H_0 D = cz \left[1 + \frac{1}{2}(1-q_0)z + \dots \right] \quad (8)$$

showing that models with small q_0 have both a large luminosity distance and a large light travel-time at given z . In many cases the curves for different models cross each other at redshifts between 0.3 and 1.0, reaching much brighter magnitudes than predicted without evolution.

It is remarkable that some models have an $m-z$ relation turning back to brighter magnitudes at large enough redshifts, because of the great increase in luminosity of the galaxies at early times, especially at short wavelengths, as shown in Figure 7. There is considerable uncertainty in the luminosity early in the computed history of the galaxies because of the artificial starting point chosen, but it is not likely that the computed values are so much in error as to

falsify the qualitative effects found. The rapid early drop in luminosity, especially at short wavelengths, seems well established since sequences not showing this phenomenon did not result in good final galaxies.

For the highest density model studied, 10, the magnitude becomes brighter with increasing redshift then fainter again, even without evolution. In this model, the 'equator' of the universe ($u = \frac{1}{2}\pi$, in notation of Appendix II) is reached at $z = .64$ but the minimum of \dot{R}/R is at $z = .71$; thus beyond the equator the geometrical focussing effect is not overcome by a rapid increase in redshift (as happens in most models), and the magnitudes of galaxies get brighter with increasing redshift until the 'opposite pole' of the universe ($u = \pi$) is reached.

The effect of present uncertainty in the evolution of galaxies may be judged by comparing the curves for sequences E2 and E4. At small redshifts ($z < .3$), the differences between sequences in most cases are less than those between models. This is not so for very similar models, which must be expected as there are any number of models between those studied in the acceptable region of Figure 8. However, at larger redshifts ($z > .5$), the effects of evolution bring the models closer together, and at earlier times the sequences are more different, so that most differences between models are obscured by uncertainties in galactic history.

and Brown Sandage (1965) has reported that the $m-z$ relation

observed in the V band agrees best with the curve for $\Lambda=0$, $q_0=+1$, if evolution is neglected, and that the dispersion at 19th magnitude is 0.8 magnitudes. This dispersion in observed magnitudes is as serious as the uncertainty in galactic history, in causing confusion between models at redshifts less than about 0.5. However, it also allows a solution to the problem that the $\Lambda=0$, $q_0=+1$ model appears too young and too dense: Figure 10 shows that with evolution none of the models studied are as much as 0.8 magnitudes away from the $q_0=+1$ curve out to $z=0.53$, and in many cases they cross to brighter magnitudes than that model. This is so for all three values of H_0 considered.

The important conclusion is that models which are consistent with present limiting estimates of the age and density of the universe, are in just as good agreement with the observed m_V - z relation as is the model with $\Lambda=0$, $q_0=+1$.

EFFECTS OF COMPOSITION OF GAS AND STARS

A source of uncertainty of which the effects are not indicated by the differences between sequences E2 and E4 is the choice of initial composition of the galaxies. Suppose a different composition, still suitable for Population I star models, had been chosen (e.g. $X=.67$, $Y=.30$, $Z=.03$, as used by Demarque and Larson, 1964). The following considerations, based on approximate homology relations, can be applied (Sears and Brownlee, 1965). The luminosities of all main sequence

stars would be changed and their times spent at equivalent stages of evolution, in such a way that $\int L dt \propto X$ at any stage, since this would give the same increase in core mass. The contribution to integrated bolometric luminosity from stars of given mass at a given stage of evolution is proportional to the luminosity \times number of stars, or to luminosity \times time at the stage, which is therefore proportional to X for hydrogen burning stars.

Such a composition change would also affect $\log T_e$, and hence bolometric corrections and colors of the stars: BC changes steeply with $\log T_e$ for the earliest stars ($\log T_e > 4.0$) and the latest ($\log T_e < 3.65$), U-V changes steeply for $\log T_e$ between 3.6 and 3.8, B-V changes quite slowly, and V-R to V-L change steeply for $\log T_e < 3.8$. For the giant stars taken from observed clusters, there would be no color changes, the BC changes would be small, and the times would be adjusted so that the contributions would be proportional to X . In computed final E galaxies, the BC and colors of the important MS stars with $\log T_e$ between 3.7 and 3.8 would be changed. If the different composition mentioned above were used, for example, $\log T_e$ would be reduced by about 0.01 for MS stars with masses near 1.0. The BC changes would be small, but colors U-V to V-L would be increased by .05 to .01, the greatest changes being in U-V and the far infrared. The whole galaxy would therefore be redder by a few hundredths of a magnitude in all colors. Since $\log T_e$ is sensitive to Z , a small reduction in

the assumed initial metal content of the gas would make the computed galaxies bluer.

These changes would probably not be great enough to change the stellar birthrate parameters found to give good galaxies. At early times in E sequences, and at all times for Im sequences, there may be noticeable changes in the colors and BC of massive stars. These are not likely to affect the choice of Im sequences, but may change somewhat the values of $E(\lambda, t)$ seen at large redshifts in E galaxies. However, it seems most unlikely that any different choice of initial composition, within the range assigned to Population I stars, could alter the m-z relations computed in this chapter to such an extent that the qualitative conclusions would have to be revised.

The same considerations apply to neglecting changes in time of the gas composition, though as discussed in Chapter III the change and its effects are probably very small for E sequences.

For cosmology, the most important effect of initial composition is on the time scale of galactic evolution. Changes in main sequence luminosity are rather small, so the time for a star of given mass to evolve to the red giant region is approximately proportional to X . Therefore the colors, mass/light ratio, and contributing star types found at 12×10^9 years with $X=.708$ would be approximately reproduced for a different X (but same stellar birthrate parameters) at

time $12(X/.708) \times 10^9$ years. It would not be possible to reproduce all the observable properties of galaxies at 12×10^9 years with a different X by changing the stellar birthrate parameters. To a first approximation, one could say the time scale of evolution of an E galaxy is proportional to X . But the time scales in cosmology are all proportional to H_0^{-1} for a given model. Thus nearly equivalent $m-z$ relations would be obtained with a slightly different initial composition if the product XH_0 were the same. For example, if $X = .65$, the final galaxy ages would be 11×10^9 years and the values of H_0 giving the same $m-z$ relations as 75, 98, 120 would be 82, 107, 131 $\text{km sec}^{-1}\text{Mpc}^{-1}$, respectively.

THE POSSIBILITY OF CHOOSING BETWEEN COSMOLOGICAL MODELS

The present calculations show that there may be cosmological models among the homogeneous, isotropic, pressure-free models of General Relativity which are consistent with the observed magnitude-redshift relation, with estimates of the minimum age of the universe based on stellar evolution theory, and with empirical limits on the mean density of matter.

The problem of choosing between such models now appears harder than was previously thought, because the effects of galactic evolution bring their $m-z$ relations closer together. It will be necessary both to reduce the scatter in observation by somehow selecting galaxies as nearly as

possible equivalent to each other (in the sense of being the same at the same local epoch), and to reduce the uncertainty left by the present calculations of evolution. Also it is clear that the distance scale must be well known, because Hubble's constant also provides the time scale.

To construct a detailed color-redshift relation (C-z), it would be necessary to subtract values of $m_B - m_V$ given by two graphs at each z value. This would be inaccurate because the graphs (Figures 10 to 12) are drawn through only two to four points and an asymptote and there is only one point and an asymptote for the S band, so it was decided not to attempt this.

However, C-z relations for very small z can be found, and B-V at z=0.22.

B-V at z=0.22. This can be found from the calculated $m_B - m_V$ given in Table 8, and from the graphs of $m_B - m_V$ (Figure 10), read at z=0.22. Uncertainties due to drawing the V graphs are a few hundredths of a magnitude, but more importantly the comparison between models and sequences is accurate to the nearest hundredth. Table 9 gives the color change,

$$(B-V) - (B-V)_0 = (m_B - m_{B0}) - (m_V - m_{V0}) \quad (8)$$

where $(B-V)_0$ is the color at 12×10^9 years. Sequences S1 and S4 are compared, and the effects of evolution shown by comparison of column (2) with the color changes for 10000000000

values of H_0 . Column (2) is calculated for sequences at
(which is very like E4 at 12×10^9 years) and is determined
of H_0 , since no past time is known and the distance modulus
cancel in equation (7).

CHAPTER V

OTHER OBSERVATIONAL COSMOLOGY

COLOR-REDSHIFT RELATIONS

To construct a detailed color-redshift relation (C-z), it would be necessary to subtract values of $m_{\lambda} - M_{0\lambda}$ given by two graphs at each z value. This would be inaccurate because the graphs (Figures 10 to 12) are drawn through only two to four points and an asymptote (and there is only one point and an asymptote for the B band), so it was decided not to attempt this.

However, C-z relations for very small z can be found, and B-V at $z=0.22$.

B-V at $z=0.22$. This can be found from the calculated $m_B - M_{0B}$, given in Table 8, and from the graphs of $m_V - M_{0V}$ (Figure 10), read at $z=0.22$. Uncertainties due to drawing the V graphs are a few hundredths of a magnitude, but more importantly the comparison between models and sequences is accurate to the nearest hundredth. Table 9 gives the color change,

$$(B-V)_0 - (B-V)_{12} = (m_B - M_{0B})_{12} - (m_V - M_{0V})_{12} \quad (9)$$

where $(B-V)_0$ is the color at 12×10^9 years. Sequences E2 and E4 are compared, and the effects of evolution shown by comparison of column (2) with the color changes for different

values of H_0 . Column (2) is calculated for sequence E2 (which is very like E4 at 12×10^9 years) and is independent of H_0 , since no past time is involved and the distance effects cancel in equation (9).

TABLE 9
CHANGE IN COLOR B-V AT REDSHIFT 0.22

Model (1)	No Evolution Sequence E2 (2)	$H_0=75$		$H_0=98$		$H_0=120$	
		E2	E4	E2	E4	E2	E4
		(3)		(4)		(5)	
1	1.09	.84	.81				
2	1.03	.80	.77				
3	1.02	.81	.78				
4	1.05	.85	.82	.88	.84	.95	.91
5	1.08	.81	.77				
6	1.08	.85	.81	.89	.85	.96	.92
7	1.02	.84	.81	.88	.84		
8	1.04	.84	.81	.87	.83		
9	1.04	.83	.80	.87	.83		
10	1.07	.77	.72	.79	.75	.92	.93

At any H_0 , the differences between models are mostly obscured by the differences between sequences, but they all differ significantly from the values with no evolution.

The differences between models (or sequences) are also comparable to the observational scatter or error, so both theoretical and observational uncertainties make it unlikely that models could be distinguished by using the C-z relation out to $z=0.22$. Even if the differences were much greater at larger z , interpretation would be difficult because in the observer's B band the wavelength at emission would be shortward of U.

Linear C-z relations have been observed out to $z=.013$ by de Vaucouleurs (1961), to $z=0.13$ by Stebbins and Whitford (1948), and to $z=0.008$ by Holmberg (1958). A weighted mean of these observations (de Vaucouleurs, 1966) would give, on extrapolation to $z=0.22$, the color change $(B-V) - (B-V)_0 = .79 \pm .07$. This agrees well with the calculations based on evolving galaxies, but not if evolution is neglected.

B-V and U-V at $z \ll 1$. Observations out to $z=0.013$ give linear relations between color change and velocity (de Vaucouleurs, 1961) equivalent to the C-z relations:

$$(B-V) - (B-V)_0 = 3.6 z (\pm 0.6 \text{ p.e. in coefficient})$$

$$(U-V) - (U-V)_0 = 7.2 z (\pm 2.2 \text{ p.e. in coefficient}).$$

Theoretical relations to first order in z can be found using the formulae given by Davidson (1959a). His equation (6.5) was used in the following form for the change in B-V, with a similar equation for U-V:

$$(B-V) - (B-V)_0 = 1.086 z \left\{ \left[\frac{\partial \log E(\lambda, t_0)}{\partial \log \lambda} \right]_{\lambda_B} - \left[\frac{\partial \log E(\lambda, t_0)}{\partial \log \lambda} \right]_{\lambda_V} + 2.30H_0^{-1} \left[\frac{\partial \log E(\lambda_B, t)}{\partial t} - \frac{\partial \log E(\lambda_V, t)}{\partial t} \right]_{t_0} \right\} \quad (10)$$

Graphs of $\log E(\lambda, t)$, versus t for λ_U , λ_B , λ_V and versus $\log \lambda$ at 12×10^9 years, were drawn for sequences E2 and E4, and their gradients used to evaluate the terms in equation (10). If evolution is neglected, the last two terms are set equal to zero. The uncertainty in evaluating the first two terms is great because of the difficulty of drawing correct slopes on the graph of $\log E(\lambda, t_0)$ versus $\log \lambda$, with data only at λ_U , λ_B , λ_V and longer wavelengths. The coefficients of z found from equation (10) are given in Table 10, with their estimated uncertainties, and compared with the observed coefficients.

Because of the large uncertainty in calculated values and large p.e. in observed values, both sequences are regarded as giving coefficients consistent with observation and the effects of evolution as not making a significant difference. The light travel-time at $z=0.013$ is approximately $0.013H_0^{-1}$ in all models, which is only 1.7, 1.3, or 1.1 $\times 10^8$ years if H_0 is 75, 98, or 120 $\text{km sec}^{-1} \text{Mpc}^{-1}$, respectively.

TABLE 10

COEFFICIENTS IN LINEAR COLOR-REDSHIFT RELATIONS

Sequence	Coefficient in (B-V,z)		Coefficient in (U-V,z)	
	With Evolution	Without	With Evolution	Without
E2	$2.32 \pm .5$	$2.34 \pm .5$	$5.4 \pm .2$	$6.5 \pm .2$
E4	$3.7 \pm .5$	$3.5 \pm .5$	$5.9 \pm .2$	$7.1 \pm .2$
Observed	$3.6 \pm .6$ (p.e.)		7.2 ± 2.2 (p.e.)	

INTEGRATED BACKGROUND RADIATION FROM DISTANT GALAXIES

The integrated background radiation from distant galaxies is usually estimated with the assumption that the luminosity and energy distribution of galaxies were the same in the past as observed locally. If accurate estimates were to be made, one would need data on the luminosities of galaxies at times more than 12×10^9 years ago and at wavelengths shorter than that of the U band, which are not available. However, the present calculations show clearly that if galactic evolution is neglected, the background radiation at optical wavelengths must be severely underestimated. For example, if the U band is redshifted into the observer's band with a light travel-time of 11×10^9 years, each giant elliptical galaxy at that distance contributes over 100 times as much light as would its present equivalent, according to any of the E sequences listed in Table 4.

NUMBER-FLUX DENSITY RELATION FOR RADIO SOURCES

The interpretation of radio source counts may be simplified on the basis of the results in Chapter IV.

A recent compilation of observations by Véron (1965) shows that the slope of $\log N$ versus $\log S$ is $-1.55 \pm .05$ for radio galaxies (all $z < .5$), $-2.2 \pm .2$ for quasistellar sources. Here N is the number of sources with monochromatic flux density brighter than S . It follows from equations (A22) - (A24) in Appendix II that for all General Relativistic models the slope is less negative than -1.50 at small z , if there is no source evolution. It is well known that the same is true for the Steady State model, as is seen, for example, in the graphs drawn by Glanfield (1966). Analyses such as those by Longair (1966), Davidson (1959b; 1962a and b), or Davidson and Davies (1964a and b) show that with source evolution, but not otherwise, the observed N-S relation can be reproduced using the cosmological model with $\Lambda = 0$, $q_0 \sim .5$ that must be postulated to give agreement with the optical m-z relation if galactic evolution is neglected. It is somewhat unsatisfactory that the evolution of the radio sources must be specified to force agreement with the N-S data, rather than being based on physical theory, but no such theory is available yet for radio galaxies or QSS.

However, at large enough redshifts, some of the models found in Chapter IV to give agreement with the optical m-z relation do have a $\log N$ - $\log S$ curve with a slope more

negative than -1.5 , without source evolution. The effect can be seen in calculations for similar models presented by Glanfield (1966): his Figure 4 shows that $|d \log N/d \log S|$ is less than 1.5 for models with $\Lambda=0$, q_0 from $.005$ to 5 ; but in his Figures 5 and 6 it can be seen that for models with high enough Λ , the slope becomes very steep at small flux densities. For example, for two of the models listed in Table 7, equation (A22) in Appendix II gives the following slopes (the spectral index being taken as $.7$): For model 10, at $z=.64$ ($r_1=1$), $d \log N/d \log S = -4.4$. For model 6, at $z=1.50$, $d \log N/d \log S = -1.20$; but at $z=2.24$ ($r_1=1$), $d \log N/d \log S = -1.97$.

No more detailed calculations with these models have been made here, because they would not differ greatly from Glanfield's, and because a theory of source evolution is definitely required. The above numbers, and Glanfield's graphs, show clearly that the observed N-S relation does not necessarily imply rapid source evolution, once the models with great enough cosmological constant are accepted as compatible with the optical observations.

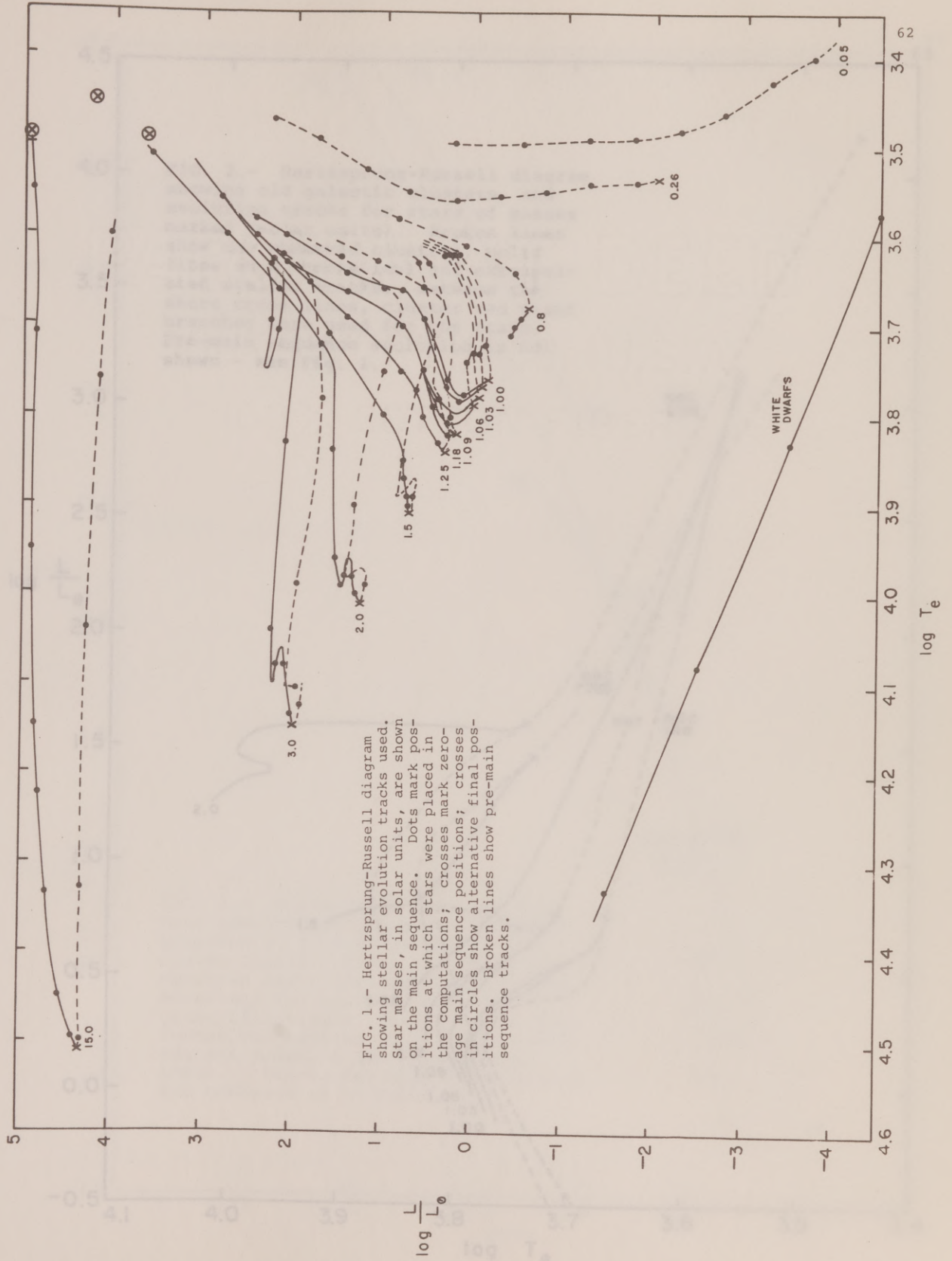
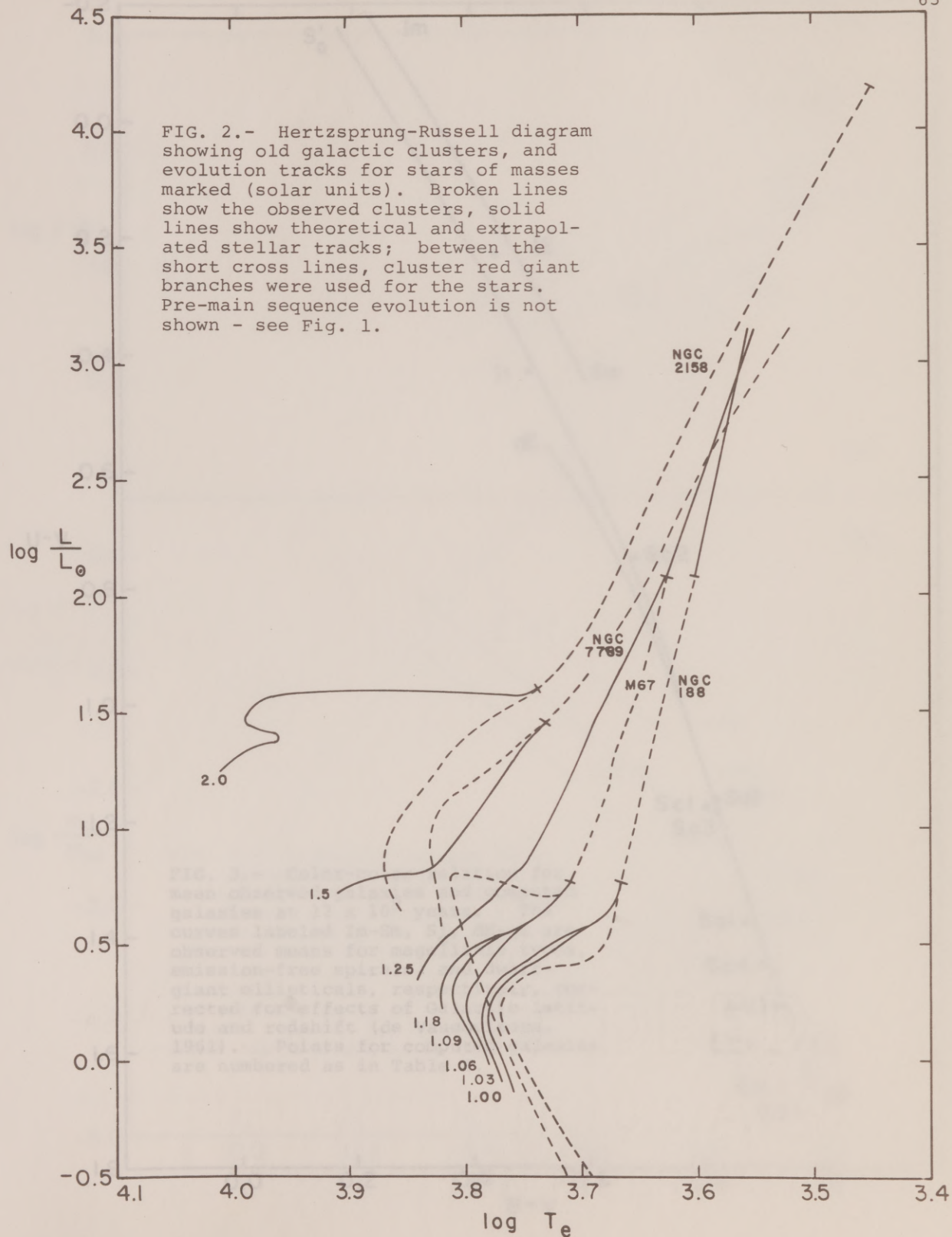
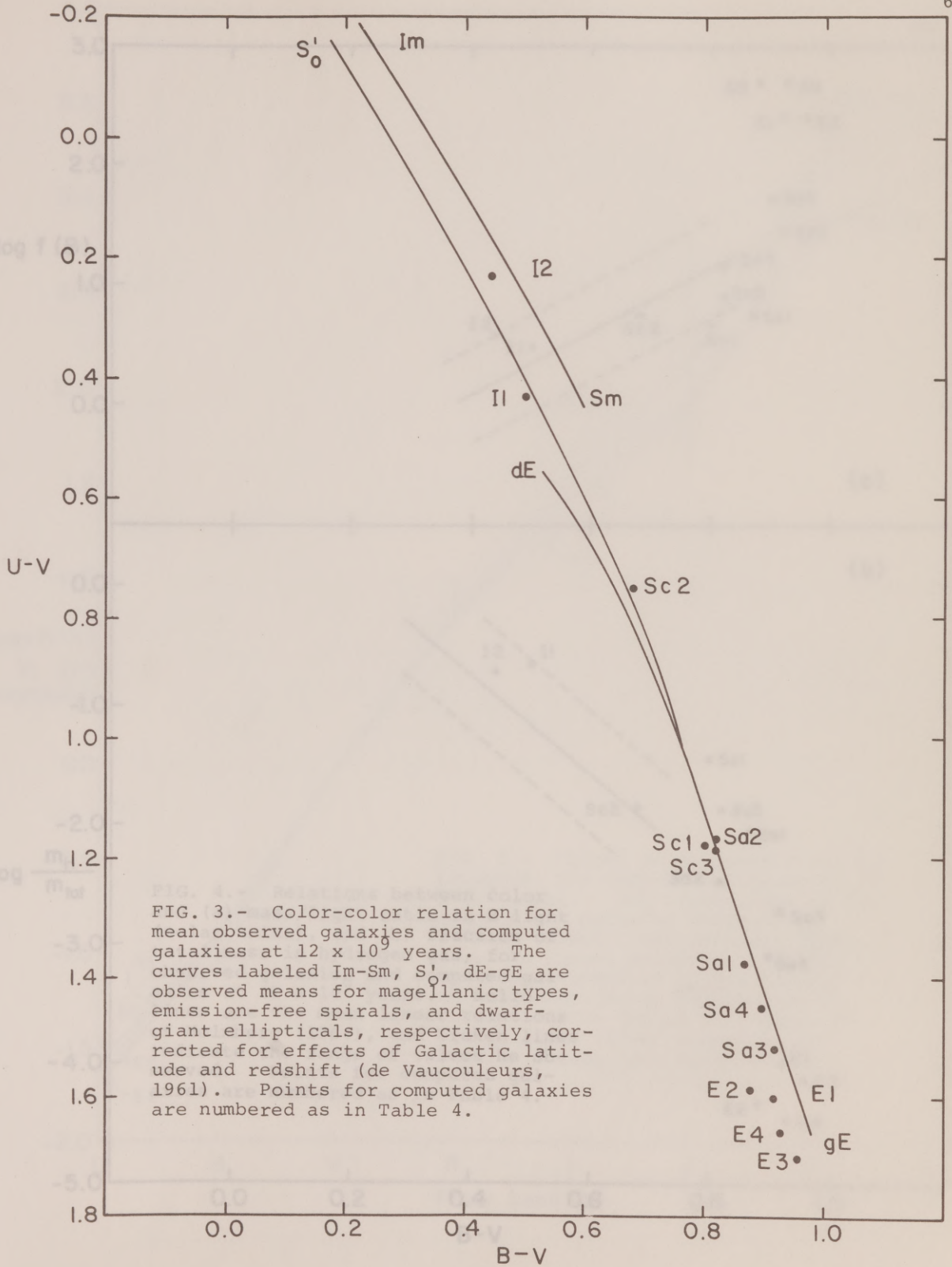


FIG. 1.- Hertzsprung-Russell diagram showing stellar evolution tracks used. Star masses, in solar units, are shown on the main sequence. Dots mark positions at which stars were placed in the computations; crosses mark zero-age main sequence positions; crosses in circles show alternative final positions. Broken lines show pre-main sequence tracks.





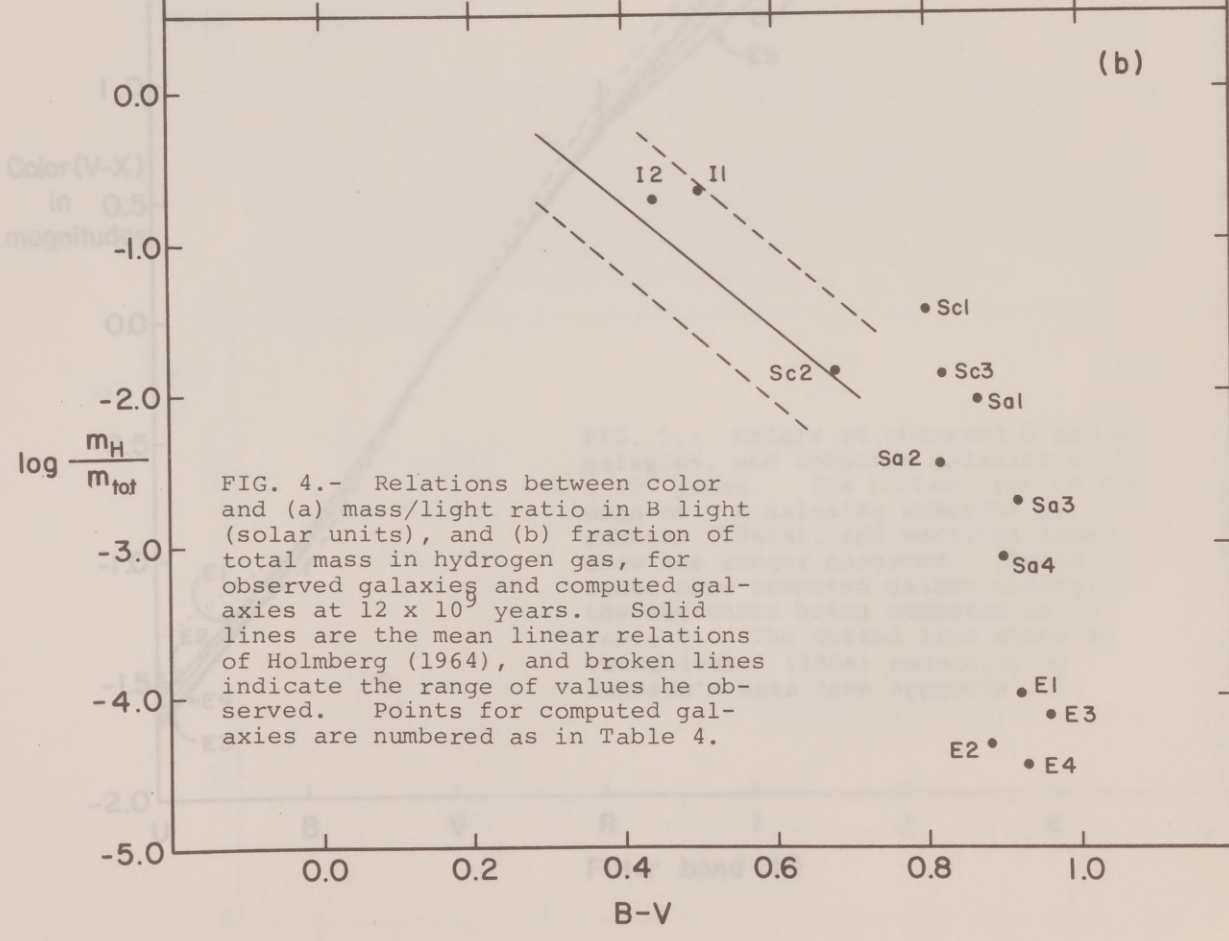
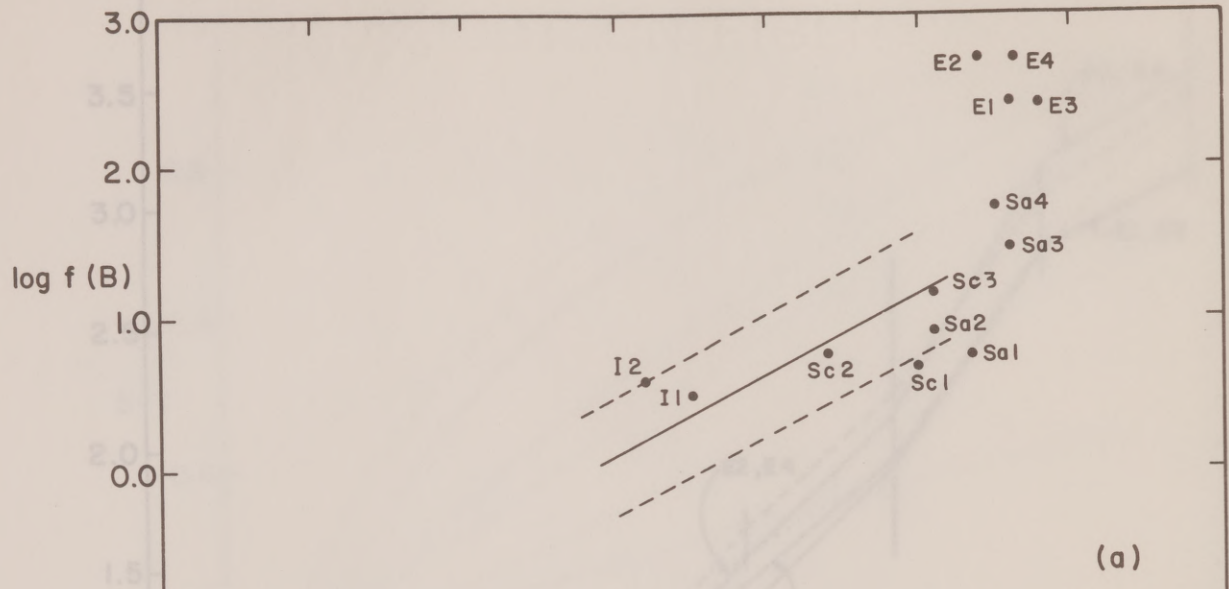


FIG. 4.- Relations between color and (a) mass/light ratio in B light (solar units), and (b) fraction of total mass in hydrogen gas, for observed galaxies and computed galaxies at 12×10^9 years. Solid lines are the mean linear relations of Holmberg (1964), and broken lines indicate the range of values he observed. Points for computed galaxies are numbered as in Table 4.

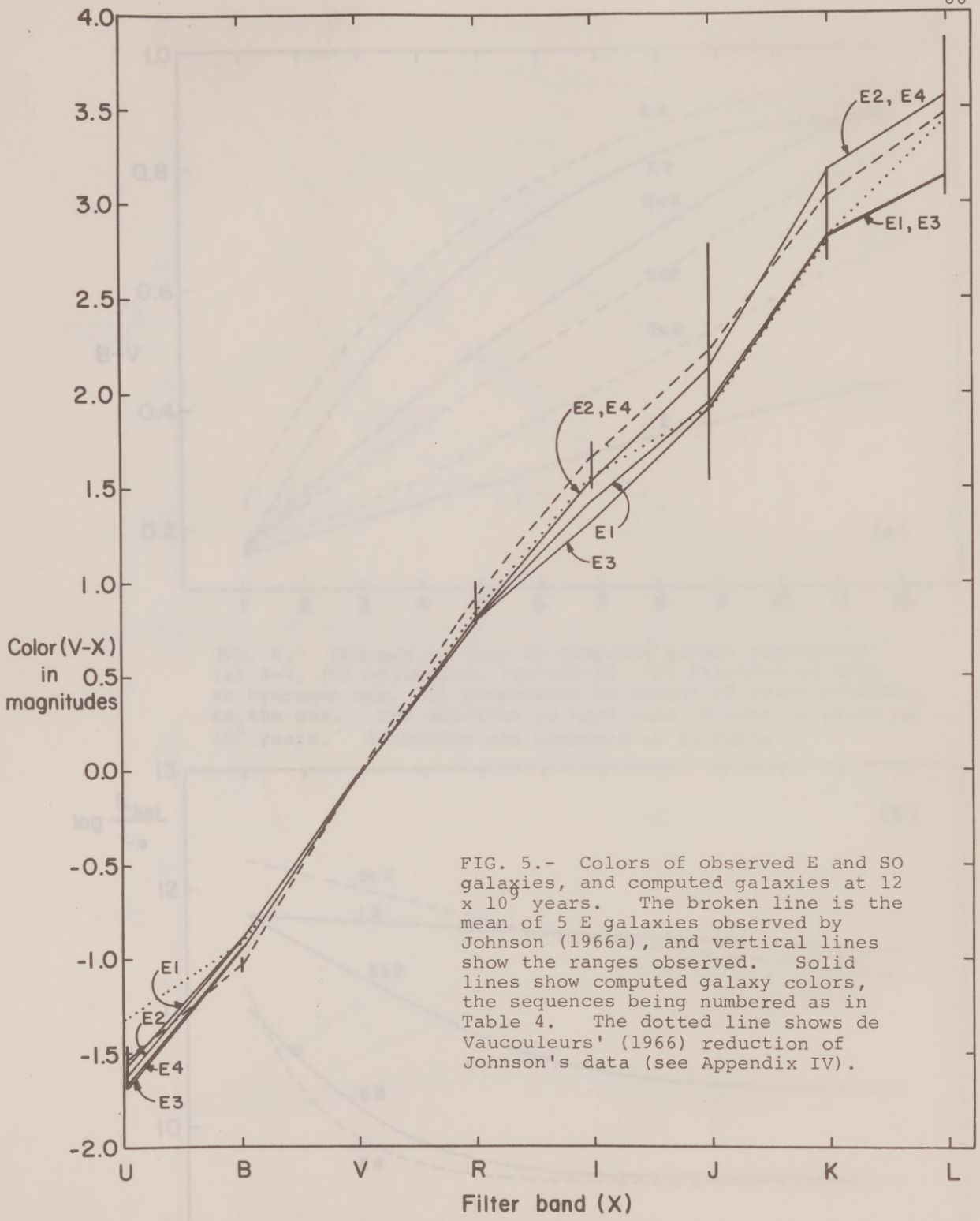


FIG. 5.- Colors of observed E and SO galaxies, and computed galaxies at 12×10^{10} years. The broken line is the mean of 5 E galaxies observed by Johnson (1966a), and vertical lines show the ranges observed. Solid lines show computed galaxy colors, the sequences being numbered as in Table 4. The dotted line shows de Vaucouleurs' (1966) reduction of Johnson's data (see Appendix IV).

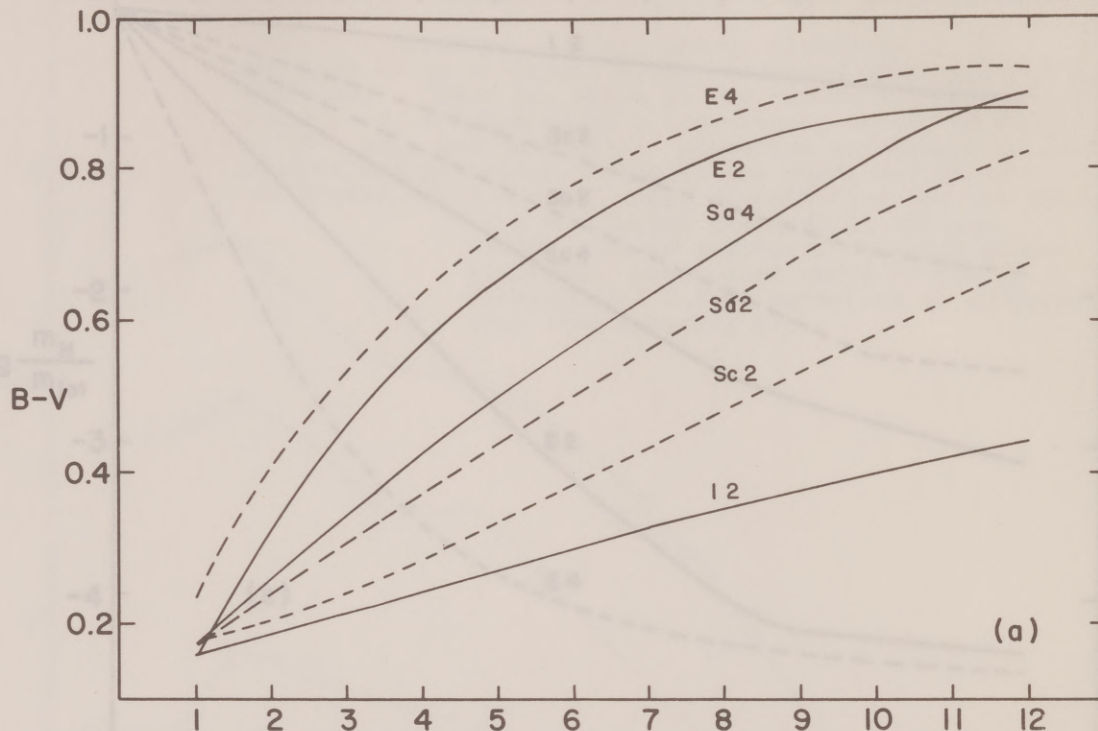
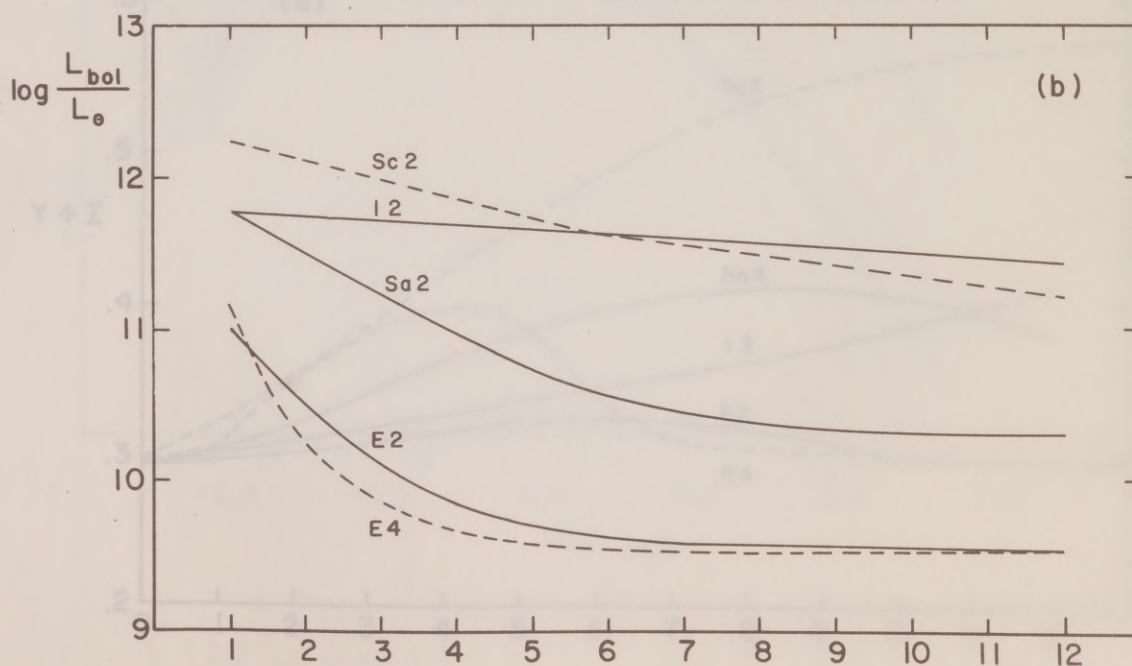
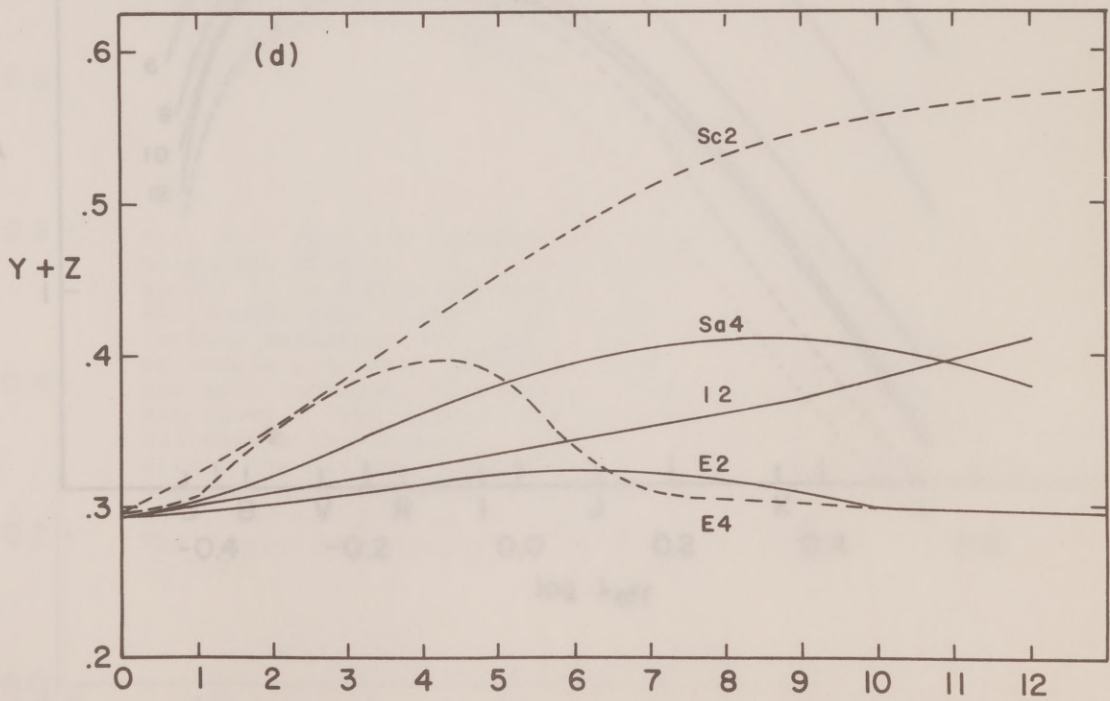
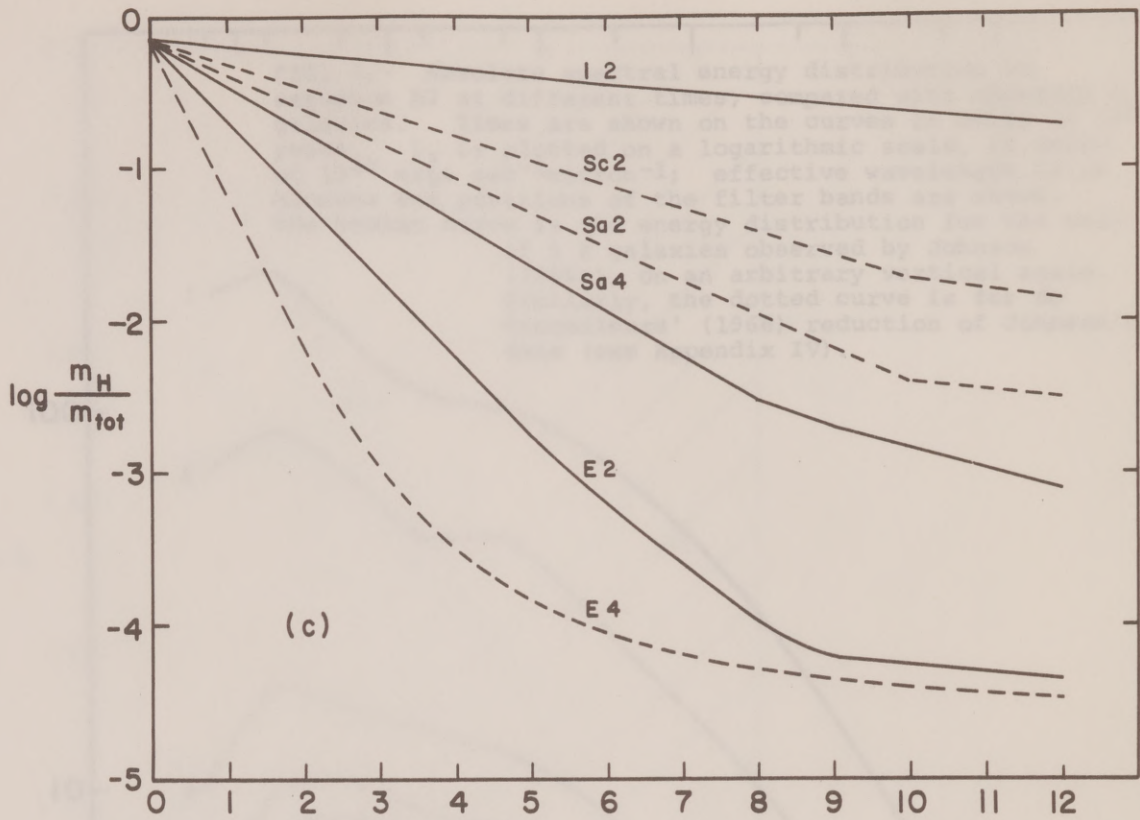
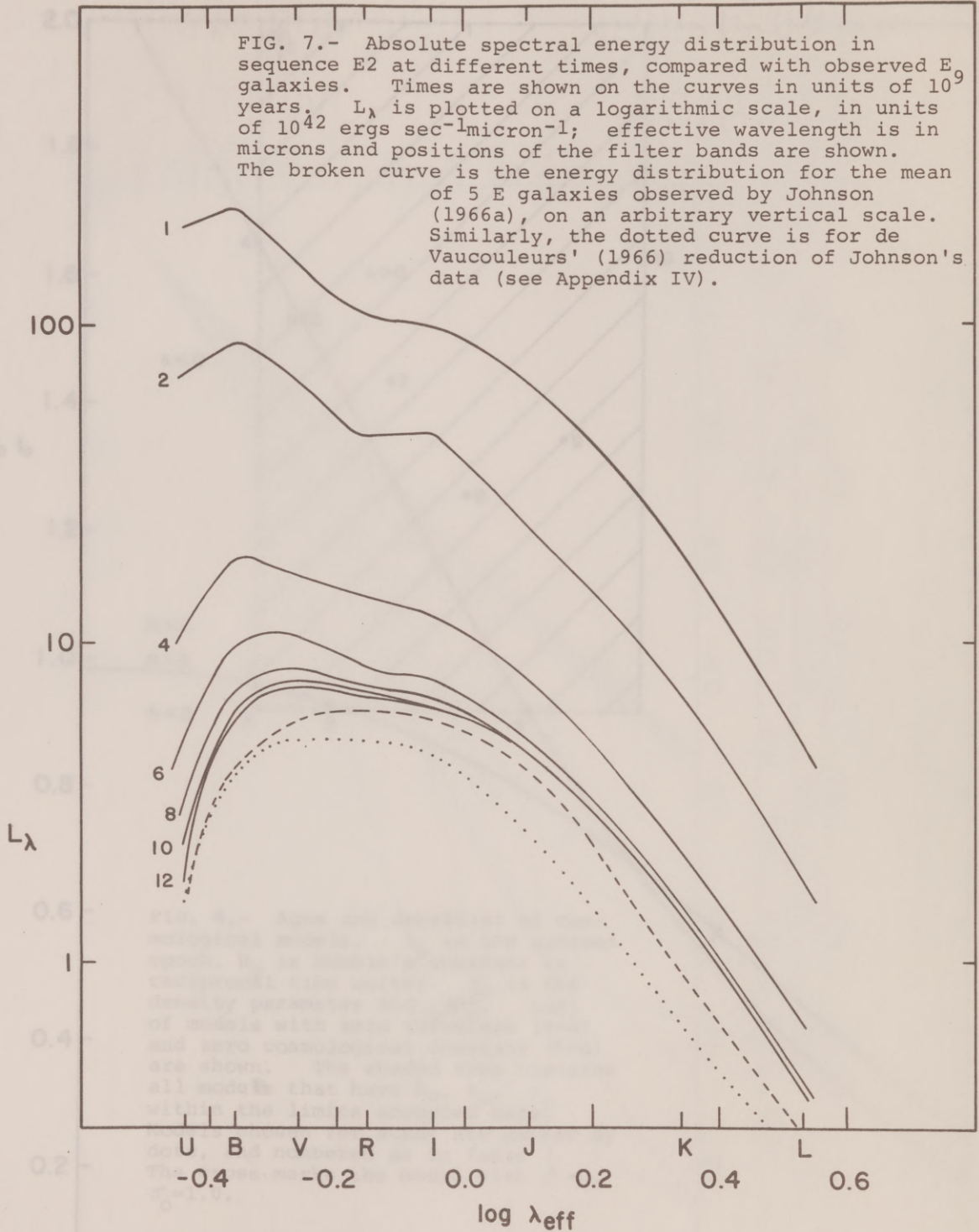


FIG. 6.- Changes in time of computed galaxy properties: (a) B-V, (b) bolometric luminosity, (c) fraction of mass as hydrogen gas, (d) proportion by weight of heavy elements in the gas. The abscissa in each case is time in units of 10^9 years. Sequences are numbered as in Table 4.







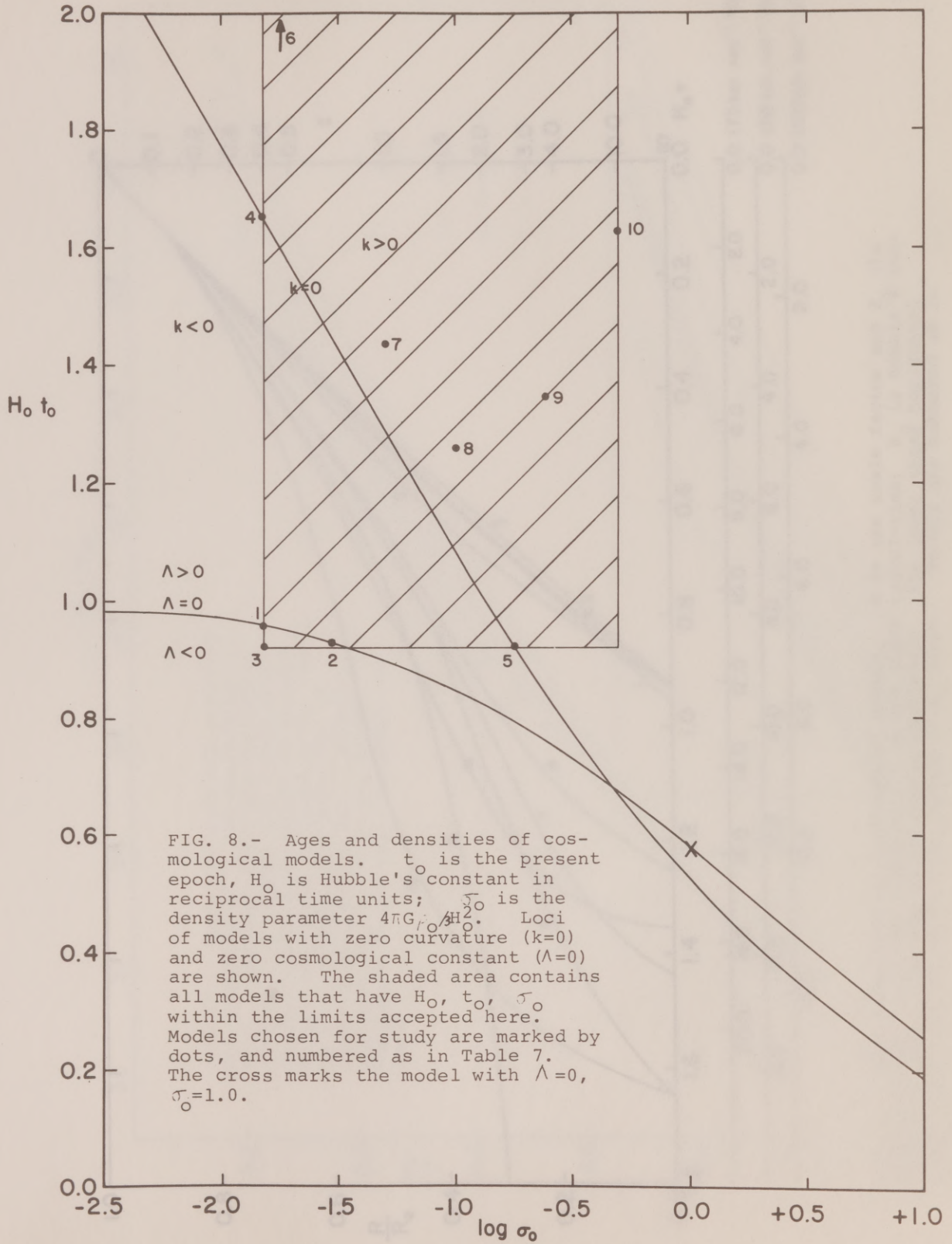


FIG. 8.- Ages and densities of cosmological models. t_0 is the present epoch, H_0 is Hubble's constant in reciprocal time units; σ_0 is the density parameter $4\pi G_0 \rho_0 / 3H_0^2$. Loci of models with zero curvature ($k=0$) and zero cosmological constant ($\Lambda=0$) are shown. The shaded area contains all models that have H_0 , t_0 , σ_0 within the limits accepted here. Models chosen for study are marked by dots, and numbered as in Table 7. The cross marks the model with $\Lambda=0$, $\sigma_0=1.0$.

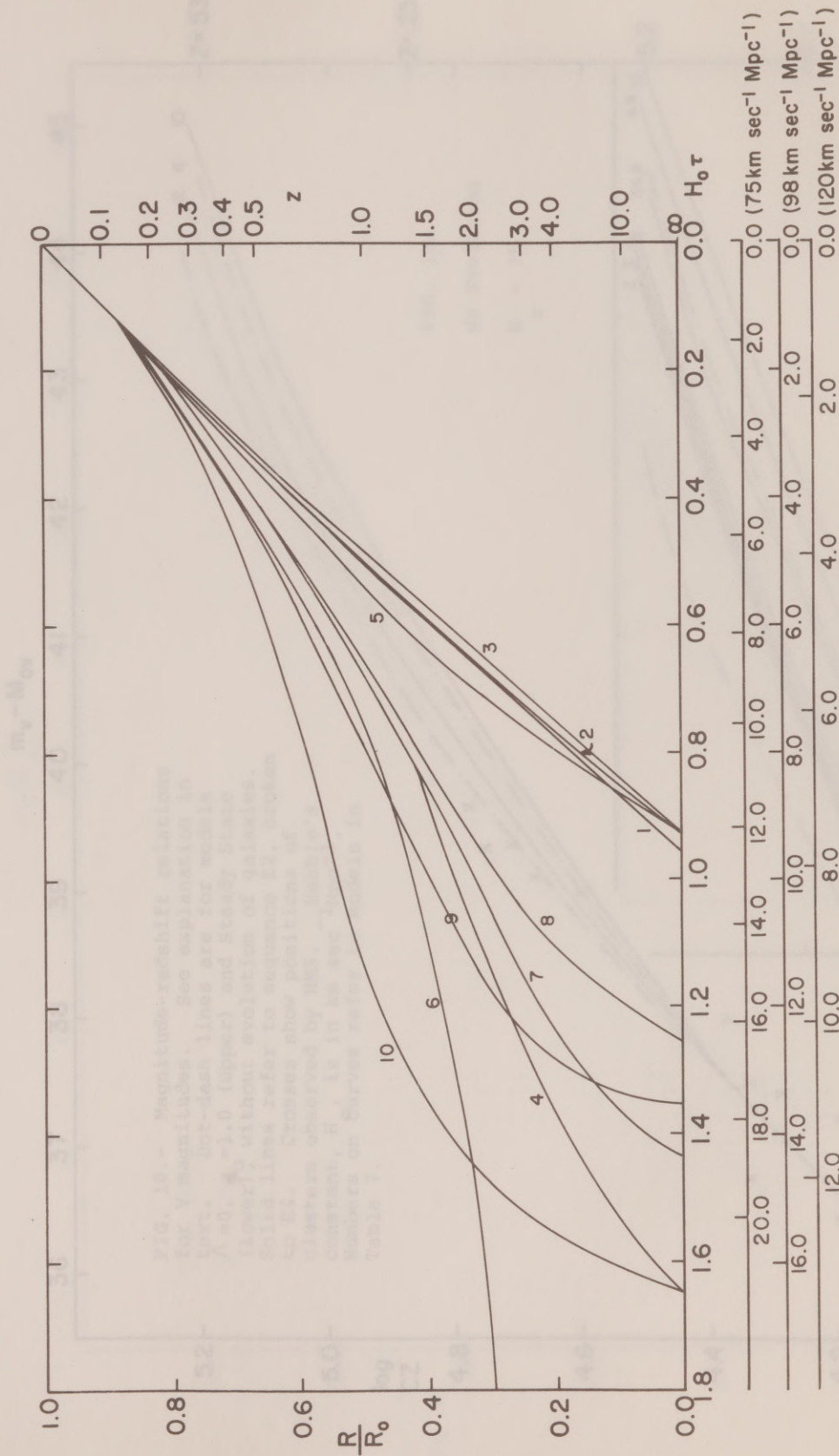


FIG. 9.- Past behaviour of cosmological models. R is the scale factor and R_0 its present value; z is the redshift; τ is the light travel-time; H_0 is Hubble's constant, in reciprocal time units unless specified. The lower three horizontal scales give τ in 10⁹ years, for values of H_0 shown. Models are numbered as in Table 7.

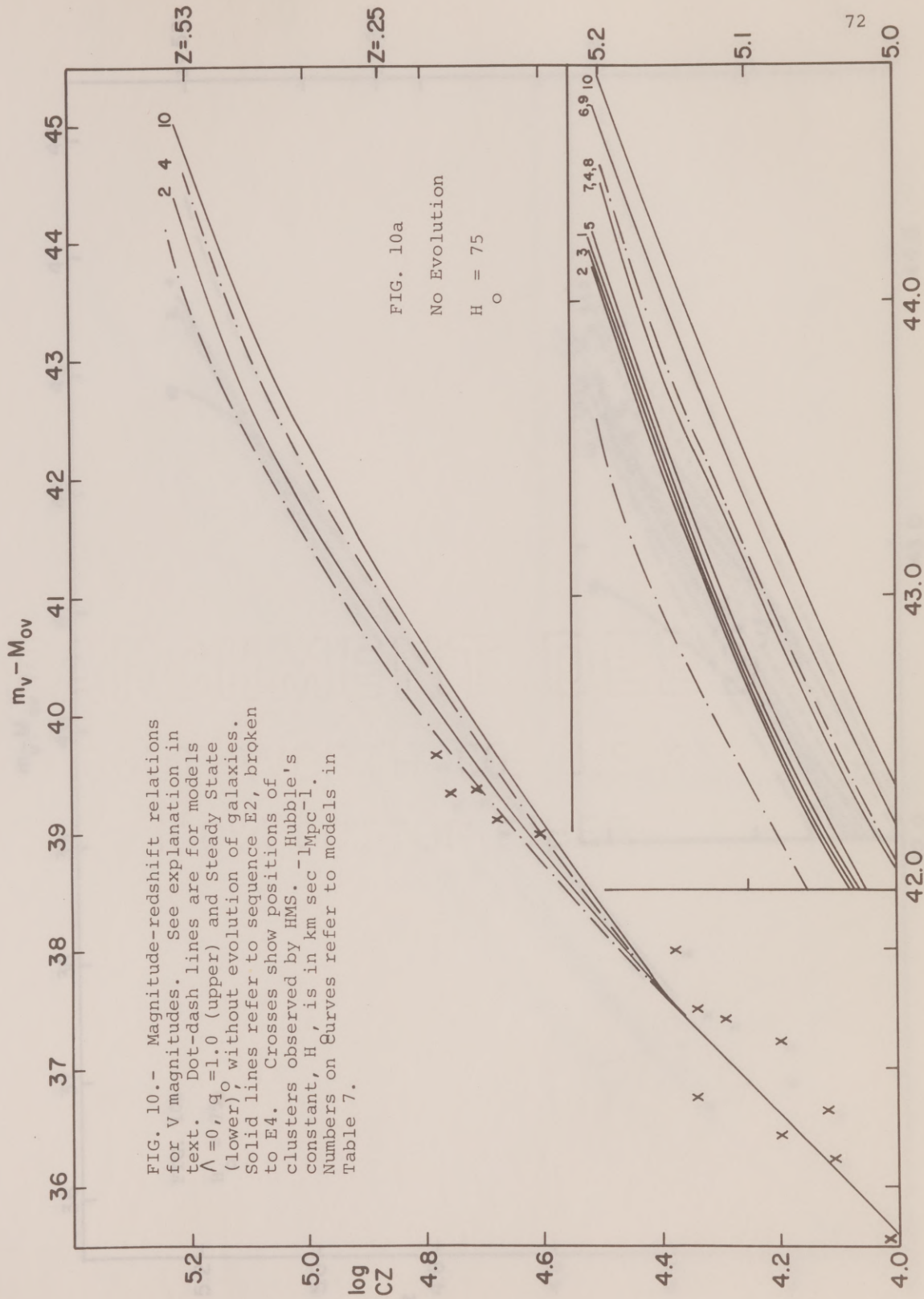
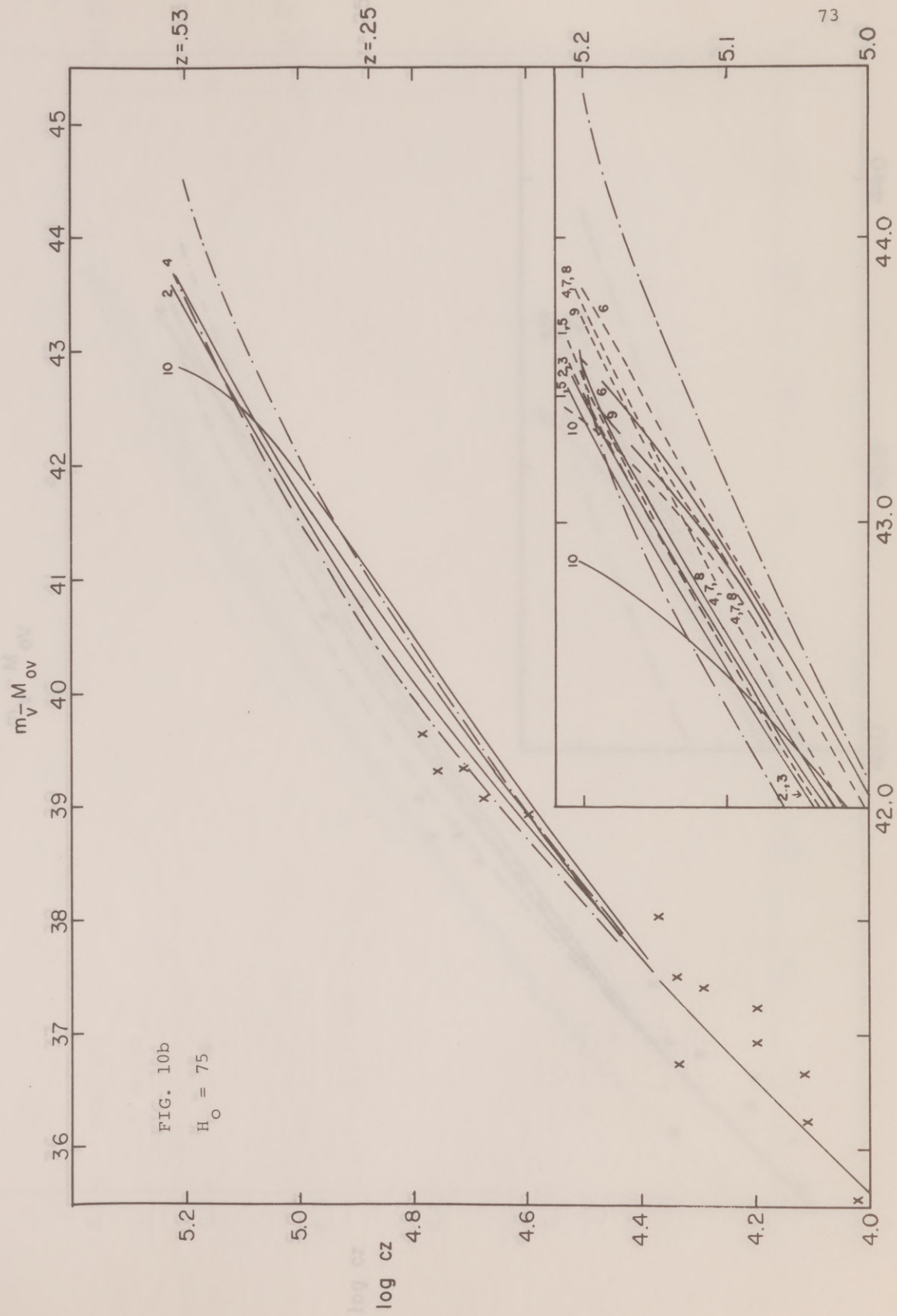
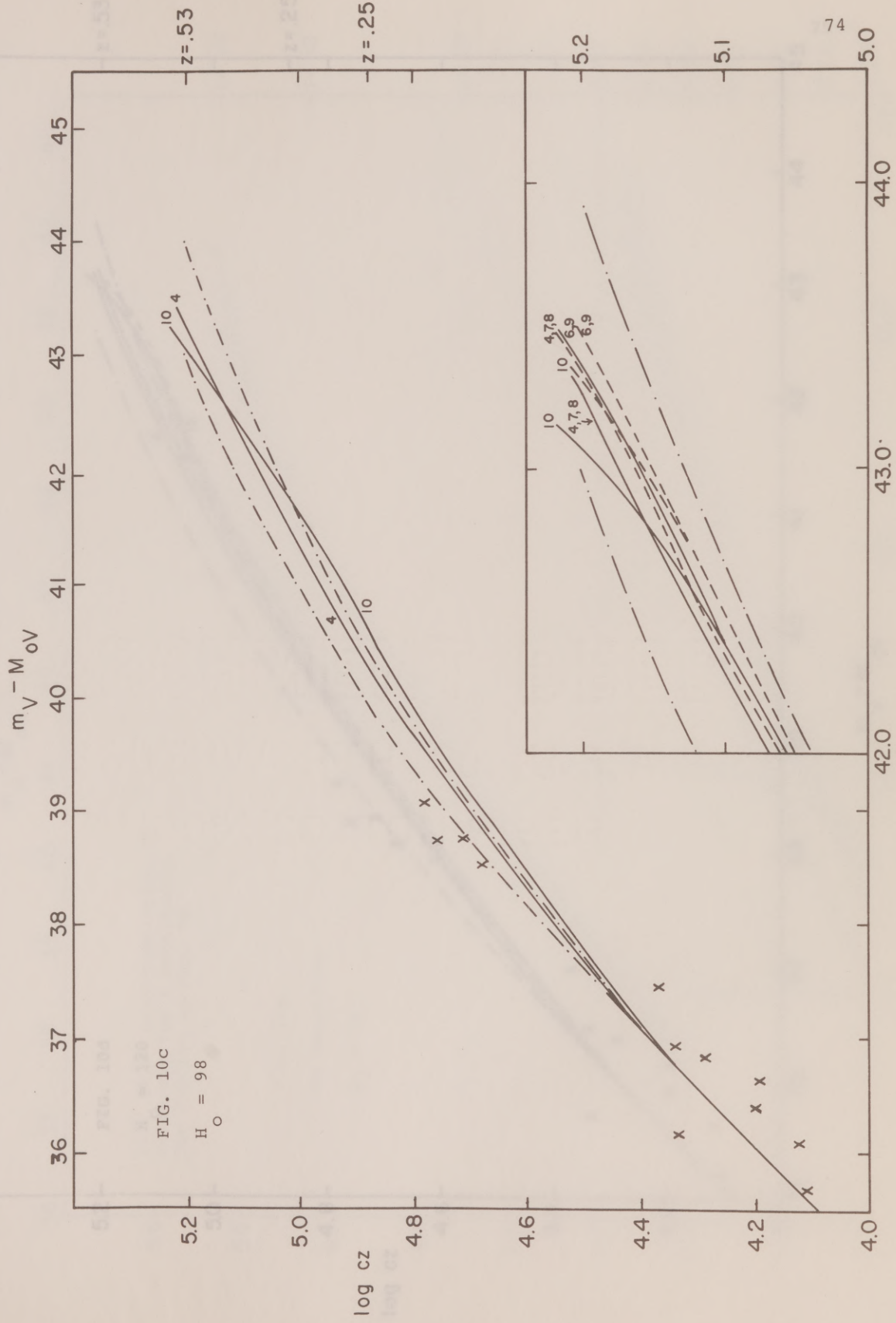
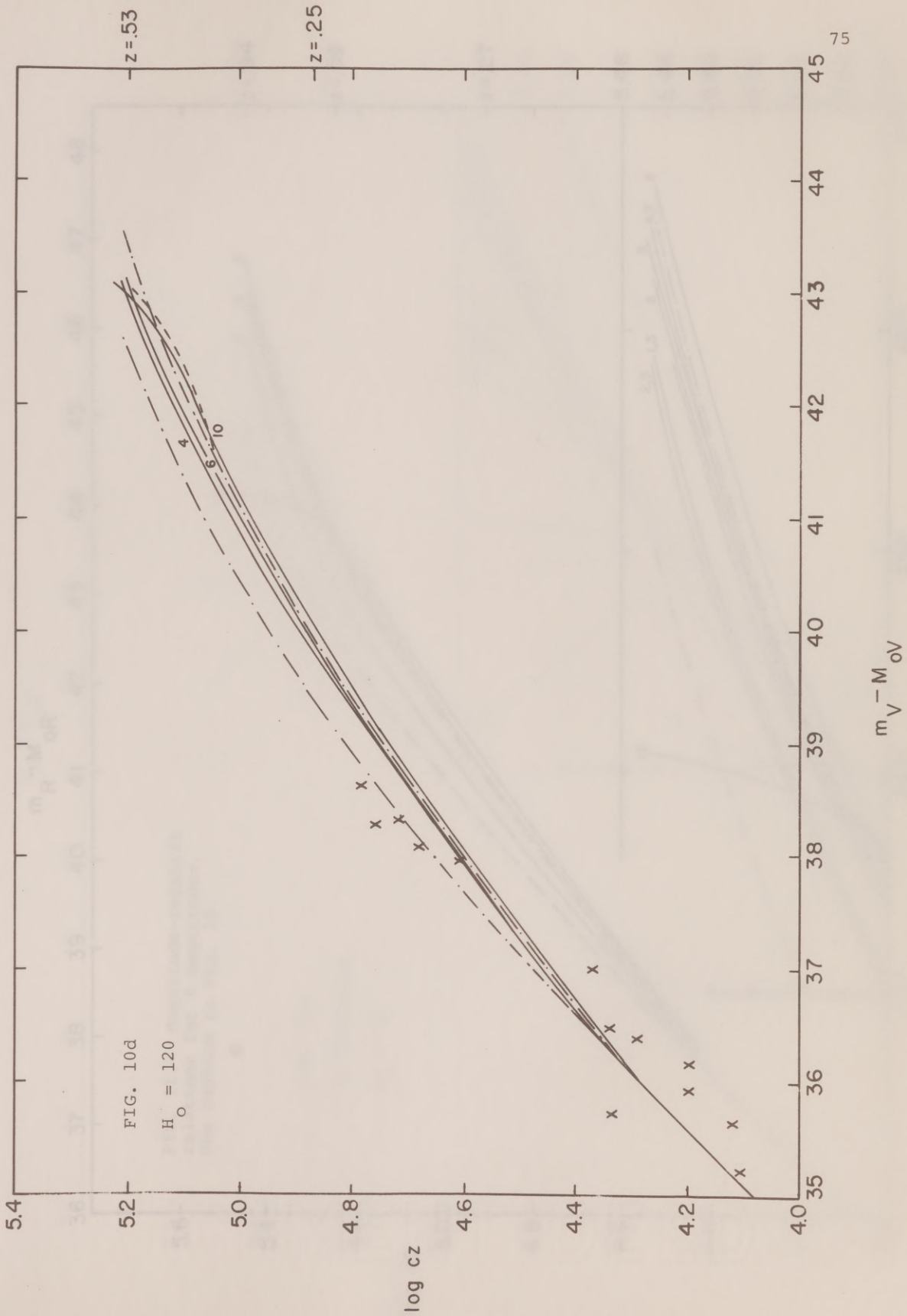
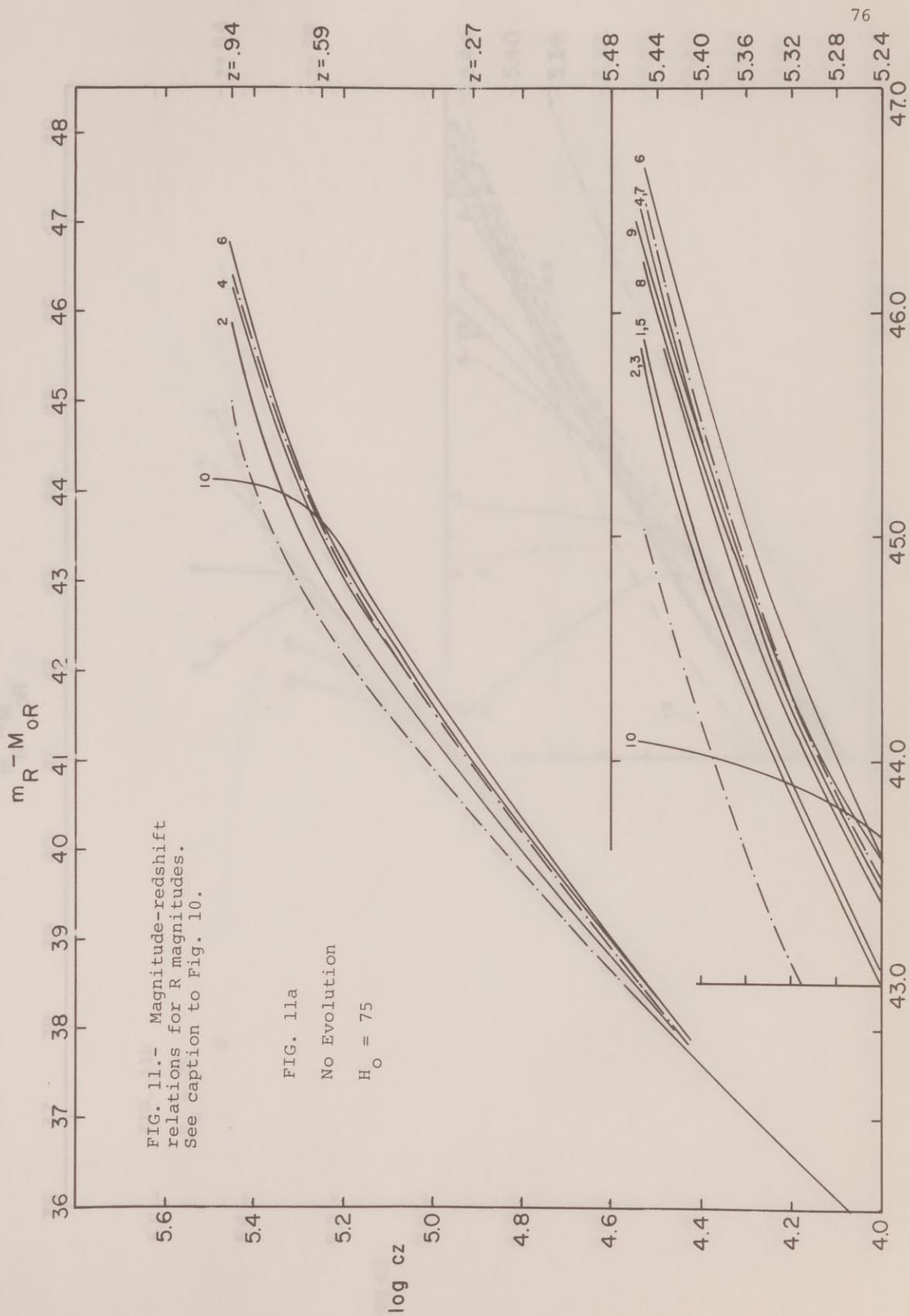


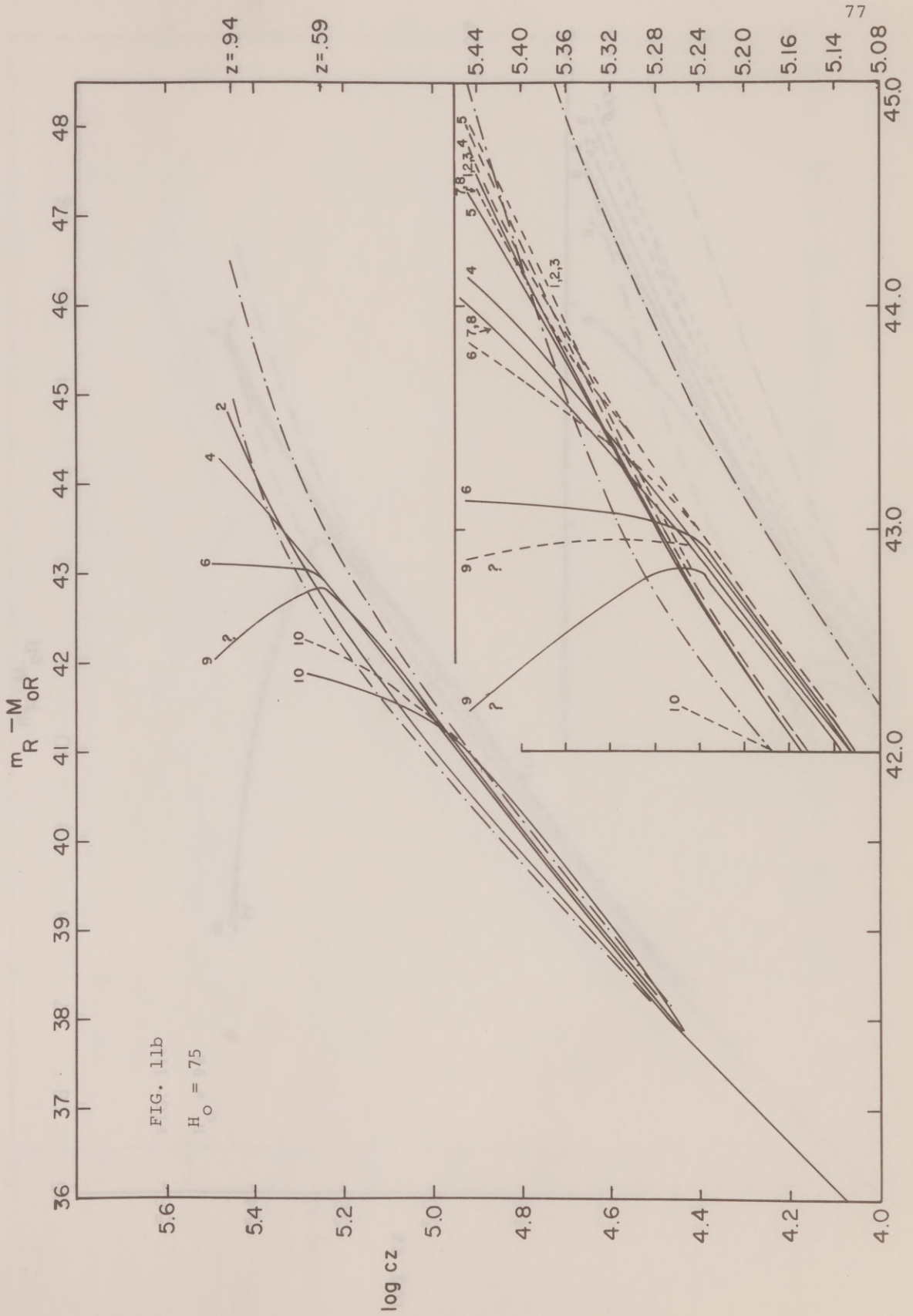
FIG. 10.- Magnitude-redshift relations for V magnitudes. See explanation in text. Dot-dash lines are for models $\Lambda = 0$, $q = 1.0$ (upper) and Steady State (lower), without evolution of galaxies. Solid lines refer to sequence E2, broken to E4. Crosses show positions of clusters observed by HMS. H_0 - Hubble's constant, H , is in $\text{km sec}^{-1} \text{Mpc}^{-1}$. Numbers on Curves refer to models in Table 7.

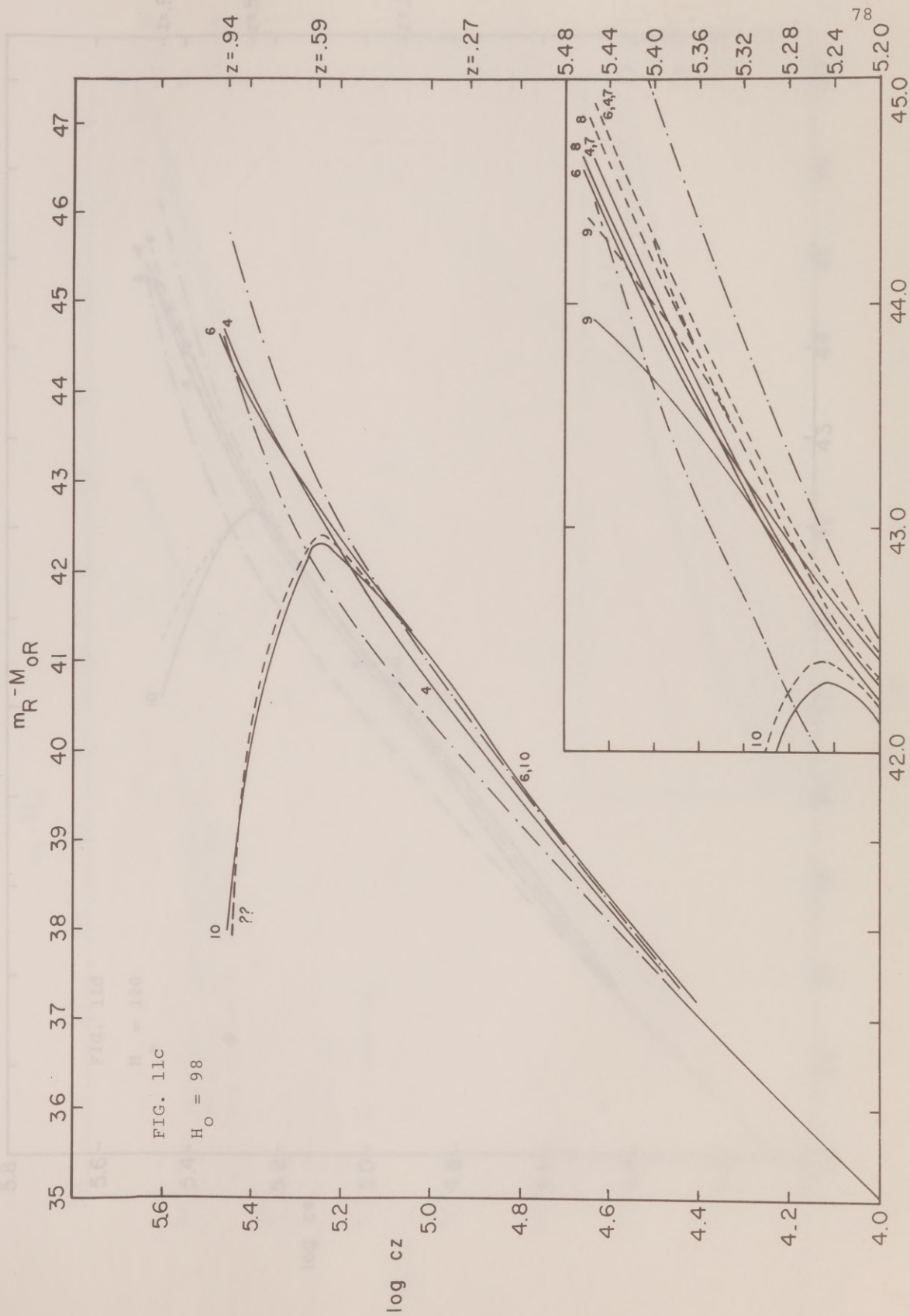


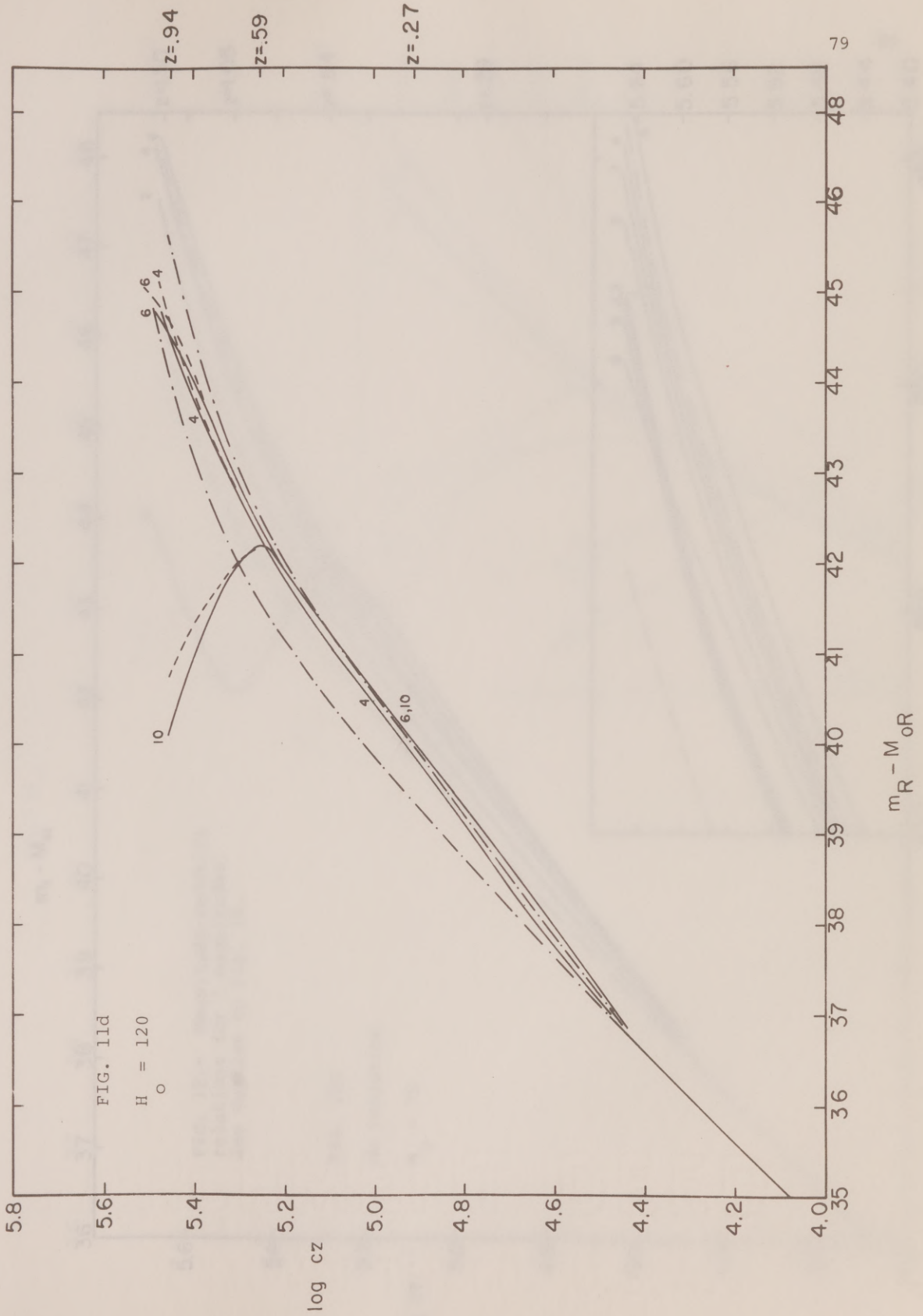












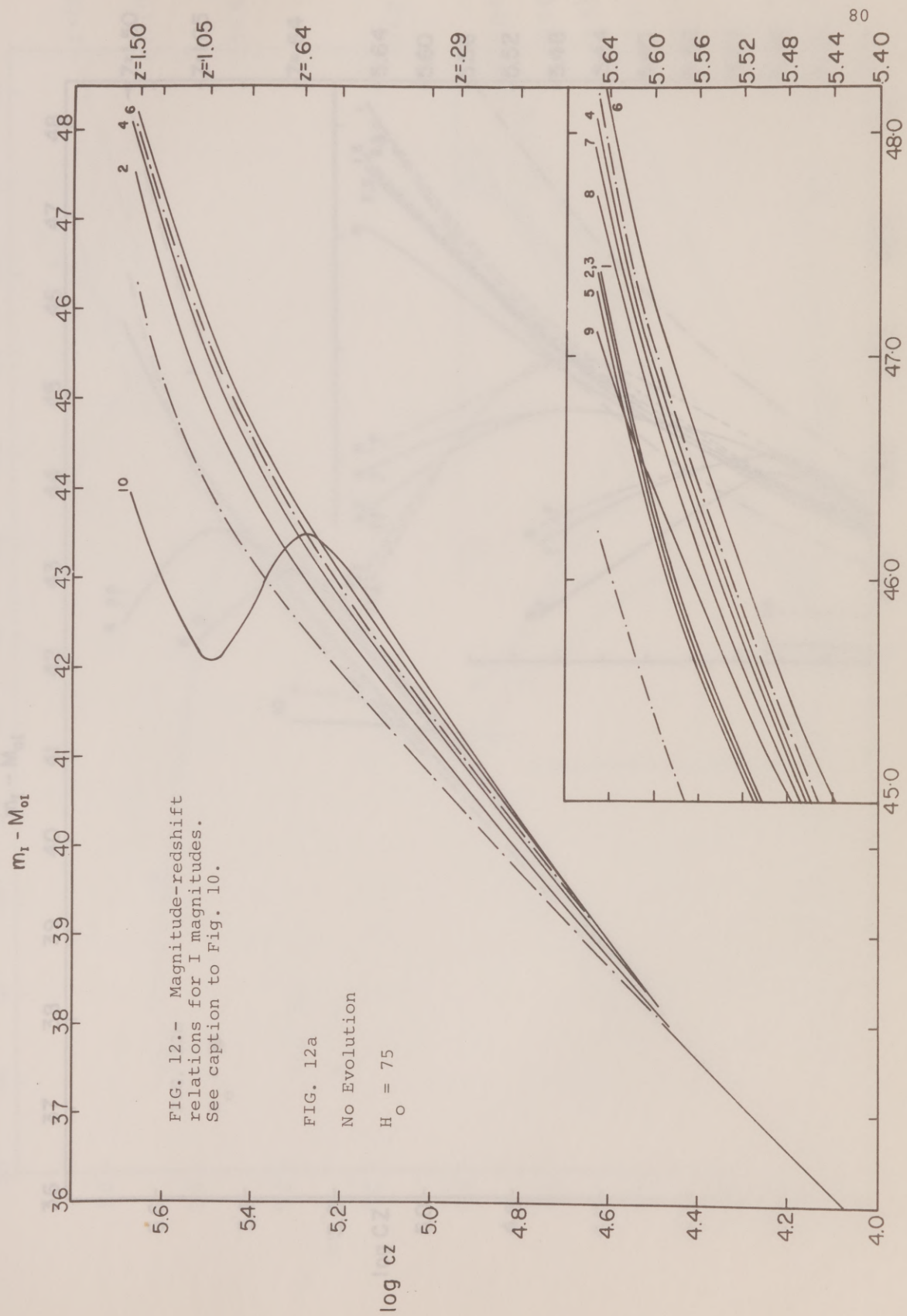
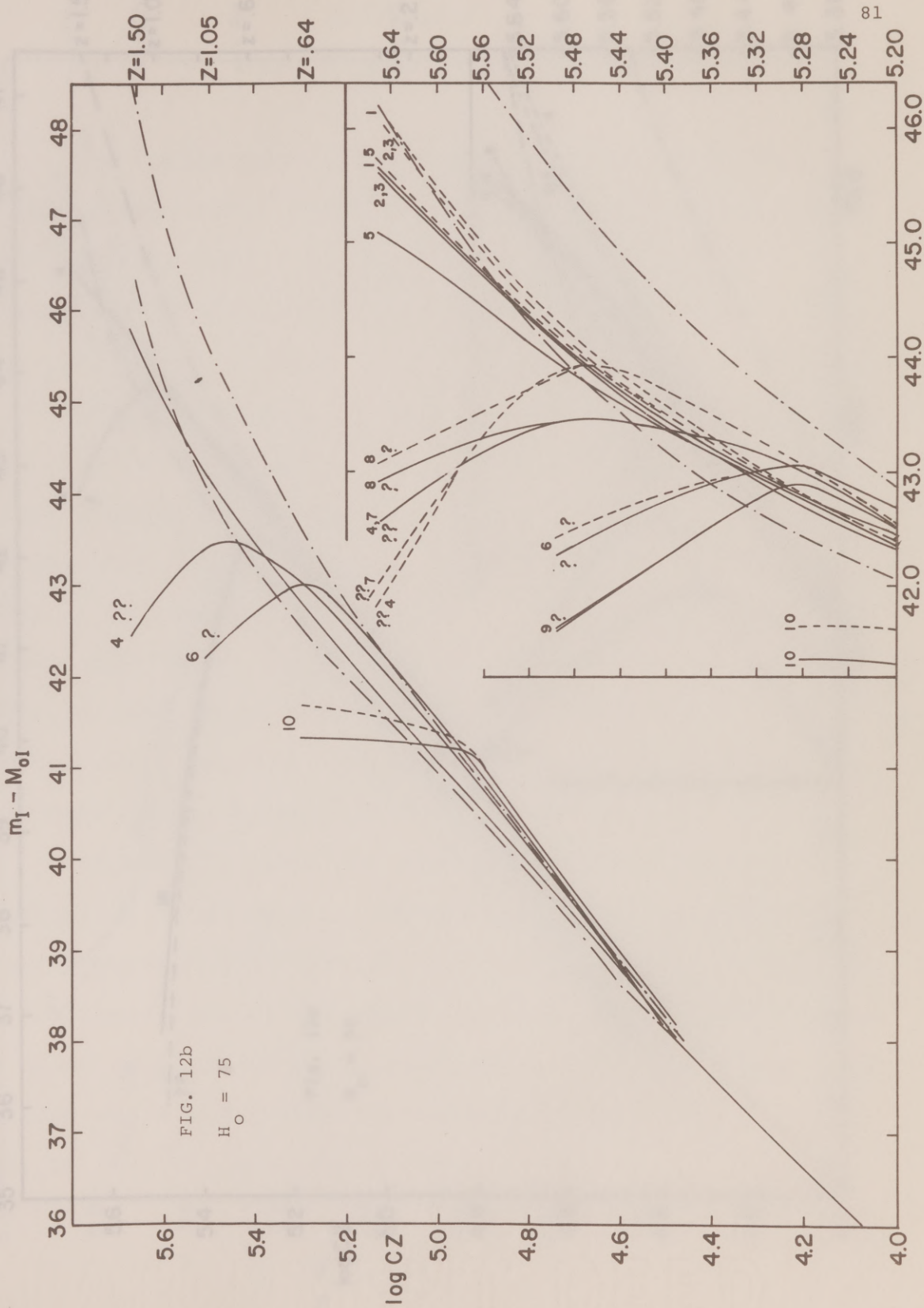
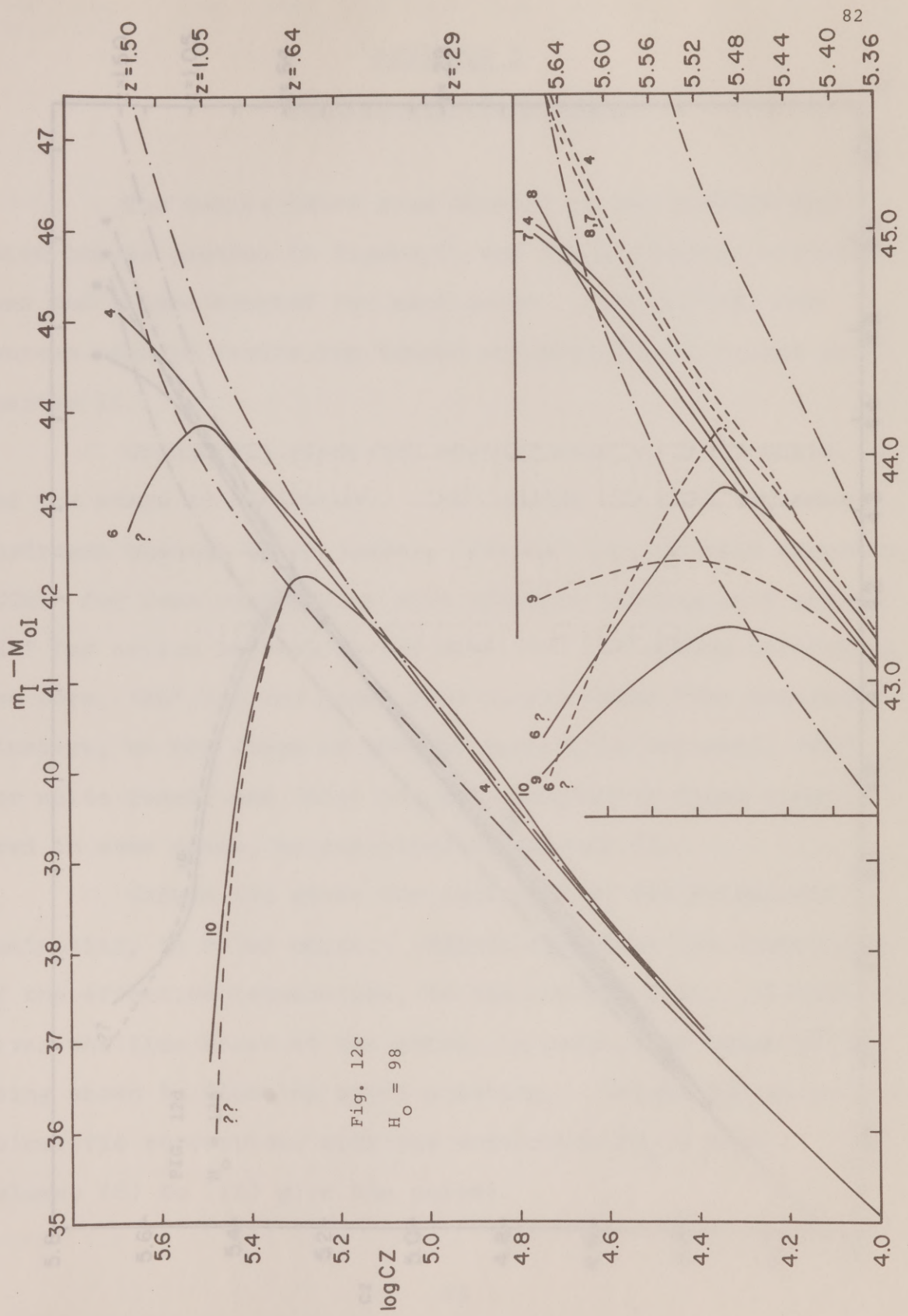


FIG. 12.- Magnitude-redshift relations for I magnitudes. See caption to Fig. 10.

FIG. 12a
No Evolution
 $H_0 = 75$





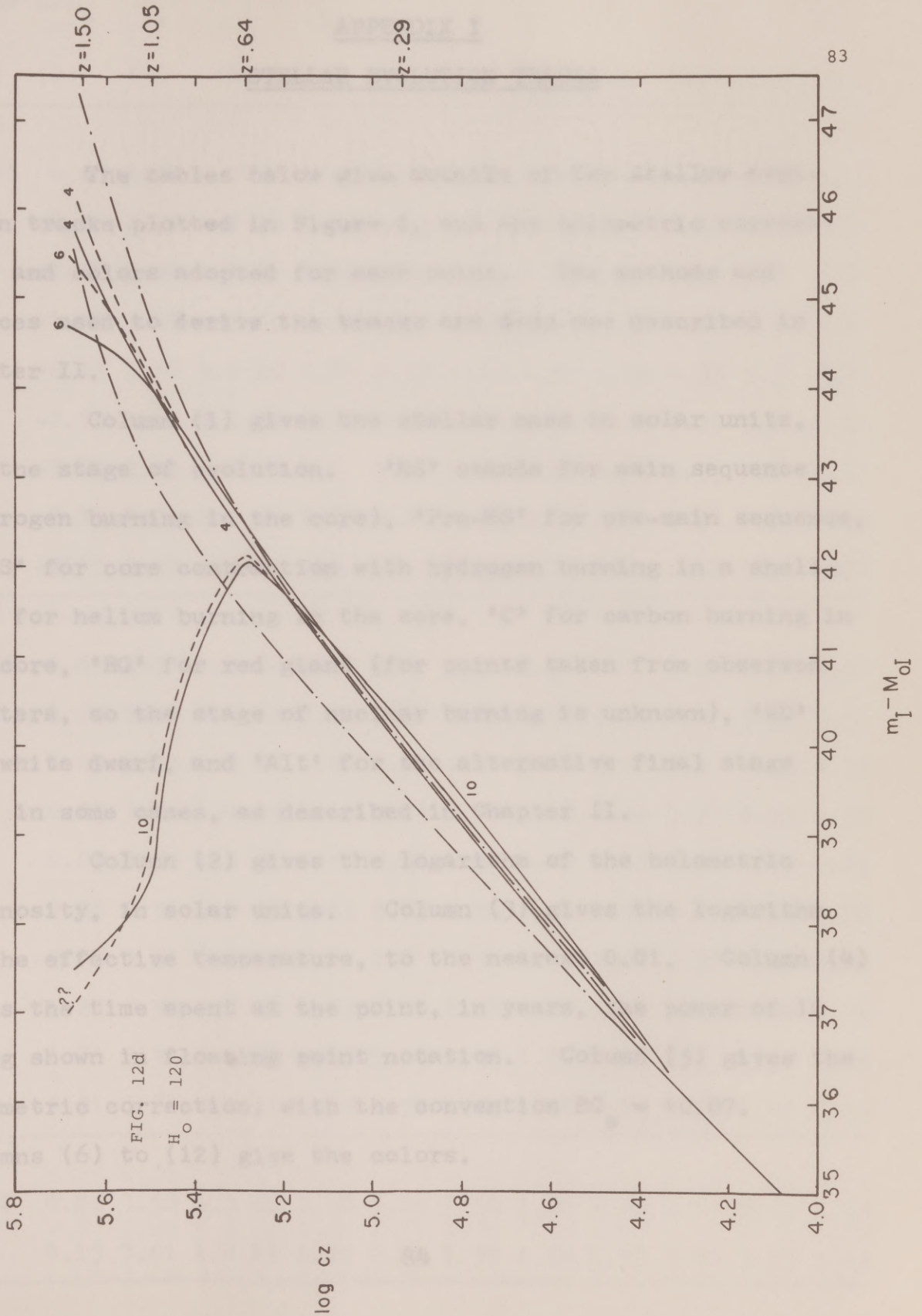


FIG. 12d

$H_0 = 120$

Mass Log Log Time BC U-V B-V Y-B Y-I

APPENDIX I

(1) (2) (3) (4) STELLAR EVOLUTION TRACKS

0.05

PreMS 0. The tables below give details of the stellar evolution tracks plotted in Figure 1, and the bolometric corrections and colors adopted for each point. The methods and sources used to derive the tracks and data are described in Chapter II.

Column (1) gives the stellar mass in solar units, and the stage of evolution. 'MS' stands for main sequence (hydrogen burning in the core), 'Pre-MS' for pre-main sequence, 'CCHS' for core contraction with hydrogen burning in a shell, 'He' for helium burning in the core, 'C' for carbon burning in the core, 'RG' for red giant (for points taken from observed clusters, so the stage of nuclear burning is unknown), 'WD' for white dwarf, and 'Alt' for the alternative final stage used in some cases, as described in Chapter II.

Column (2) gives the logarithm of the bolometric luminosity, in solar units. Column (3) gives the logarithm of the effective temperature, to the nearest 0.01. Column (4) gives the time spent at the point, in years, the power of 10 being shown in floating point notation. Column (5) gives the bolometric correction, with the convention $BC_{\odot} = +0.07$. Columns (6) to (12) give the colors.

PreMS 0.88 3.58 1.3 86 1.30 3.02 1.50 1.37 2.00

0.13 3.61 1.8 87 1.00 2.84 1.37 1.50 1.50

Mass Stage	Log L/L [⊙]	Log T _e	Time	BC	U-V	B-V	V-R	V-I	V-J	V-K	V-L
(1)	(2)	(3)	(4)	(5)	(6)	(7)	(8)	(9)	(10)	(11)	(12)
0.05											
PreMS	0.0:	3.5:	1.0:E5	2.55	3.55	1.65	1.73	3.25	4.00	5.18	5.4
MS	-0.5	3.50	1.0 E6	2.55	3.55	1.65	1.73	3.25	4.00	5.18	5.4
	-1.25	3.49	2.0 E6	2.68	3.57	1.65	1.75	3.35	4.14	5.3	5.5
	-1.75	3.49	1.7 E7	2.68	3.57	1.65	1.75	3.35	4.14	5.3	5.5
	-2.25	3.48	3.0 E7	2.85	3.58	1.65	1.82	3.50	4.35	5.5	5.7
1.00	-2.75	3.46	5.0 E7	3.20	3.58	1.70	2.00	3.80	4.70	5.9	6.1
PreMS	-3.25	3.43	2.0 E8	4.1	3.58	1.70	2.37	4.75	5.55	7.0	7.5
	-3.75	3.33	>12.E9	7.8	3.6	1.80	3.95	7.0	8.3	9.85	10.4
Alt	-3.75	3.22	>12.E9	10.9	3.6	2.53	5.95	10.02	12.20	14.05	14.88
0.26											
PreMS	2.0:	3.45:	1.0:E2	3.5	3.6	1.7	2.3	4.2	5.2	6.0	6.0
	1.75	3.49	1.0 E3	2.68	3.57	1.65	1.75	3.35	4.0	5.3	5.5
1.03	1.25	3.53	1.0 E4	2.00	3.3	1.6	1.56	3.78	3.4	4.55	4.72
PreMS	0.75	3.55	1.0 E5	1.65	3.15	1.57	1.45	2.52	3.2	4.15	4.37
	-0.25	3.56	5.0 E5	1.55	2.95	1.55	1.42	2.45	3.1	4.00	4.25
	-0.25	3.56	3.0 E6	1.65	2.85	1.55	1.45	2.55	3.2	4.05	4.32
MS	-0.75	3.55	6.0 E6	1.70	2.8	1.54	1.51	2.62	3.32	4.15	4.40
	-1.25	3.54	3.0 E7	1.85	2.70	1.54	1.57	2.77	3.5	4.30	4.55
	-1.75	3.54	7.0 E7	1.85	2.70	1.54	1.57	2.77	3.5	4.30	4.55
MS	-2.01	3.54	>12.E9	1.95	2.70	1.55	1.58	2.85	3.57	4.40	4.65
0.8											
PreMS	0.88	3.58	1.3 E6	1.30	3.02	1.50	1.27	2.20	2.75	3.65	3.85
	0.13	3.61	1.8 E7	1.00	2.75	1.37	1.14	1.90	2.40	3.25	3.45

Mass Stage	Log L/L _o	Log T _e	Time	BC	U-V	B-V	V-R	V-I	V-J	V-K	V-L
(1)	(2)	(3)	(4)	(5)	(6)	(7)	(8)	(9)	(10)	(11)	(12)
	-0.43	3.64	5.5 E7	0.73	2.31	1.16	1.02	1.65	2.13	2.83	3.14
MS	-0.57	3.68	4.4 E9	0.45	1.98	1.02	0.88	1.45	1.79	2.45	2.60
	-0.50	3.69	4.4 E9	0.37	1.84	1.00	0.84	1.36	1.67	2.26	2.44
	-0.44	3.70	2.2 E9	0.30	1.68	0.94	0.77	1.29	1.59	2.15	2.33
	-0.37	3.71	2.2 E9	0.27	1.54	0.90	0.73	1.21	1.49	2.04	2.21
1.00											
PreMS	0.20	3.62	9.0 E6	0.85	2.70	1.30	1.07	1.77	2.28	3.1	3.3
	-0.10	3.72	1.6 E7	0.18	1.35	0.82	0.68	1.13	1.40	1.9	2.1
	-0.15	3.76	2.5 E7	0.07	0.82	0.63	0.55	0.90	1.10	1.48	1.62
MS	-0.05	3.77	5.4 E9	0.07	0.72	0.60	0.51	0.84	1.02	1.40	1.52
	0.11	3.78	3.2 E9	0.05	0.62	0.57	0.48	0.79	0.96	1.32	1.45
	0.28	3.76	2.2 E9	0.07	0.82	0.63	0.55	0.90	1.10	1.48	1.62
1.03											
PreMS	0.26	3.62	8.0 E6	0.85	2.70	1.30	1.07	1.77	2.28	3.1	3.3
	-0.03	3.73	1.5 E7	0.18	1.24	0.80	0.65	1.07	1.33	1.83	1.98
	-0.09	3.77	2.3 E7	0.07	0.72	0.60	0.51	0.84	1.02	1.40	1.52
MS	0.01	3.78	4.7 E9	0.05	0.62	0.57	0.48	0.79	0.96	1.32	1.45
	0.17	3.78	2.9 E9	0.05	0.62	0.57	0.48	0.79	0.96	1.32	1.45
	0.34	3.77	1.9 E9	0.07	0.72	0.60	0.51	0.84	1.02	1.40	1.52
1.00, 1.03											
CCHS	0.58	3.69	1.0 E9	0.35	1.72	0.95	0.75	1.27	1.63	2.20	2.35
RG	0.83	3.66	3.3 E8	0.50	2.10	1.08	0.88	1.43	1.85	2.52	2.65
	1.44	3.64	1.6 E8	0.65	2.47	1.20	0.92	1.58	2.05	2.75	3.00

Mass Stage	Log L/L _☉	Log T _e	Time	BC	U-V	B-V	V-R	V-I	V-J	V-K	V-L
(1)	(2)	(3)	(4)	(5)	(6)	(7)	(8)	(9)	(10)	(11)	(12)
CCHS	2.10	3.60	3.5 E7	0.90	3.15	1.43	1.07	1.82	2.36	3.26	3.40
1.06	2.45	3.58	1.1 E7	1.13	3.33	1.51	1.16	2.04	2.65	3.55	3.70
1.06											
PreMS	0.32	3.62	7.0 E6	0.85	2.70	1.30	1.07	1.77	2.28	3.1	3.3
	0.04	3.73	1.4 E7	0.18	1.24	0.80	0.65	1.07	1.33	1.83	1.98
	-0.04	3.77	2.2 E7	0.07	0.72	0.60	0.51	0.84	1.02	1.40	1.52
MS	0.07	3.79	4.2 E9	0.05	0.56	0.55	0.45	0.75	0.90	1.25	1.37
1.25	0.23	3.80	2.6 E9	0.02	0.53	0.50	0.44	0.72	0.85	1.18	1.28
PreMS	0.40	3.78	1.7 E9	0.05	0.62	0.57	0.48	0.79	0.96	1.32	1.45
CCHS	0.58	3.75	8.0 E8	0.11	0.96	0.70	0.58	0.95	1.18	1.61	1.74
1.09											
PreMS	0.37	3.62	6.0 E6	0.85	2.70	1.30	1.07	1.77	2.28	3.1	3.3
	0.11	3.74	1.3 E7	0.12	1.10	0.72	0.60	1.02	1.25	1.70	1.85
	0.02	3.78	2.1 E7	0.05	0.62	0.57	0.48	0.79	0.96	1.32	1.45
MS	0.14	3.80	3.7 E9	0.02	0.53	0.50	0.44	0.72	0.85	1.18	1.28
	0.30	3.81	2.3 E9	0.02	0.48	0.48	0.42	0.65	0.78	1.1	1.2
	0.47	3.79	1.5 E9	0.05	0.56	0.55	0.45	0.75	0.90	1.25	1.37
CCHS	0.58	3.75	7.0 E8	0.11	0.96	0.70	0.58	0.95	1.18	1.61	1.74
1.18											
PreMS	0.54	3.63	5.0 E6	0.75	2.60	1.25	1.00	1.67	2.18	2.95	3.2
	0.31	3.76	1.1 E7	0.07	0.82	0.63	0.55	0.90	1.10	1.48	1.62
	0.19	3.80	1.7 E7	0.02	0.53	0.50	0.44	0.72	0.85	1.18	1.28
MS	0.31	3.82	2.7 E9	0.01	0.45	0.45	0.40	0.60	0.73	1.03	1.10
	0.50	3.79	2.8 E9	0.05	0.56	0.55	0.45	0.75	0.90	1.25	1.37

Mass Stage	Log L/L _☉	Log T _e	Time	BC	U-V	B-V	V-R	V-I	V-J	V-K	V-L
(1)	(2)	(3)	(4)	(5)	(6)	(7)	(8)	(9)	(10)	(11)	(12)
CCHS	0.58	3.75	4.0 E8	0.11	0.96	0.70	0.58	0.95	1.18	1.61	1.74
1.06, 1.09, 1.18	0.80	3.85	1.6 E8	0.00	0.39	0.33	0.32	0.49	0.73	0.96	1.18
RG	0.83	3.70	3.3 E8	0.30	1.68	0.94	0.77	1.29	1.59	2.15	2.33
	1.44	3.66	1.6 E8	0.40	2.07	1.07	0.76	1.30	1.73	2.39	2.49
	2.10	3.63	3.5 E7	0.67	2.72	1.30	0.92	1.60	2.10	2.91	3.10
	2.45	3.60	1.1 E7	0.90	3.15	1.43	1.07	1.82	2.36	3.26	3.40
1.25											
PreMS	0.65	3.63	4.0 E6	0.75	2.60	1.25	1.00	1.67	2.18	2.95	3.2
	0.45	3.78	1.0 E7	0.05	0.62	0.57	0.48	0.79	0.96	1.32	1.45
PreMS	0.30	3.82	1.6 E7	0.01	0.45	0.45	0.40	0.60	0.73	1.03	1.10
MS	0.44	3.83	2.2 E9	0.00	0.40	0.40	0.37	0.59	0.70	0.95	1.04
	0.59	3.80	2.2 E9	0.02	0.53	0.50	0.44	0.72	0.85	1.18	1.28
RG	0.83	3.75	3.3 E8	0.11	0.96	0.70	0.58	0.95	1.18	1.61	1.74
	1.44	3.69	1.6 E8	0.30	1.58	0.95	0.69	1.18	1.56	2.15	2.23
	2.10	3.63	3.5 E7	0.67	2.72	1.30	0.92	1.60	2.10	2.91	3.10
	2.45	3.60	1.1 E7	0.90	3.15	1.43	1.07	1.82	2.36	3.26	3.40
1.5											
PreMS	1.19	3.63	2.35E5	0.75	2.60	1.25	1.00	1.65	2.15	2.93	3.17
CCHS	0.63	3.66	2.12E6	0.50	2.10	1.08	0.88	1.43	1.85	2.52	2.65
	0.67	3.77	8.07E6	0.06	0.72	0.60	0.51	0.84	1.02	1.40	1.52
	0.70	3.89	7.8 E6	0.00	0.28	0.20	0.17	0.28	0.36	0.49	0.54
MS	0.74	3.90	5.45E8	0.00	0.26	0.16	0.16	0.25	0.33	0.40	0.50
	0.78	3.89	3.85E8	0.00	0.28	0.20	0.17	0.28	0.36	0.49	0.54

Mass Stage	Log L/L _☉	Log T _e	Time	BC	U-V	B-V	V-R	V-I	V-J	V-K	V-L
(1)	(2)	(3)	(4)	(5)	(6)	(7)	(8)	(9)	(10)	(11)	(12)
	0.80	3.87	3.1 E8	0.00	0.35	0.30	0.28	0.44	0.52	0.70	0.76
	0.80	3.85	1.6 E8	0.00	0.37	0.35	0.30	0.47	0.58	0.82	0.88
CCHS	1.09	3.80	2.7 E8	0.02	0.53	0.50	0.44	0.72	0.85	1.18	1.28
RG	1.67	3.71	9.8 E7	0.20	1.54	0.90	0.73	1.21	1.49	2.04	2.21
	2.28	3.63	2.8 E7	0.67	2.72	1.30	0.92	1.60	2.10	2.91	3.10
	2.87	3.56	1.2 E7	1.45	3.52	1.60	1.27	2.32	2.94	3.97	4.14
1.0 -											
1.5											
Alt	3.65	3.49	7E5 to 2E6	2.60	3.60	1.67	1.77	3.39	4.13	5.29	5.49
2.0											
PreMS	1.52	3.63	1.1 E5	0.70	2.65	1.28	0.98	1.63	2.15	2.91	3.15
	1.05	3.66	7.9 E5	0.50	2.10	1.08	0.87	1.40	1.83	2.50	2.63
CCHS	1.03	3.75	1.75E6	0.08	0.96	0.70	0.58	0.95	1.18	1.61	1.74
	1.32	3.90	1.30E6	0.00	0.26	0.16	0.16	0.25	0.33	0.40	0.50
	1.33	3.98	7.5 E5	0.03	0.00	0.00	0.00	0.00	0.00	0.00	0.00
MS	1.24	3.99	3.6 E6	0.06	0.00	0.00	0.00	-0.02	0.00	0.00	0.00
	1.30	4.00	4.02E8	0.12	0.00	-0.02	0.00	-0.03	-0.03	-0.3	0.00
	1.37	3.98	2.02E8	0.03	0.00	0.00	0.00	0.00	0.00	0.00	0.00
	1.43	3.98	2.6 E7	0.03	0.00	0.00	0.00	0.00	0.00	0.00	0.00
CCHS	1.50	3.99	8.3 E7	0.06	0.00	0.00	0.00	-0.02	0.00	0.00	0.00
PreMS	1.56	3.96	5.86E7	0.03	0.08	0.06	0.05	0.06	0.08	0.12	0.15
	1.58	3.84	0.0	0.00	0.38	0.38	0.33	0.51	0.65	0.88	0.93
RG	1.74	3.72	1.05E8	0.13	1.35	0.82	0.62	1.10	1.41	1.93	2.10
	2.19	3.66	5.5 E7	0.40	2.07	1.07	0.76	1.30	1.73	2.39	2.49

Mass Stage	Log L/L _☉	Log T _e	Time	BC	U-V	B-V	V-R	V-I	V-J	V-K	V-L
(1)	(2)	(3)	(4)	(5)	(6)	(7)	(8)	(9)	(10)	(11)	(12)
	2.77	3.60	2.95E7	0.90	3.15	1.43	1.07	1.82	2.36	3.26	3.40
MS	3.62	3.51	8.4 E6	2.20	3.60	1.64	1.63	3.00	3.60	4.85	5.05
Alt	4.21	3.45	1.0 E6	3.40	3.60	1.75	2.10	4.08	4.95	6.15	6.36
3.0	4.55	4.45	3.0 E6	2.95	-1.25	-1.30	-1.33	-1.40	-1.47	-1.50	-1.50
PreMS	2.18	3.55	3.0:E3	1.0	3.5	1.6	1.5	2.5	3.0	4.0	4.0
	1.85	3.65	2.1 E5	0.50	2.30	1.15	0.82	1.40	1.86	2.52	2.65
He	1.70	3.78	5.5 E5	0.05	0.80	0.59	0.48	0.80	0.90	1.32	1.42
	1.97	3.99	5.0 E5	0.07	-.05	0.00	0.00	-.02	-.02	0.00	0.03
	1.99	4.11	2.0 E5	0.72	-.30	-.06	-.02	-.10	-.14	-.15	-.15
	1.94	4.13	2.0 E5	0.80	-.38	-.10	-.03	-.12	-.18	-.22	-.20
MS	2.02	4.13	1.4 E8	0.85	-.40	-.10	-.04	-.13	-.18	-.24	-.22
Alt	2.10	4.08	8.5 E7	0.60	-.25	-.05	-.03	-.07	-.09	-.10	-.10
CCHS	2.18	4.08	1.0 E7	0.60	-.25	-.05	-.03	-.07	-.09	-.10	-.10
WD	2.23	4.04	1.3 E7	0.37	-.13	-.03	-.02	-.05	-.05	-.05	-.02
	2.10	3.83	2.0 E6	0.00	0.40	0.35	0.35	0.50	0.67	0.90	1.00
He	2.19	3.65	4.0 E6	0.50	2.30	1.15	0.82	1.36	1.87	2.52	2.65
	2.29	3.64	2.5 E7	0.64	2.65	1.25	0.90	1.60	2.07	2.80	3.05
	2.24	3.71	2.9 E7	0.25	1.60	0.90	0.70	1.25	1.55	2.08	2.27
	2.34	3.70	1.9 E7	0.30	1.70	0.95	0.68	1.25	1.60	2.20	2.35
15.0											
PreMS	4.5:	3.56	6.0:E2	1.5	3.6	1.7	1.5	2.4	3.0	3.75	4.0
	4.16	3.76	3.0 E3	0.05	1.27	0.75	0.55	0.90	1.07	1.50	1.52
	4.29	4.04	5.6 E3	0.37	-.56	-.05	0.00	0.00	-.05	-.05	-.02
	4.31	4.33	3.1 E4	2.15	-1.3	-.23	-.10	-.32	-.53	-.70	-.70

Mass Stage	Log L/L _☉	Log T _e	Time	BC	U-V	B-V	V-R	V-I	V-J	V-K	V-L
(1)	(2)	(3)	(4)	(5)	(6)	(7)	(8)	(9)	(10)	(11)	(12)
	4.31	4.50	2.2 E4	3.34	-1.43	-.30	-.15	-.44	-.73	-.93	-.92
MS	4.31	4.51	8.0 E4	3.40	-1.44	-.31	-.15	-.44	-.73	-.94	-.92
	4.40	4.50	6.6 E6	3.30	-1.42	-.30	-.15	-.43	-.72	-.93	-.91
	4.55	4.45	3.6 E6	2.95	-1.33	-.30	-.12	-.40	-.67	-.90	-.90
CCHS	4.70	4.34	3.0 E5	2.20	-1.2	-.24	-.10	-.33	-.56	-.72	-.72
	4.80	4.23	6.0 E5	2.12	-1.1	-.17	-.05	-.24	-.40	-.51	-.45
He	4.85	4.15	7.9 E5	0.95	-0.9	-.12	0.00	-.16	-.25	-.32	-.25
	4.88	3.95	1.7 E5	0.00	-.23	0.04	0.06	0.10	0.14	0.18	0.23
	4.88	3.71	1.0 E4	0.20	1.75	0.95	0.68	1.08	1.42	1.93	2.04
	4.91	3.55	3.0 E4	1.55	3.60	1.70	1.36	2.40	3.07	4.15	4.35
C	4.97	3.49	2.3 E5	2.70	3.63	1.72	1.75	3.40	4.13	5.29	5.5
Alt	4.97	3.49	6.0 E5	2.70	3.63	1.72	1.75	3.40	4.13	5.29	5.5
0.5											
WD	-1.50	4.33	8.0 E7	2.00	-1.38	-.18	-.10	-.31	-.51	-.70	-.75
	-2.50	4.08	3.4 E8	0.80	0.18	0.09	-.03	-.07	-.10	-.10	-.10
	-3.50	3.83	1.78E9	0.70	3.00	0.58	0.37	0.55	0.70	0.95	1.02
	-4.50	3.57	>11.E9	1.70	7.11	1.53	1.42	2.45	3.05	3.88	4.1

$R(r)$ is the 'static' metric tensor
radial coordinate, r is the
observers, α is the
the curvature and is Ω .

APPENDIX II

FORMULAE FOR COSMOLOGICAL CALCULATIONS

Below are summarized the formulae for cosmological calculations, in the form in which they were used here, which was very convenient for machine computation. The basic cosmological constant, Λ , is assumed to be zero. Derivations and field equations are also given. Derivations of most of the General Relativistic formulae are given by McVittie (1965); others follow similarly from the basic equations. Results for the Steady State model were derived by Bondi and Gold (1948).

GENERAL FORMULAE FOR RELATIVISTIC MODELS

Units. Ordinary units of physics, such as c.g.s., are used, unless otherwise stated.

Hubble's constant:

Metric. The Robertson-Walker line element for homogeneous, isotropic world models is used, in the form:

$$ds^2 = c^2 dt^2 - R^2(t) \left\{ \frac{dr^2}{1-kr^2} + r^2 (d\theta^2 + \sin^2\theta d\phi^2) \right\} \quad (A1)$$

$R(t)$ is the 'scale factor' for the model, r is a convenient radial coordinate, t is the proper time for all fundamental observers, c is the speed of light, and k gives the sign of the curvature and is +1, -1, or 0.

Field Equations for General Relativistic Models.

$$\frac{\dot{R}^2}{R^2} + \frac{2\ddot{R}}{R} + \frac{8\pi G p}{c^2} = -\frac{kc^2}{R^2} + \Lambda c^2 \quad (A2)$$

$$\frac{\dot{R}^2}{R^2} - \frac{8\pi G \rho}{3} = -\frac{kc^2}{R^2} + \frac{\Lambda c^2}{3} \quad (A3)$$

p, ρ are the pressure and mean density of matter, Λ is the cosmological constant, G is the Newtonian gravitational constant, and dots represent differentiation with respect to time.

Here it is assumed that $p=0$, so (A2) can be replaced by $\rho R^3 = \text{constant}$. (A4)

GENERAL FORMULAE FOR RELATIVISTIC MODELS

Parameters for the present time, t_0 .

$$R(t_0) \equiv R_0$$

Hubble's constant: $H_0 = \dot{R}_0 / R_0$ (A5)

Deceleration parameter: $q_0 = -\ddot{R}_0 / (R_0 H_0^2)$ (A6)

Density parameter: $\sigma_0 = 4\pi G \rho_0 / (3H_0^2)$ (A7)

A model, i.e. a solution to (A3) and (A4), is specified uniquely by 3 parameters, e.g. H_0, q_0, σ_0 , or H_0, t_0, σ_0 . Other quantities are related by:

$$\Lambda c^2 / H_0^2 = 3(\sigma_0 - q_0) \quad (A8)$$

$$kc^2 / (R_0^2 H_0^2) = 3\sigma_0 - 1 - q_0 \quad (A9)$$

Age of the Universe, t_0 (if finite), measured from $R(0)=0$.

$$H_0 t_0 = H_0 \int_0^{R_0} dR / \dot{R} = \int_0^1 y^{\frac{1}{2}} f^{-\frac{1}{2}} dy \quad (A10)$$

$$\text{where } f(y) = 2\sigma_0 + (1 + q_0 - 3\sigma_0)y + (\sigma_0 - q_0)y^3 \quad (\text{A11})$$

Relation between coordinates at emission and observation

of light. Time t_1 , radial coordinates r_1 and u , and scale factor $R_1 (=R(t_1))$, at emission from an object seen at the origin at t_0 with redshift z , are related by:

$$1 + z = R_0/R_1 \quad (\text{A12})$$

$$u = \int_0^{r_1} dr/\sqrt{1-kr^2} = c \int_{t_1}^{t_0} dt/R(t) = \begin{cases} \sin^{-1} r_1 & \text{if } k=+1 \\ r_1 & \text{if } k=0 \\ \sinh^{-1} r_1 & \text{if } k=-1 \end{cases} \quad (\text{A13})$$

$$\text{If } k=+1, \quad u = \sqrt{3\sigma_0 - q_0 - 1} \int_{(1+z)^{-1}}^1 y^{-\frac{1}{2}} r^{-\frac{1}{2}} dy \quad (\text{A14})$$

$$\text{If } k=0, \quad u = \frac{c}{H_0 R_0} \int_0^z dx / \left\{ 1 - 2\sigma_0 + 2\sigma_0(1+x)^3 \right\}^{\frac{1}{2}} \quad (\text{A15})$$

$$\text{If } k=-1, \quad u = \sqrt{1+q_0-3\sigma_0} \int_{(1+z)^{-1}}^1 y^{-\frac{1}{2}} r^{-\frac{1}{2}} dy \quad (\text{A16})$$

Light travel-time, τ .

$$\text{Definition: } \tau = t_0 - t_1 \quad (\text{A17})$$

$$H_0 \tau = \int_{(1+z)^{-1}}^1 y^{\frac{1}{2}} r^{-\frac{1}{2}} dy \quad (\text{A18})$$

Luminosity distance, D .

$$\text{Definition: } D^2 = L/(4\pi l) \quad (\text{A19})$$

L is the bolometric luminosity of the source, in proper units at the source (ergs sec^{-1}); l is the observed luminosity, in proper units at the observer ($\text{ergs cm}^{-2}\text{sec}^{-1}$).

General formula: $D = R_o r_1 (1+z)$ (A20)

with $R_o r_1$ given by (A9) and (A13) - (A16).

Minimum rate of expansion. The minimum of \dot{R}/R occurs at z_m ,
where $(1+z_m)^3 = 1 - q_o / \sigma_o$ (A21)

Number-flux density relation. Of interest is the slope of the curve $\log N$ versus $\log S$, where N is the number of sources with monochromatic flux density (in $\text{ergs cm}^{-2} \text{sec}^{-1} \text{ster}^{-1} (\text{cps})^{-1}$, in proper units at the observer) greater than S . If sources do not evolve, and have spectral index x , i.e. monochromatic luminosity at frequency $f \propto f^{-x}$, then:

$$\text{If } k=+1, \frac{d \log N}{d \log S} = \frac{-r_1^2}{\left[-\frac{1}{2} r_1 \sqrt{1-r_1^2} + \frac{1}{2} \sin^{-1} r_1 \right] \left[(x+1) \dot{R}_1 / c + 2\sqrt{1-r_1^2} / r_1 \right]} \quad (\text{A22})$$

$$\text{If } k=0, \frac{d \log N}{d \log S} = \frac{-r_1^2}{\frac{r_1^3}{3} \left[(x+1) \frac{\dot{R}_1}{c} + \frac{2}{r_1} \right]} \quad (\text{A23})$$

$$\text{If } k=-1, \frac{d \log N}{d \log S} = \frac{-r_1^2}{\left[\frac{1}{2} r_1 \sqrt{1+r_1^2} - \frac{1}{2} \ln(r_1 + \sqrt{1+r_1^2}) \right] \left[(x+1) \dot{R}_1 / c + 2\sqrt{1+r_1^2} / r_1 \right]} \quad (\text{A24})$$

r_1, R_1 refer to the position of a source observed with flux density S . All reduce to $|d \log N / d \log S| \leq 1.5$ when $r_1 \ll 1$.

FORMULAE FOR CERTAIN GENERAL RELATIVISTIC MODELS

$\Lambda = 0$.

$$\sigma_0 = q_0 \geq 0 \quad (\text{A25})$$

If $q_0 = 0$, $H_0 D/c = z(1 + \frac{1}{2}z)$ (A26)

If $q_0 > 0$, $H_0 D/c = q_0^{-2} [1 - q_0 + q_0 z + (q_0 - 1)\sqrt{2q_0 z + 1}]$ (A27)

Formulae for $H_0 t_0$ are given by Sandage (1961a) and for $H_0 \tau$ by Sandage (1961b).

$\Lambda > 0$, $k = 0$.

$$\Lambda = 3H_0^2(1 - 2\sigma_0) \quad (\text{A28})$$

$$q_0 = 3\sigma_0 - 1 \quad (\text{A29})$$

$$H_0 t_0 = \frac{1}{3\sqrt{1-2\sigma_0}} \cosh^{-1} (\sigma_0^{-1} - 1) \quad (\text{A30})$$

$H_0 \tau =$

$$\frac{1}{3\sqrt{1-2\sigma_0}} \ln \left\{ \frac{1 - \sigma_0 + \sqrt{1-2\sigma_0}}{\sigma_0 + (1-2\sigma_0)(1+z)^{-3} + (1-2\sigma_0)^{\frac{1}{2}}(1+z)^{-3/2} \sqrt{(1-2\sigma_0)(1+z)^{-3+2\sigma_0}}} \right\} \quad (\text{A31})$$

$$H_0 D/c = (1+z) \int_0^z dx / [1 - 2\sigma_0 + 2\sigma_0(1+x)^3]^{\frac{1}{2}} \quad (\text{A32})$$

$\Lambda = \Lambda_c$, $k = +1$. These are the Eddington-Lemaitre models,

with a finite minimum radius, R_m , from which expansion starts in the infinite past.

$$\Lambda_c = (4G\pi\rho_0 R_0^3)^{-2} = R_m^{-2} = 3\sigma_0 H_0^2 (1+z_m)^3 / c^2 \quad (\text{A33})$$

$$z_m^2 (z_m + 3) = 1/\sigma_0 \quad (\text{A34})$$

$$q_0 = -1 - 3\sigma_0 z_m \quad (\text{A35})$$

$$\begin{aligned}
 H_0 \tau \frac{(1+z_m)^{3/2}}{(z_m+3)^{1/2} z_m} &= \frac{1}{\sqrt{3}} \ln \frac{(z_m - z)(-3 - 2z_m + \sqrt{3(1+z_m)(3+z_m)})}{z_m(-3 - 2z_m - z + \sqrt{3(1+z_m)(3+z_m+2z)})} \\
 &+ \ln \frac{(2+z+z_m - \sqrt{(1+z_m)(3+z_m+2z)})}{(1+z)(2+z_m - \sqrt{(1+z_m)(3+z_m)})} \quad (A36)
 \end{aligned}$$

$$\sin^{-1} r_1 = u = \ln \frac{(z_m - z)(3+2z_m - \sqrt{3(1+z_m)(3+z_m)})}{z_m(3+2z_m+z - \sqrt{3(1+z_m)(3+z_m+2z)})} \quad (A37)$$

$$\text{In (A22), } \frac{\dot{R}_1}{c} = \frac{(z_m - z) \sqrt{3+z_m+2z}}{(1+z) \sqrt{1+z_m}} \quad (A38)$$

$\Lambda > \Lambda_c$, $k = +1$. These are Lemaitre models. No simplification of the general formulae is possible, and numerical integration is necessary to find $H_0 t_0$, $H_0 \tau$, and $H_0 D$.

FORMULAE FOR THE STEADY STATE MODEL

The only quantity required in the present calculations is the luminosity distance, given by:

$$H_0 D/c = z(1+z) \quad (A39)$$

APPENDIX III

MAGNITUDE-REDSHIFT RELATIONS

The tables below give the data plotted in Figures 10 to 12, and explained in Chapter IV.

The first column gives the observer's filter band. In the second column, the first line gives the redshift and the second line the corresponding band at emission. Succeeding columns give data for the cosmological models: models numbered 1 to 10 are as in Table 7, ' $q_0=1$ ' refers to the model with $\Lambda = 0$, and 'SS' is the Steady State model. The lines are labeled in the final column: τ is the light travel-time, in 10^9 years; lines labeled E2 or E4 give $m_\lambda - M_{0\lambda}$ for those sequences. For models ' $q_0=1$ ' and 'SS', no value of τ is shown since they are taken with $\tau = 0$ always, and $m_\lambda - M_{0\lambda}$ values are given for sequence E2 only since it differs negligibly from E4 at $\tau = 0$. The symbol '?' is added if $\tau = 10$ to 11×10^9 years, '??' is added if $\tau = 11$ to 12×10^9 years, and there is no magnitude value given if τ is greater than 12×10^9 years.

The table headed 'No Evolution' is for Hubble's constant $H_0 = 75 \text{ km sec}^{-1} \text{ Mpc}^{-1}$, and τ is zero. The other tables are for evolution, with H_0 given in the heading, in $\text{km sec}^{-1} \text{ Mpc}^{-1}$.

No Evolution

Obs. band	z	SS	1	2	3	4	5	6	7	8	9	10		
V	.25 B	40.48	40.97	40.76	40.72	40.71	40.95	40.81	41.05	40.96	40.95	41.06	41.21	E2
	.53 U	43.57	44.50	44.11	44.05	44.07	44.46	44.16	44.61	44.50	44.46	44.62	44.76	E2
R	.27 V	40.37	40.89	40.67	40.63	40.58	40.87	40.72	40.97	40.84	40.84	40.95	41.10	E2
	.59 B	42.54	43.55	43.13	43.08	43.05	43.51	43.18	43.67	43.50	43.46	43.62	43.68	E2
	.94 U	45.01	46.46	45.86	45.80	45.82	46.38	45.85	46.61	46.39	46.28	46.25	44.08	E2
I	.29 R	40.49	41.04	40.83	40.77	40.73	41.05	40.89	41.13	41.00	40.99	41.11	41.27	E2
	.64 V	42.45	43.52	43.07	43.01	43.00	43.48	43.11	43.64	43.47	43.42	43.57	43.50	E2
	1.05 B	43.99	45.55	44.91	44.85	44.83	45.45	44.87	45.71	45.40	45.28	45.17	42.09	E2
	1.5 U	46.23	48.22	47.44	47.38	47.36	48.07	47.29	48.40	47.95	47.73	47.10	43.79	E2

$H_0 = 75$

Obs. band	z Em. band	$\alpha_0=1$ SS										τ	E2	E4	
		1	2	3	4	5	6	7	8	9	10				
V	.25 B	2.60	2.60	2.58	2.90	2.72	3.05	2.91	2.91	2.91	3.08	3.35			
		40.64	40.60	40.59	40.81	40.68	40.90	40.82	40.81	40.81	40.91	41.03			
		40.66	40.62	40.61	40.84	40.71	40.93	40.85	40.84	40.93	41.07				
	.53 U	4.50	4.48	4.47	5.48	4.81	5.90	5.58	5.54	6.28	7.94				
		43.43	43.37	43.39	43.53	43.45	43.56	43.54	43.51	43.46	42.85				
		43.54	43.48	43.51	43.76	43.58	43.81	43.78	43.75	43.73	43.37				
R	.27 V	2.76	2.76	2.71	3.11	2.90	3.27	3.07	3.07	3.07	3.27	3.58			
		40.56	40.52	40.48	40.75	40.61	40.83	40.72	40.72	40.72	40.81	40.95			
		40.56	40.52	40.47	40.75	40.60	40.83	40.72	40.72	40.82	40.95				
	.59 B	4.82	4.80	4.72	5.97	5.17	6.47	5.98	5.92	6.78	8.83				
		42.77	42.73	42.71	42.94	42.77	42.97	42.93	42.90	42.83	41.85				
		42.83	42.79	42.76	43.02	42.84	43.07	43.01	42.98	42.95	42.18				
	.94 U	6.28	6.24	6.21	8.41	6.78	9.58	8.57	8.37	10.07	14.56				
		44.70	44.65	44.68	44.13	44.52	43.13	44.01	44.08	42.18	-				
		44.94	44.89	44.92	44.73	44.81	43.84	44.63	44.66	42.87	-				

H₀ = 75, Continued

Obs. band	Z	Em. band	σ ₀ =1	SS	1	2	3	4	5	6	7	8	9	10	
I	.29 R		40.49	41.04	2.89	2.89	2.83	3.27	3.04	3.44	3.24	3.23	3.46	3.81	τ
					40.78	40.72	40.69	40.99	40.84	41.06	40.94	40.93	41.04	41.18	E2
					40.80	40.74	40.71	41.01	40.86	41.09	40.96	40.95	41.07	41.22	E4
	.64 V		42.45	43.52	5.06	5.04	4.97	6.35	5.44	6.93	6.38	6.32	7.30	9.79	τ
					42.78	42.73	42.72	43.00	42.78	43.04	42.99	42.95	42.89	41.35	E2
					42.89	42.83	42.84	43.08	42.90	43.06	43.06	43.03	42.89	41.66	E4
B	1.05		43.99	45.55	6.62	6.58	6.46	9.04	7.15	10.47	9.04	8.80	10.63	15.30	τ
					44.16	44.11	44.14	43.43	43.96	42.29	43.38	43.47	41.59	-	E2
					44.33	44.27	44.29	43.90	44.17	42.43	43.83	43.85	41.62	-	E4
U	1.5		46.23	48.22	7.76	7.70	7.56	11.32	8.35	14.30	11.24	10.73	12.96	17.73	τ
					45.65	45.63	45.68	42.58	45.09	-	42.56	42.92	-	-	E2
					46.14	46.12	46.14	41.81	45.73	-	42.00	43.09	-	-	E4

$$H_0 = 98$$

Obs. band	z Em. band	$q_0=1$	SS	4	6	7	8	9	10	
V	.25 B	39.90	40.39	2.22	2.33	2.23	2.22	2.36	2.57	τ
				40.26	40.36	40.27	40.27	40.37	40.51	E2
				40.30	40.39	40.30	40.30	40.40	40.54	E4
	.53 U	42.99	43.92	4.20	4.52	4.27	4.24	4.81	6.08	τ
				43.25	43.34	43.28	43.25	43.33	43.06	E2
				43.34	43.46	43.37	43.34	43.46	43.33	E4
R	.27 V	39.79	40.31	2.38	2.50	2.35	2.35	2.50	2.74	τ
				40.20	40.30	40.18	40.17	40.28	40.41	E2
				40.19	40.29	40.16	40.15	40.27	40.41	E4
	.59 B	41.96	42.97	4.57	4.95	4.58	4.53	5.19	6.76	τ
				42.61	42.71	42.60	42.56	42.62	42.31	E2
				42.66	42.78	42.65	42.61	42.70	42.42	E4
	.94 U	44.43	45.88	6.44	7.33	6.56	6.41	7.71	11.14	τ
				44.59	44.47	44.56	44.50	43.91	38.21	E2
				44.85	44.84	44.82	44.75	44.34	37.74	E4
									??	
I	.29 R	39.91	40.46	2.50	2.63	2.48	2.47	2.65	2.92	τ
				40.43	40.51	40.38	40.37	40.49	40.64	E2
				40.46	40.54	40.41	40.40	40.52	40.66	E4
	.64 V	41.87	42.94	4.86	5.31	4.89	4.83	5.59	7.49	τ
				42.63	42.75	42.62	42.58	42.63	42.19	E2
				42.74	42.87	42.73	42.68	42.75	42.16	E4
	1.05 B	43.41	44.97	6.92	8.02	6.92	6.73	8.14	11.71	τ
				44.04	43.87	44.00	43.92	43.24	36.78	E2
				44.23	44.13	44.17	44.08	43.52	35.93	E4
									??	
	1.5 U	45.65	47.64	8.67	10.94	8.60	8.22	9.92	13.57	τ
				44.99	42.79	44.95	45.08	42.63	-	E2
				45.69	42.55	45.63	45.67	43.39	-	E4
					?					

$$H_o = 120$$

Obs. band	z Em. band	$q_o=1$	SS	4	6	10		
V	.25 B	39.46	39.97	1.82	1.91	2.10	τ	
				39.85	39.94	40.10	E2	
				39.89	39.98	40.13	E4	
	.53 U	42.55	43.48	3.43	3.69	4.96	τ	
				42.95	43.06	42.95	E2	
				42.95	43.08	43.11	E4	
R	.27 V	39.35	39.87	1.94	2.04	2.24	τ	
				39.77	39.87	40.00	E2	
				39.76	39.86	39.99	E4	
	.59 B	41.52	42.53	3.73	4.04	5.52	τ	
				42.27	42.40	42.18	E2	
				42.29	42.42	42.25	E4	
	.94 U	43.99	45.44	5.26	5.99	9.10	τ	
				44.49	44.51	40.14	E2	
				44.66	44.73	40.84	E4	
	I	.29 R	39.47	40.02	2.04	2.15	2.38	τ
					40.01	40.08	40.22	E2
					40.04	40.11	40.24	E4
.64 V		41.43	42.50	3.97	4.33	6.12	τ	
				42.48	42.40	42.06	E2	
				42.34	42.48	42.13	E4	
1.05 B		42.97	44.53	5.65	6.55	9.56	τ	
				43.95	43.96	38.55	E2	
				44.05	44.12	39.13	E4	
1.5 U		45.21	47.20	7.08	8.94	11.08	τ	
				45.60	44.59	37.53	E2	
				45.99	45.33	37.19	E4	
					??			

APPENDIX IV

REVISED COLORS OF ELLIPTICAL GALAXIES

CORRECTED COLORS FROM OBSERVATIONS

After the study of galactic evolution and cosmology described above was completed, a reinterpretation of Johnson's (1966a) observations of colors of galaxies was made by G. de Vaucouleurs, and communicated to the author.

The observed colors of elliptical galaxies were revised by applying corrections for aperture size and internal color distribution, Galactic absorption, and redshift. Also, NGC 4168 was excluded from the mean since it is a dwarf elliptical and consequently slightly bluer than the others (de Vaucouleurs, 1961). The means of the corrected colors obtained by de Vaucouleurs for four giant elliptical galaxies are tabulated below, with the uncorrected means for comparison.

Color	U-V	B-V	V-R	V-I	V-J	V-K	V-L
Mean for 5 observed E galaxies (Johnson, 1966a)	1.56	1.02	0.92	1.67	2.23	3.04	3.48
Corrected mean for 4 gE galaxies (de Vaucouleurs)	1.296	0.909	0.850	1.580	1.919	2.803	3.433

The corrected colors are shown (dotted line) in Figure 5, and the corresponding absolute energy distribution in Figure 7.

The corrected mean U-V and B-V agree well with the values obtained by de Vaucouleurs (1961) for gE galaxies, 1.35 and 0.89, respectively, also corrected to zero redshift and galactic absorption.

COMPARISON WITH COMPUTED SEQUENCES

It can be seen from Figure 5 that the above revision seriously affects the agreement between observed and computed U-V. For the far infrared colors, the discrepancies are not so serious because of the wide scatter in observed colors and the difficulties of the measurements. Agreement between observed and computed B-V, V-R, and V-I is improved by this revision.

None of the galactic evolution sequences constructed as described in Chapter II showed, at any age, good agreement with all the observed E properties listed in Table 3, if U-V as low as 1.30 or 1.35 were required. However, the considerations in Chapter IV suggested that a change in the assumed initial stellar composition might reduce the computed U-V at 12×10^9 years sufficiently. This possibility was tested by computing a sequence with the same stellar birthrate parameters as E2, but with four important lower main sequence stars moved to positions with $\log T_e$ greater by .06. The calculations of Demarque and Larson (1964) indicate that this change would take place if the composition were changed either by reducing

X by about 0.1, or by reducing Z by about 0.015. Also, the more recent relations between $\log T_e$, BC, and colors (Johnson, 1966b) were used for these four stars. The resulting colors at 12×10^9 years were all lower than those in sequence E2.

Below are tabulated these reductions in color, and the reductions required to sequence E2 to bring it into agreement with the revised observations.

Color	U-V	B-V	V-R	V-I	V-J	V-K	V-L
Reduction in test	.53	.17	.10	.17	.18	.19	.18
Reduction needed	.31	.03	.01	.01	.27	.43	.19

Changing $\log T_e$ for four stars can be expected to give only a very crude indication of the possible effects of changing the composition of all the stars in the galaxy. The test shows that U-V could be reduced to the observed value by a smaller change in composition than that tried. The very low mass star ($0.05 M_{\odot}$) that is the most important contributor in the J, K, and L bands was not changed in the test, since the calculations of Demarque and Larson do not apply to it, so a discussion of possible changes in the far infrared cannot be given at present.

A more detailed attempt to obtain final colors in agreement with the corrected observations should be made, by changing the assumed initial composition. It appears likely from the above rough test that this attempt would be success-

ful. The magnitude-redshift relations would be altered, but the history of the sequence computed in the rough test indicates that the changes would be small and would not affect the qualitative conclusions drawn in Chapter IV.

- Abell, G.O. 1965, *Annual Review of Astronomy and Astrophysics*, 3, 1.
- Allen, C.W. 1963, *Astronomical Quantities* (George Allen and Unwin Press).
- Auman, J.R. 1965, *Ap.J.*, 133, 663.
- App, H. 1962, *Ap.J.*, 136, 66.
- App, H., and Cuffey, J. 1967, *Ap.J.*, 125, 100.
- Bondi, H. 1968, *Cosmology* (Cambridge: Cambridge University Press, 2nd ed., Part 1-4).
- Bondi, H., and Gold, T. 1948, *M.N.*, 110, 469.
- Burbidge, E.M. 1947, *Diagnose sobre Evolucao de Estrelas*, ed. S. B. Burbidge (La Plata: Observatorio Astronomico), p. 47.
- Burbidge, G.S. 1962, *Distribution and Motion of Interstellar Matter in Galaxies*, ed. L. Spitzer (New York: J.A. Sereno), p. 251.
- Burbidge, E.M., and Burbidge, G.S. 1958, *Ap.J.*, 128, 170.
- Cole, A.B. 1959, *Pub. A.S.P.*, 22, 190.
- Craspin, J., and Hoyle, F. 1961, *M.N.*, 121, 77.
- Davidson, W. 1959a, *M.N.*, 112, 64.
- _____. 1959b, *ibid.*, p. 665.
- _____. 1962a, *ibid.*, 122, 425.
- _____. 1962b, *ibid.*, 124, 79.

BIBLIOGRAPHY

- Abell, G.O. 1965, Annual Review of Astronomy and Astrophysics, 3, 1.
- Allen, C.W. 1963, Astrophysical Quantities (London: Athlone Press).
- Auman, J.R. 1965, Ap.J., 142, 462.
- Arp, H. 1962, Ap.J., 136, 66.
- Arp, H., and Cuffey, J. 1962, Ap.J., 136, 51.
- Bondi, H. 1960, Cosmology (Cambridge: Cambridge University Press, 2nd ed.), Figs. 1-4.
- Bondi, H., and Gold, T. 1948, M.N., 108, 252.
- Burbidge, E.M. 1962, Simposia Sobre Evolución Estelar, ed. J. Sahada (La Plata: Observatorio Astronómico), p. 273.
- Burbidge, G.R. 1962, Distribution and Motion of Interstellar Matter in Galaxies, ed. L. Woltjer (New York: W.A. Benjamin), p. 291.
- Burbidge, E.M., and Sandage, A.R. 1958, Ap.J., 128, 174.
- Code, A.D. 1959, Pub.A.S.P., 71, 118.
- Crampin, J., and Hoyle, F. 1961, M.N., 122, 27.
- Davidson, W. 1959a, M.N., 119, 54.
- _____. 1959b, *ibid*, p.665.
- _____. 1962a, *ibid*, 123, 425.
- _____. 1962b, *ibid*, 124, 79.

- Davidson, W., and Davies, M. 1964a, M.N., 127, 241.
- _____. 1964b, *ibid*, 128, 363.
- Demarque, P.R., and Larson, R.B. 1964, Ap.J., 140, 544.
- Deutsch, A.J. 1961, Stars and Stellar Systems (Chicago: University of Chicago Press), Vol. 6, Chapter 15.
- Eastmond, T.S. 1965, Pub.A.S.P., 77, 385.
- Epstein, E.E. 1964, A.J., 69, 490.
- Field, G.B., Solomon, P.M., and Wampler, E.J. 1966, Ap.J., 145, 351.
- Glanfield, J.R. 1966, M.N., 131, 271.
- Gratton, L. 1964, Ann. d'Ap., 127, 114.
- Gunn, J.E., and Peterson, B.A. 1965, Ap.J., 142, 1633.
- Hamada, T., and Salpeter, E.E. 1961, Ap.J., 134, 683.
- Harris, D.L., III, 1963, Stars and Stellar Systems (Chicago: University of Chicago Press), Vol. 3, p. 269.
- Hayashi, C., Hoshi, R., and Sugimoto, D. 1962, Prog. Theoret. Phys. Suppl., No. 22 (HHS).
- Hayashi, C., and Nakano, T. 1963, Prog. Theoret. Phys., 30, 460.
- Heney, L.G., Le Levier, R., and Levee, R.D. 1959, Ap.J., 129, 2.
- Holmberg, E. 1958, Medd. Lunds Obs., Ser. II, No. 136.
- _____. 1964, Ark. Astron., 3, 387.
- Hoyle, F., and Schwarzschild, M. 1955, Ap.J. Suppl., 2, No. 13.
- Humason, M.L., Mayall, N.U., and Sandage, A.R. 1956, A.J., 61, 97 (HMS).

- Iben, I. 1965a, Ap.J., 141, 993. *Letters*, 16, 410.
- Reddish. 1965b, *ibid*, 142, 1447. *81*, 19.
- _____. 1966a, *ibid*, 143, 483.
- _____. 1966b, *ibid*, p. 516. *50*, 835.
- Johnson, H.L. 1964, Bol. Obs. Tonantzintla y Tacubaya, 3, 305.
- Roberts. 1965a, Ap.J., 141, 170. *of Astronomy and Astro-*
- _____. 1965b, *ibid*, p. 923.
- Roberts. 1965c, Contr. Lunar and Planetary Obs., 53.
- _____. 1966a, Ap.J., 143, 187. 1965, *Nature*, 208, 993.
- _____. 1966b, Annual Review of Astronomy and Astrophysics, 4, 193. *59*, 1818, 122, 608.
- Johnson, H.L., and Sandage, A.R. 1955, Ap.J., 121, 616.
- Kelsall, T. 1965, Stars and Stellar Systems (Chicago: University of Chicago Press), Vol. 8, p. 274.
- Kinman, T.D. 1966, Ap.J., 144, 1232.
- Koehler, J.A. 1965, paper presented on Conference on Relativity and Astrophysics, Miami Beach, Florida, Dec. 15-17.
- Limber, D.N. 1960, Ap.J., 131, 168.
- Longair, M. 1966, M.N., 133, 421.
- McVittie, G.C. 1965, General Relativity and Cosmology (Urbana: University of Illinois Press).
- Mendoza, E.E., and Johnson, H.L. 1965, Ap.J., 141, 161.
- Morgan, W.W. 1959a, Pub.A.S.P., 70, 364.
- _____. 1959b, *ibid*, 71, 92.
- Morgan, W.W., and Mayall, N.U. 1957, Pub.A.S.P., 69, 291.
- Page, T. 1964, Science, 146, 804.

- Peebles, P.J.E. 1966, Phys. Rev. Letters, 16, 410.
- Reddish, V.C. 1961, Observatory, 81, 19.
- _____. 1962a, *ibid*, 82, 14.
- _____. 1962b, Science Progress, 50, 235.
- _____. 1965, Observatory, 85, 35.
- Roberts, M.S. 1963, Annual Review of Astronomy and Astrophysics, 1, 149.
- Robertson, H.P. 1955, Pub.A.S.P., 67, 82.
- Robinson, B.J., and Koehler, J.A. 1965, Nature, 208, 993.
- Salpeter, E.E. 1955, Ap.J., 121, 161.
- _____. 1959, *ibid*, 129, 608.
- _____. 1965, The Structure and Evolution of Galaxies (London: John Wiley & Sons), p. 71.
- Sandage, A.R. 1957, Ap.J., 126, 326.
- _____. 1961a, *ibid*, 133, 355.
- _____. 1961b, *ibid*, 134, 916.
- _____. 1962a, *ibid*, 135, 333.
- _____. 1962b, *ibid*, p. 349.
- _____. 1962c, Problems of Extragalactic Research, ed. G.C. McVittie (New York: Macmillan), p. 359.
- _____. 1965, paper presented at Conference on Relativity and Astrophysics, Miami Beach, Florida, Dec. 15-17.
- Schmidt, M. 1959, Ap.J., 129, 243.
- _____. 1962, Problems of Extragalactic Research, ed. G.C. McVittie (New York: Macmillan), p. 170.
- _____. 1963, Ap.J., 137, 758.

- Schwarzschild, M. 1958, Structure and Evolution of the Stars
(Princeton, N.J.: Princeton University Press), pp. 230-
245.
- Sears, R.L. 1964, Ap.J., 140, 477.
- Sears, R.L., and Brownlee, R.R. 1965, Stars and Stellar Systems
(Chicago: University of Chicago Press), Vol. 8, Chapter
11.
- Sérsic, J.L. 1962, Ann. d'Ap., 25, 206
- Spinrad, H. 1962, Ap.J., 135, 715.
- Spitzer, L. 1965, The Structure and Evolution of Galaxies
(London: John Wiley & Sons), p. 46.
- Stebbins, J., and Whitford, A.E. 1948, Ap.J., 108, 413.
- Tull, R.G. 1966, private communication.
- Vaucouleurs, G. de. 1959, Hdb.d.Phys. (Berlin: Springer-
Verlag), 53, 360.
- _____. 1961, Ap.J. Suppl., 5, No. 48.
- _____. 1966, private communication.
- Vaucouleurs, G. de., and Vaucouleurs, A. de. 1958, Lowell
Obs. Bulletin, 4, No. 92, p. 58.
- _____. 1959, Pub.A.S.P., 71, 83.
- Véron, P. 1965, paper presented at Conference on Relativity
and Astrophysics, Miami Beach, Florida, Dec. 15-17.
- Walker, M.F. 1958, Ap.J., 128, 562.
- Walker, M.F., and Bidelman, W.P. 1960, Pub.A.S.P., 72, 50.
- Weymann, R. 1963, Annual Review of Astronomy and Astro-
physics, 1, 97.

Wood, D.B. 1966, Ap.J., 145, 36.

Woolf, N.J. 1962, Ap.J., 135, 644.

_____. 1966, private communication.

Beatrice Marie Hill Tinsley was born in Chester, England on January 27, 1931, the daughter of Jean O'Hagan Hill and Edward Owen Herbert Hill. She attended the Girls' High School, New Plymouth, New Zealand from 1953 to 1957, and entered the University of Canterbury, Christchurch, New Zealand in 1958. She received from the University of Canterbury the degrees of Bachelor of Science in 1961 and Master of Science in 1963, each with a major in physics. Her Masters' thesis research work, 'Analysis of the Optical Absorption Spectrum of Neodymium Magnesium Nitrate', was published in The Journal of Chemical Physics, Vol. 38, p. 3503, 1963. During 1962 and 1963 she was employed as a part-time physics teacher at the Christchurch Girls' High School, and in 1963 gave private tuition to University students. In 1964 she attended The University of Texas, and entered the Graduate School in 1965. She married Brian Alfred Tinsley of Christchurch in 1961, and they have a son, Alan Roger, born in 1962.

Permanent address: 8739 Southbrook Avenue
Dallas, Texas 75231

This dissertation was typed by Beatrice M. Tinsley.

The vita has been removed from the digitized version of this document.